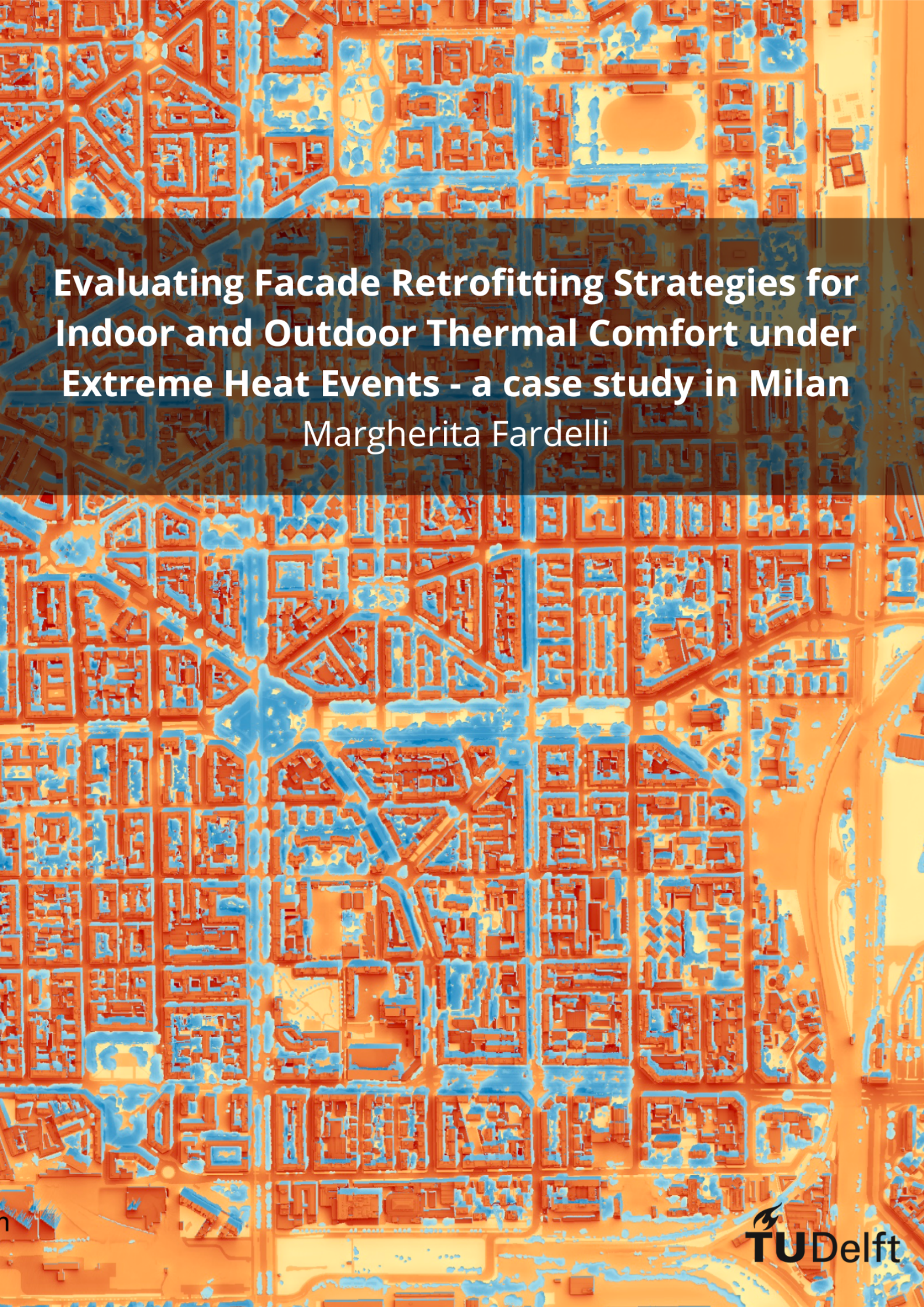

Evaluating Facade Retrofitting Strategies for Indoor and Outdoor Thermal Comfort under Extreme Heat Events - a case study in Milan

Margherita Fardelli

TUDelft

Delft University of Technology
Civil Engineering and Geosciences Faculty

Evaluating Facade Retrofitting Strategies for Indoor and Outdoor Thermal Comfort under Extreme Heat Events - a case study in Milan

Master's Thesis

Presented by:
Margherita Fardelli

Number of EC: 30

Date of Completion: 14/08/2025

Chair Supervisor:
Dr.ir. H.R. Schipper

Supervisor:
Dr. A. Luna Navarro

Advisor:
Dr. D. Maiullari

Academic Year 2024–2025

Abstract

Due to climate change, heatwaves have increased their frequency, intensity and extent. In particular, in cities the phenomena is exacerbated due to the urban heat island effect. More than half of the global population lives in urban areas. As a result, adapting the built environment to these changing climatic conditions is becoming a priority. To address this need, the present research aims to evaluate how different retrofit strategies influence outdoor and indoor thermal comfort during heatwaves, bridging two aspects which are usually studied separated. The Acquabella district in Milan is used as a case study.

The study includes a review on thermal comfort metrics , followed by an assessment of which metrics are most suitable for comparing outdoor and indoor thermal comfort. An RC thermal model of a facade was developed to identify the parameters who were mainly influencing the heat transfer, which were then used to define the retrofit scenarios to be tested. The scenario considered include two different aspect ratios, cool facades, external and internal insulation, and their combinations. The outdoor microclimate was simulated with Envi-met, while indoor thermal conditions with EnergyPlus. The outputs from Envi-met were used as boundary conditions for EnergyPlus.

The simulations outcomes revealed a strong correlation between the buildings and street geometry and the varying impact of facade retrofitting on outdoor thermal comfort. Cool facade showed a marked negative effect on outdoor thermal comfort particularly in courtyards, where inter-reflection phenomena occurred more intensely. Nevertheless, cool facades also achieved the greatest improvement in SET, with a reduction of about 0.25°C. Across all scenarios, the wider street canyon consistently gave a better performance. While most existing studies focus exclusively on either the indoor or outdoor effects of facade retrofitting, the findings of the present study demonstrate the importance of assessing both, as interventions on the facade affect the two environments simultaneously and, in some cases, in contrasting ways.

Contents

List of Figures

List of Tables

Acknowledgements

I would like to thank my supervisors, Alessandra, Daniela, and Roel, for their incredible and invaluable help and guidance. They have been fundamental in my academic journey, and their support has helped me grow both personally and professionally. This thesis would not have been possible without their direction. My thanks also go to the staff of the VR Lab, and in particular to the coordinator @Hok Student ICT Support Aytaç, for always being kind and ready to help whenever things were not working.

A big thank you to my family for always supporting and encouraging my studies. To my little sister Alessandra, for being —despite the distance — my faithful study companion throughout these years.

Thanks to all my friends in Rome for always making me feel as if I had never left: my friends from Parcoschuster and my neighborhood friends. Thanks to Irene, Sofia, Giusy, and Laura for bringing lightness and joy even during the heaviest times.

To Paola, my therapist, thank you for helping me always put myself first in every decision I make.

A sincere thank you goes to Marco, for always being by my side in the most difficult moments, for loving me with patience, and for cheering at every small success, ti amo.

Finally, to all my friends in Delft, thank you. A special thanks to my housemates Camilla, Sofia, and Margherita: you have been my sunshine during these two years in the Netherlands. You made Balpol feel like home, and you became my family. Every small step and accomplishment along the way, you were always the first ones I wanted to share my smiles and tears with.

Introduction

Importance

One of the most critical issues of the 21st century is rapid urbanization. It is estimated that 68% of the world's population will live in urban areas by 2050. Cities only cover 2% of the world's surface, yet they consume 78% of the world's energy and produce more than 60% of greenhouse gas emissions [1]. As the urban population grow, cities are expanding to meet housing needs. As a result, the urban fabric is significantly changing, leading to the Urban Heat Island (UHI) effect. The UHI effect is defined as the temperature difference between the urban areas and the rural ones. Studies have shown that high urban temperatures lead to detrimental effects on a broad variety of aspects, such as: outdoor thermal comfort, energy consumption, air quality, human health and affect the indoor environments of buildings as well. Moreover, hotter summers increase the reliance on cooling systems, which in turn release anthropogenic heat into the environment. This additional heat contributes to the urban energy balance, further exacerbating the problem.

In this context, cities have to be dynamic, to adapt to changes and to respond to extreme conditions. Resilience of the built environment is what is needed to face raising temperatures and their consequences on cities. The metropolitan area of Milan is one of the most densely populated in Italy and Europe. It faced in the last decades several extreme heat waves. For this reason, Milan is an interesting case study in the context of thermal comfort during heatwaves. Facade retrofitting strategies for UHI mitigation for existing buildings have been widely studied. Retrofitting strategies give the opportunity to engineers and urban planners to mitigate UHI effect and improve thermal comfort, by acting on the existing built environment, where the facade represents the medium between the indoor environment and the outdoor environment.

Problem statement

The research in retrofitting the building envelope system is led by two major aims: either mitigating the UHI effect, or improving the building energy efficiency. However, the effective strategies for UHI mitigation do not always align with those that enhance pedestrian thermal comfort, and those who improve indoor thermal comfort may not benefit outdoor thermal conditions.

Retrofitting the facades of existing buildings reflects the process of continual adaptation to the changing environmental conditions due to climate change and adjustment to evolving user needs, such as enhanced energy efficiency or a change in the building's function. In this context, cities can be considered responsive to changing conditions, taking part in the wide concept of "resilience" [2].

Under these circumstances, buildings take a key role ensuring occupants' safety, especially when considering extreme heat events. In the scenario of a heatwave, the heat island effect is not only detrimental during the day time, where pedestrian comfort is negatively impacted, but also during the night time inside buildings. This happens because, if the sleeping environment is too warm, the human body has to actively work to release its own heat, which in the long term could harm occupants' health. [3].

Current mitigation strategies for the UHI effect, rarely take indoor thermal comfort into account, and sometimes are in contrast with outdoor thermal comfort too. Retrofitting strategies are designed by facade engineers and urban planners focusing on either outdoor or indoor conditions. This fragmented approach results in a partial evaluation and assessment of the strategies. Ensuring a

thermal comfortable indoor environment in a hot summer often involve the use of air conditioning. However, this would release anthropogenic heat in the air and increase the outdoor thermal discomfort. Similarly, applying a highly reflective coating on a building facade could effectively reduce the solar heat gain inside the building, but at the same time would exacerbate pedestrian discomfort contributing to the outdoor rising mean radiant temperature.

A holistic approach to retrofitting strategies that address both indoor and outdoor comfort is needed. The absence of an integrated retrofitting plan could undermine long-term efficiency and overlook the relationship between indoor and outdoor thermal environments, which significantly affects urban living conditions.

Research questions

Research question:

How do different retrofitting strategies influence outdoor and indoor thermal comfort during a heatwave?

Research sub-questions:

- What are the appropriate metrics for describing thermal comfort indoor and outdoor?
- Which are the facade parameters, environmental parameters and urban geometry characteristics that influence thermal comfort indoor and outdoor?
- How do the facade parameters, environmental parameters and urban geometry characteristics influence thermal comfort indoor and outdoor?

Objective

The objective of this research is to investigate the relationship between facade design, environmental conditions, and urban geometry, and their combined effects on both indoor and outdoor thermal comfort. To this end, a case study was used, which is the Acquabella district of Milan. This study aims to identify and analyze the key parameters influencing thermal comfort through simulation-based assessment. To achieve this, the following research objectives have been formulated:

- To review and identify suitable metrics for quantifying thermal comfort in both indoor and outdoor environments.
- To analyze the urban and climatic context of the Acquabella district and define the most relevant facade and urban geometry parameters affecting thermal comfort.
- To set up and perform simulations to evaluate the impact of different facade characteristics and urban morphology on thermal comfort, both indoor and outdoor.
- To interpret the simulation results in order to draw conclusions on the effects that different retrofitting strategies have on outdoor and indoor thermal comfort.


Outline of the thesis
State of the art
1
Explorative review on retrofitting strategies, urban heat island and thermal comfort
Identify literature gap
outcome: research basis, overall understanding of the existing literature
Methodology
2
Thesis workflow
Thermal comfort metrics
3
Systematic review on thermal comfort models and thermal comfort indices
Comparison of thermal comfort indices
outcome: comparative tables, indices choice
Parameters selection
4
Systematic review on the parameters who are involved in the research and RC thermal model development
Selection of relevant parameters, developing scenario planning based on the chosen parameters
outcome: RC thermal model, scenario planning for simulations
Case study
5
Selection of the focus area and selection of the simulation day
Clustering of the buildings on the focus area
outcome: clustering of the buildings that have to be modeled and selection of the simulation day
Simulation and scenario testing
6
Set-up of models for indoor and outdoor simulations
Scenario testing
outcome: results of the impact of different scenarios on indoor and outdoor thermal comfort
Evaluation
7
Post-processing of the results
Results visualization
outcome: clear overview of the results (i.e. maps and graphs)
Discussion
8
Discussion of the results
Conclusion
9
Conclusions and recommendations for future research, including limitations

1

State of the art

Climate change is driving a rise in the frequency and intensity of extreme heat events. In urban areas, these effects are further amplified by the urban heat island phenomenon. With a significant part of the global population living in cities and much of the built environment already in place, adapting existing structures to a changing climate is an urgent priority. In this chapter, concepts such as the Urban Heat Island and thermal comfort will be explored in depth, as they are essential for understanding the research context. In addition, facade retrofitting strategies will be examined to clarify what retrofitting is, why it is undertaken, how it is implemented, and which aspects are not clear yet with the current knowledge.

1.1. Urban heat island

Rapid urbanization and rising urban density has led to increasing temperatures in cities. This phenomenon is referred to as Urban Heat Island (UHI). UHI effect can be explained as the difference in temperature between the rural and the urban areas. There are various reasons why cities are hotter than countrysides, and the most influential factor appears to be the type of materials employed in the urban built environment [4]. It is the result of urban and rural energy balance differences.

The energy that reaches the earth's surface is of two types:

- Shortwave (solar) radiation, in the visible ultraviolet and near-infrared spectrum;
- Longwave (terrestrial, or thermal) radiation, in the infrared spectrum.

A part of this incoming energy is reflected back to the space and what remains is the Net Radiation ($Q*$), and it is the energy available at the surface. The overall radiation balance is:

$$Q* = SW\downarrow - SW\uparrow + LW\downarrow - LW\uparrow \tag{1.1}$$

Where the downward sign means that the energy wave is going into the system, and the upward sign means it is going outside the system.

The net radiation is used for three purposes: to heat up the air (i.e. sensible heat flux Q_H), to evaporate water (i.e. latent heat flux Q_E) and to heat the ground (i.e. ground heat Q_G). Hence the surface energy balance is:

$$Q* = Q_H + Q_E + Q_G \tag{1.2}$$

The UHI effect is influenced by several key factors that amplify heat retention and reduce cooling in urban areas. The heat storage component Q_G increases as urban materials such as concrete and asphalt absorb and retain heat during the day. This heat is gradually released at night, maintaining elevated temperatures. This process heats up the air directly, contributing to the overall rise in temperature. The latent heat flux (Q_E) is reduced in urban areas due to the replacement

of vegetation with a greater proportion of impervious surfaces. As a result, the cooling effect of evapotranspiration is significantly reduced. Meanwhile, the sensible heat flux (Q_H) increases, as the heat that would go into latent heat is instead directed towards sensible heat.

Moreover, in urban canyons the heat is trapped inside the canyon itself. By urban canyon is meant "*urban street configurations where buildings are arranged on either side, creating a canyon-like effect that influences airflow and ventilation*" [5]. The urban layout (building and narrow streets) reduces the longwave radiation loss (LW ↑), causing heat trapping. Additionally, in cities there is a decrease of wind speed due to the urban roughness. Lower wind speeds limit the mixing and dissipation of heat, further exacerbating the UHI effect. Furthermore, water bodies have considerable capacity to reduce the UHI effect in cities, providing marked cooling benefits. They influence the nearby temperature and humidity through evaporation, heat convection, and solar radiation absorption. Water has an incredible high heat capacity, meaning that a substantial amount of energy is required to evaporate even a small quantity.

The UHI effect not only depends on building materials but also on the way buildings are set up. There are two important parameters that describe this: the aspect ratio and the sky view factor (SVF). The aspect ratio is defined as "the ratio between the average height (H) of the canyon walls and the canyon width (W)" [6]. The sky view factor (which can have values between 0 and 1) governs incoming and outgoing radiation. SVF is defined as “the ratio of the amount of the sky which can be seen from a given point on a surface to that potentially available". The obstacles that obstruct the sky sight are buildings and vegetation. SVF and H/W ratio are directly related.

There is a missing term in the energy balance equation, when the urban context is tried to be described. The missing term is the anthropogenic heat flux (Q_f). Hence, the urban energy balance equation becomes Equation 1.3, according to Oke [7].

$$Q^* + Q_f = Q_E + Q_H + \Delta Q_G \tag{1.3}$$

Where:

- Q^* is the surface net flux density;
- Q_f is the anthropogenic heat flux density;
- Q_E is the convection of latent heat to/from air;
- Q_H is the convection of sensible heat to/from the air;
- ΔQ_G is the heat storage.

In Oke’s paper the heat storage is referred to as ΔQ_S, but in this research it will be referred to as ΔQ_G.

The Urban Heat Island Intensity (UHII), which is the magnitude of the temperature differences between urban and rural areas, depends on heat absorption during day-time and heat release during night-time from urban components [8]. The UHI has been shown to have a seasonality: it has its maximum values in summer, and in winter is approximately a half [9] [10]. Indeed, changes in the indoor environments due to the UHI effect are more evident in summer [10].

Mitigation strategies

According to Connors, Galletti, and Chow [11], the urban variations in temperatures, which are a consequence of the UHI, largely result from modification to:

1. Urban structure (e.g. H/W ratio);
2. Urban cover (e.g. the proportion of building vs. vegetated surface per urban area);
3. Urban layout (e.g. physical properties of the envelope materials);
4. Urban metabolism (e.g. anthropogenic heat waste).

To mitigate the UHI effect, several strategies have been studied by researchers, which can be grouped in three categories: green strategies, water strategies and white strategies [12]. Mitigation strategies should have the scope to achieve better living conditions and comfort, considering both outdoor and indoor environments [2]. This is essential because outdoor thermal conditions have an indirect effect on indoor environment [10]. The methods applied directly on the building envelope are usually two: increasing solar reflection and/or increasing evaporation and transpiration [12]. Urban greening is always recommended as a mitigation strategy since vegetation's presence can alter micro-climate parameters and guarantee a decrease of air temperature [13] through the process of evapotranspiration [14].

1.2. Thermal comfort

ISO 7730 standard defines comfort as "That condition of mind which expresses satisfaction with the thermal environment" [15]. This definition of thermal comfort highlights how the judgment of comfort is a cognitive process, involving psychological, physiological and physical factors [16].

The human body produces heat and exchanges heat with the surrounding environment, trying to maintain an energy equilibrium in a process called "thermoregulation" [16]. The thermoregulatory system actively operates to keep the body core's temperature at 37°C and the skin temperature at 34°C [17]. If the body temperature is too high, the human body tries to restore energy balance in two ways: blood vessels vasodilate, or sweat. While, when the body is too cold, the thermoregulatory system gives input for blood vessels to vasoconstruct and for shivering. The perception of being cold or being warm is determined by skin sensors (i.e. skin thermoreceptors), which signal cold when the skin temperature is lower than 34°C, or warm when the skin temperature is higher than 34°C. The brain then interprets the signals sent by the sensors, and reacts with muscle movement, sweating or changing the blood flow in the skin. At the same time, also the blood temperature is received in the hypothalamus and controlled to be 37°C.
The environment is finally considered comfortable if no body reaction is present [17].

There are 6 parameters defining thermal comfort, which affect the energy transfer to and from the body, and therefore affect thermal sensation [17].

1. Activity level (metabolism, expressed in terms of metabolic rate);
2. Resistance of clothing;
3. Air temperature Ta;
4. Relative humidity RH (usually for a comfortable and healthy environment should be around 30-70%);
5. Air speed v and turbulence (below 0.15 m/s during cold season, increased up to 0.5 m/s during the hot season);
6. Mean Radiant Temperature (MRT) (defined as the average surface temperature of the enclosure).

The first two are defined as personal variables, whereas the remaining four are considered fundamental environmental variables affecting human responses to the thermal environment. [16].

Factors beyond physics and physiology also influence thermal perception, as demonstrated by human adaptation to the thermal environment. Some of these factors are: population demographic (gender, age, economic status), context (season, climate, social conditioning) and cognition (attitude, preference, and expectation) [17]. The literature on thermal comfort shows two different approaches: the (rational) heat-balance model and the adaptive model [16] [18].

1.2.1. Outdoor thermal comfort

The difference between indoor and outdoor thermal comfort is that indoor thermal comfort is generally achieved by creating a stable and neutral thermal environment, while outdoor thermal comfort can be achieved in highly asymmetric and dynamic thermal conditions. There are some studies that investigated into the wider comfort range that people experience in outdoor settings[19], arguing that the comfort range of indoors could be expanded learning from the outdoor. As an example, natural ventilation is a concept that is being recently proposed to reproduce the dynamic outdoor environment and widening the comfort zone of the indoor environment [20].

Compared to indoor thermal comfort, outdoor thermal comfort is still challenging to be quantitatively described by researchers. This is due to the complexity of outdoor environments [16] and to to the fact that people are directly exposed to local microclimate conditions [21]. In outdoor environments the human body is exposed to different types of radiation that contribute to exchange heat with the body: incident solar radiation (direct and diffuse), reflected radiation (from horizontal and vertical surfaces) and longwave radiation emitted by the sky and the surrounding surfaces. The net impact of radiant exchange with the human body is expressed by the Mean Radiant Temperature (T_{mrt}) [22].

1.2.2. Local thermal discomfort

Thermal discomfort can arise not only when the entire body is too warm or too cool, but also when localized body parts experience thermal imbalance. There are various reasons why the body can be in thermal discomfort, which are: draughts, asymmetric thermal radiation, vertical air temperature differences and local discomfort caused by surface contact [23].

Draughts are defined as unwanted local cooling of the body used by air movements. The magnitude of the perception of the draughts depends on air velocity, air temperature, degree of air disturbance, area of the body exposed and thermal state of the person. Asymmetric thermal radiation is due to the asymmetric nature of the radiation field in real thermal environments. If the environment is thermally neutral, the effect of the radiation asymmetry is reduced. Vertical air temperature differences happen in all real environments. This is due to the fact that warm air tends to rise, resulting in cooler temperatures near the floor and warmer temperatures near the ceiling. Consequently, the lower parts of the body may feel cooler, while the upper body may be warmer. Discomfort by surface contact is highly reduced by clothing, which provide thermal insulation. This type of thermal discomfort can occur, for instance, when a person is seated and the feet, being in contact with the colder floor, experience lower temperatures compared to the rest of the body.

1.3. Facade Retrofitting Strategies

Rising temperatures in cities due to the climate change and extreme heat events exacerbated by the heat island effect, are becoming a threat to human health and well-being in the built environment. For this reason, the already existing built environment has to be modified to respond better to this phenomena. In this section the types, applications, and trade-offs of existing retrofitting strategies will be studied. In the present research, facade retrofit is intended as any modification or addition to the facade system to respond to environmental considerations and occupants' well-being [24].

A clear understanding of the aims and scope of prior retrofitting interventions is a necessary first step. A survey conducted by Martinez et al. [24] on more than 300 retrofit building projects found that even if operational energy use is the main driver for retrofitting, comfort is one of the main goals of retrofit projects, as shown in Figure 1.1.
The scope of the retrofit work was also investigated, revealing that the main emphasis in the reviewed projects was the replacement of the entire facade, as shown in Figure 1.2.

The findings from these two surveys highlighted how full facade replacement is more frequent than

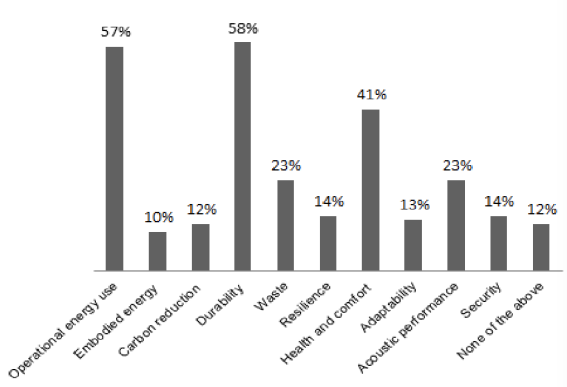

Figure 1.1: Goals included in retrofit plans in the survey conducted by Martinez et al. [24]

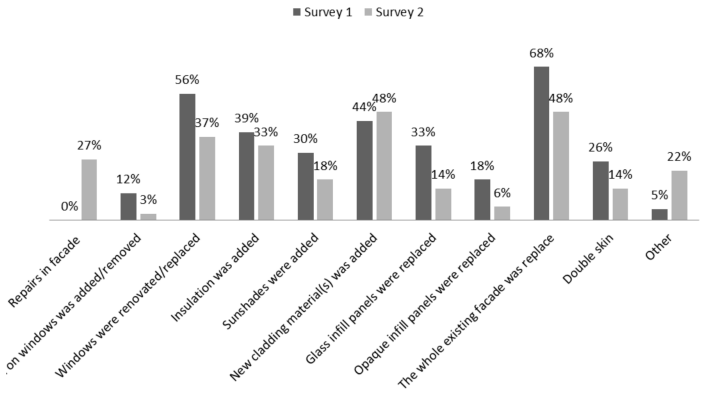

Figure 1.2: Scope of facade retrofitting projects reported in both of the surveys conducted by Martinez et al. [24]

other partial measures. This indicated that retrofitting is often considered as a general opportunity to integrate multiple improvements at once to the building envelope, rather than a targeted measure.

Even if specific retrofit strategies are studied only with the objective of mitigating the UHI effect, they will have repercussions on the indoor environment as well. Likewise, energy retrofit of facades aims to make the building envelope more energy efficient, but could have effects on the microclimate. Therefore, when designing a retrofit strategy is essential to understand the overall effects of it. The importance of focusing on both indoor and outdoor environments when designing retrofitting strategies is recognized by various researchers as Camporeale and Mercader-Moyano [25] and Lassandro and Di Turi [26]. The study conducted by Wonorahardjo et al. [8], reviewed relevant studies regarding the effect of different building facade systems on thermal comfort. Figure 1.3 shows an outline of the main findings.

The facade systems are divided in three categories: heavyweight blockwork facade (such as brick and concrete), sandwich wall facade and glazing facade. In the central column of the figure there is the wall treatment technology. The arrows that go from the wall treatment technology to the right show the outdoor effects of the treatment, divided in the impact on heat transfer and the effect on microclimate. The arrows that go from the wall treatment technology to the left, bring to the indoor effects, divided in heat transfer and effect on air temperature. For this study, it is interesting to look in detail at those wall treatment technologies that have an effect on both indoor and outdoor environments. For no treated heavyweight blockwork facade (i.e. simple brick or concrete facade), the heat transfer indoor is governed by the thermal inertia (see section 4.1.2) of the facade, the indoor air temperature is stabilized. When an additional panel (e.g. metal panel) is added to this type of facade, there is a shading effect which causes a higher surface temperature on the external wall, causing an increasing in outdoor air temperature. However, this shading effect reduces the

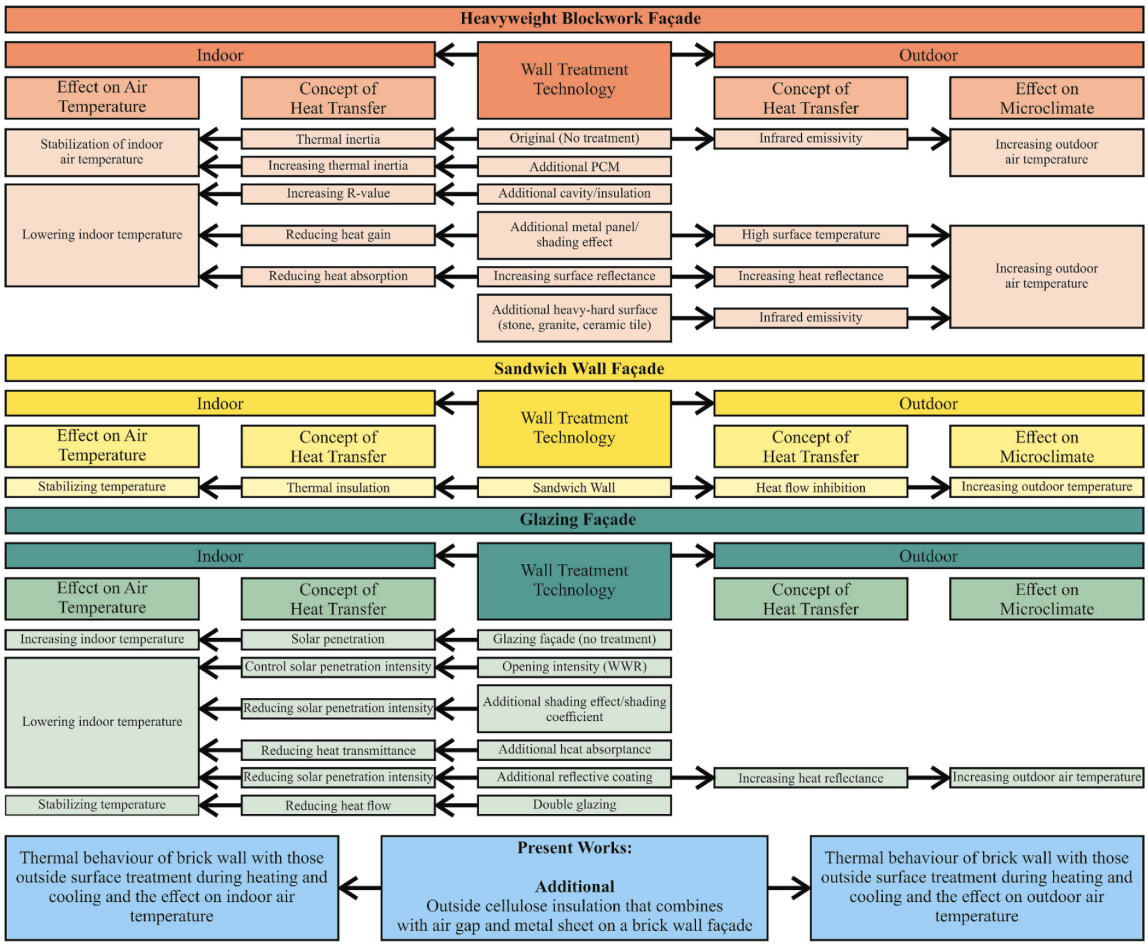

Fig. 1. Summary of façade treatment studies and the present works.

Figure 1.3: Summary of facade treatment studies and the present works [8]

heat gain of the facade, lowering indoor temperature. Increasing surface reflectance is also reviewed as a wall treatment technology, which cause an increase in heat reflectance of the exterior surface, leading to an increasing outdoor temperature. However, it lowers the indoor temperature, reducing the heat absorption. For the sandwich wall facade, the thermal insulation helps stabilizing the air temperature indoor. However, it increases the outdoor temperatures by inhibition of the heat flow. For glazing facades, the addition of reflective coatings have similar implications than heavyweight blockwork facades.

Objective of retrofitting

In this study these two objectives of retrofitting will be considered: retrofit to enhance outdoor thermal comfort, and retrofit to improve indoor thermal comfort. There are two main research direction in the existing literature: retrofit to mitigate the UHI effect, and energy retrofit.

The research in retrofitting strategies to mitigate the UHI effect seems to have two main trends: the implementation of building integrated vegetation technologies and the optimization of reflectance and emissivity of facade materials through cool coatings.

There is extensive literature on energy facade retrofitting. With "energy retrofit" is intended the practice that involves changing the facade to improve the building's energy efficiency. Even if the scope of this research is to study retrofitting for indoor thermal comfort, there are few studies

addressing this specific topic. Most of the studies are on energy retrofit, and some of them mention comfort as a side note. However, reviewing the energy retrofit gives a good idea of the methods of retrofit for indoor environments. Moreover, there is a direct relationship between energy consumption in buildings and the residents' thermal sensation [27].

The strategies used to retrofit facades for indoor and outdoor purposes are not always the same. This chapter focuses on three approaches—vertical greening, cool materials, and insulation—as they are among the most frequently discussed in the literature and the most widely implemented in practice.

Vertical greening

Greening has been shown to improve livability in cities, as it improves the surrounding environment and the air quality. Vegetation technologies can significantly decrease the incoming solar radiation (depending on leaf density) through shading. They also convert part of the sensible heat (Q_H) in latent heat (Q_E) through evapotranspiration, which bring a significant reduction in outdoor air temperature [14]. Thus, urban vegetation can reduce the UHI effect [28]. The effects of green façades on the thermal environment are mainly due to the shading of the leaves, insulation, transpiration, and wind barrier effects [29]. Surface temperature reduction goes from 2 to 16°C degrees in the hot season when vertical greening is applied. The maximum impact happens during the day time, when there is solar radiation and evapotranspiration [28]. The vertical greening systems have special relevance in high density cities, where the potential tree-planting area is limited and conversely there is a great building façade area.
Studies have shown that when these technologies are applied to a single building, the mitigation effect is smaller than when there is a wide application, suggesting neighborhood-scale interventions rather than single-building ones [30].

Building integrated vegetation technologies are: living wall systems (LWS), green façades (GF) and green roofs (GR). In this research, the focus will be on LWS and GF. The differences from the two are summarized in Table 1.1 according to [31].

Table 1.1: Types of vertical greening and main characteristics.

type of vertical greening		supporting elements	growing media	vegetation	drainage	irrigation
green façades	*direct*	no		climbing plants; evergreen or deciduous; up to ~25 m; full wall coverage may require several years	—	—
	indirect	structural support for vegetation growth with continuous or modular guides (tensile cables, stainless steel, grids, etc.)	ground or box	climbing plants (as above)		
living wall systems	*continuous*	frame indirectly fixed to the wall	lightweight, absorbent screens (e.g., fabric/felt) cut to form pockets	wide variety of plants (grasses, perennial plants, shrubs, succulents, etc.)	drainage through a permeable layer	hydroponic technique: irrigation system installed at the top of the structure
	modular	pre-vegetated panels with specific supports (vessels, trays, flexible bags, planter tiles) in which plants grow	organic and/or inorganic substrate with good water-retention capacity allowing root proliferation		water drains through the panel and is collected at the bottom	irrigation system generally installed between the panels

Green facades use climbing plants (e.g. common ivy, boston ivy) to cover the vertical surfaces, and the plants are rooted into the ground. The plant can have evergreen foliage or deciduous and could reach until 25 meters of height. However, the full coverage of the wall could take up some years. Green facades can be direct or indirect 1.4. In direct green facades the plants are directly attached

to wall, while indirect green facades use a supporting system for the plants. The use of a supporting structure (i.e. indirect green facades) offers the benefit to have space between the green facade structure and the wall, that could be use with insulation purposes or to ease the maintenance. Moreover, it gives the system resistance to environmental actions (rain, snow, etc.) [31].

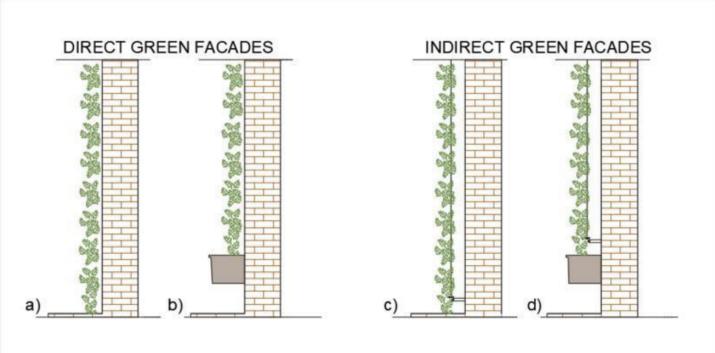

Figure 1.4: Green facade [31]

Living wall systems are designed using pre-vegetated panels, vertical modules or planted blankets. They use as a rooting medium planter boxes, mineral wool, foam or felt layers [29]. They can be divided into continuous living walls and modular living walls 1.5. The growing media of continuous LWs is a lightweight and absorbent screen cut to form pockets and they are attached to a frame which is indirectly fixed to the wall. The modular LWs are pre-vegetated panels with specific supporting elements in which the plants grow. The growing media is organic ad/or inorganic substrate, where the roots can proliferate. There is also a third typology of living wall system mentioned in the literature called linear green wall [32], which result from cascading elements, affixed to the wall in a liner way.

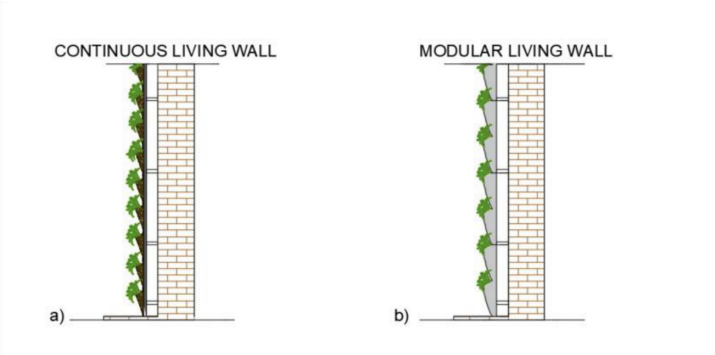

Figure 1.5: Living wall [31]

There are multiple studies that explore the beneficial effects on indoor thermal comfort and energy savings of applying vertical greening [33]. For example, a study conducted by Alsaad et al. [34] demonstrated that using vertical greening could reduce the indoor air temperature by 3.77°C. Hao et al.[35] conducted an experimental study on the effect of vertical greening and green roofs by building two experimental rooms, one with green façades and a green roof, and the other one without, in Xiangtan, China, which is characterized by hot summers and cold winters. The results showed that the OT of the first room was was reduced in average of 0.4°C, and a maximum of 2.1°C compared to the second room. Moreover, the OT in the first room had less oscillation, resulting in a stabilization of it. A review on the thermal effects of vertical greening systems conducted by Medl et al. [32] divided the findings in three main area: surface cooling potential, indoor cooling potential (T_a) and energy saving potential. This review reported the values of 11 studies on the surface cooling potential, 2 studies on the door cooling potential and 3 studies on the energy saving potential.

However, most of the studies on the effect of green façades on the indoor environment do not consider the window components of the buildings, overlooking an important factor. Li et al. [36] studied the effect of vertical greening on indoor air temperature considering the window-to-wall ratio, and reported a maximum reduction of temperature of 0.56°C, which is considerably lower than the reduction of temperature of the other reviewed studies. This difference is due to the high solar heat gain coefficient (SHGC) and high heat conductivity coefficient that characterizes glasses. In general, the effect of vertical greening found by this study, was an increase in the cold perception duration and a reduced perception duration of heat throughout the year. However, in this study, even if the windows were considered, they were assumed to always be close, leaving an open question on how the performance of green facades changes if natural ventilation or infiltration are considered in buildings. Moreover, most of the studies are carried in hot summer days, while it is important to analyze the effect of these systems all over the year, due to their possible controversial effect on winter, aiming to a passive design solution which is beneficial throughout the entire year.

The benefits achievable by vertical greening systems depend on many factors involving plant and building characteristics and local climate. Among these factors, the thermal functioning of green façades are heavily influenced by the plant characteristics and the Leaf Area Index (LAI) is the most crucial one [37]. LAI is a dimensionless quantity, define as the leaf cross-sectional area per unit covered area. Higher values of LAI corresponds to a better thermal performance of the building. However, many studies found that there is a threshold value of the index after which the benefits are negligible. In the research conducted by Convertino et al. [37] an experimental green façade was built at the experimental center of the University of Bari and the threshold value was found to be $LAI = 6$. In correspondence of this value, the cooling effect of the green façade was increasing less than 1%. Widiastuti et al. [38] found that the effect of green facades on indoor temperature, humidity, and thermal comfort is determined by the leaf coverage areas. A greater leaf coverage area lead to a lower indoor air temperature. However, it also increased the relative humidity indoors, thus the indoor thermal comfort is not necessarily improved [33].

There is extensive literature on how greening improves the outdoor thermal comfort, for all the reason discussed in the introduction of this section. However, different façade greening arrangements have different impacts on outdoor thermal comfort [39]. Cui et al. [39] investigated different vertical greening dispositions and the related change in PET. They found that the most significant reduction in the average PET (0.49°C) was achieved when the greenery was placed in the lower half of the façade, closed to pedestrian level. Similar findings were made by Acero et al. [28]. The study revealed that vertical greening systems have a greater impact on pedestrian comfort when they are located at the bottom of the façade. When greenery is placed above 6 meters in height, there is no significant benefit to pedestrian comfort.

Cool materials

Currently trending in research is the application on facades of cool materials, which are materials characterized by high thermal emittance and high solar reflectance [2]. Having a high solar reflectance, cool materials decrease solar absorption, having a beneficial effect on the daytime surface temperature, and, consequently, they could help in reducing the urban air temperature. Having a lower surface temperature also means that the solar heat gain of the building envelope is reduced, with beneficial effect on the indoor thermal conditions in summer. However, some studies highlighted the possible detrimental effect cool facades could have on outdoor comfort at the street-level. This happens because the body in the outdoor environment is exposed to different types of radiation: incident solar radiation (direct and diffuse), reflected radiation (from horizontal and vertical surfaces) and long-wave radiation (emitted by the sky and surrounding surfaces) [22]. This net radiant exchange can be expressed in terms of Mean Radiant Temperature (T_{mrt}).

Increasing solar reflectance on facades could have controversial effects on thermal comfort, and multiple and interconnected consequences. Defining the scale of the discussion is essential, especially

in research such as the present study, which spans from the district scale down to the individual building level. When there is this big variability in the scales, the same considerations can have different consequences, depending on the scale that is considered. This is particularly evident when the albedo (i.e. the overall reflective behavior of surfaces across the solar spectrum) of the vertical surfaces is studied.

The albedo can be can be quantified at three different scales: the surface albedo, the urban albedo and the urban canyon albedo. The Surface Albedo (or Surface Reflectance, SR) represents the reflective power of single surfaces. It is given by the ratio of the reflected solar radiation to the incident one over a horizontal plane and goes from 0 to 1, where closer to 0 there are dark materials and closer to 1 white ones. However, single surfaces' albedo do not accurately describe the overall albedo of a city, due to other factors that also play a role when the scale gets bigger. In general, urban surfaces have a lower reflecting power due to urban roughness. Compared to planar surfaces of the same material, urban surfaces result in a 10-40% increase in solar absorption due to radiation trapping. For this reason, the concept of Urban Albedo (UA) was developed. The urban albedo concept was developed to characterize the ability of cities to reflect radiation back to the sky, considering both urban materials albedo and urban roughness, which cause an increase in solar absorption. To investigate the urban canyon at the microscale, the Urban Canyon Albedo (UCA) was introduced. The urban canyon is defined as the planar intersection between the roof and the external wall. Figure 1.6 is a schematic representation of the interconnections between surface albedo, urban canyon albedo, outdoor thermal comfort and building indoor thermal environment, according to Salvati et al. [22].

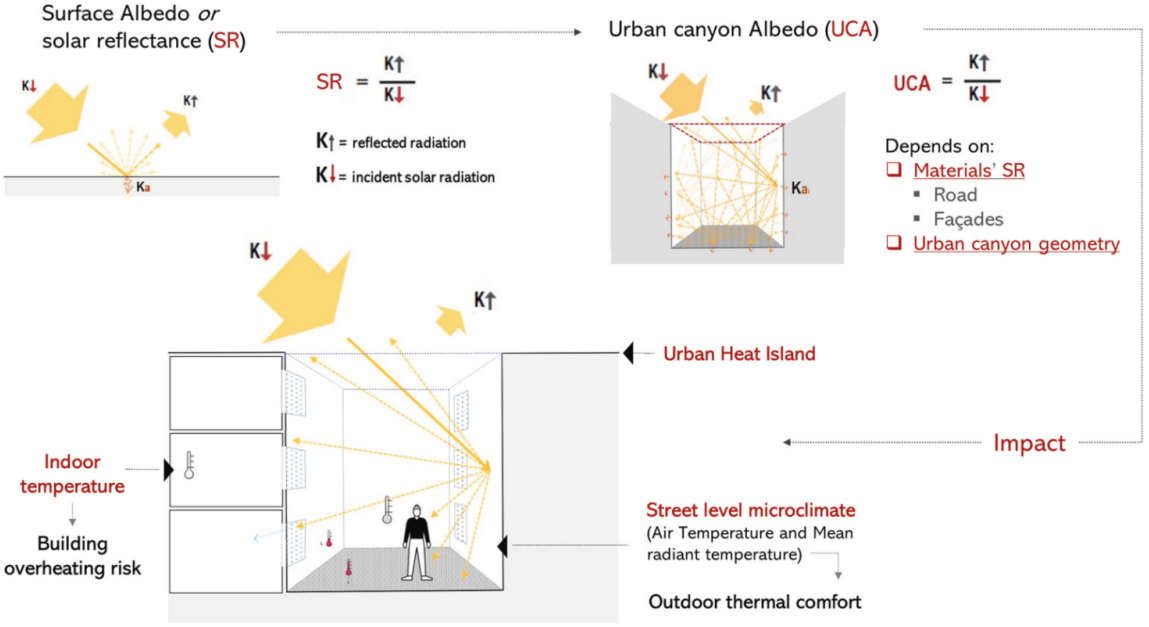

Figure 1.6: interconnections between surface albedo, urban canyon albedo, outdoor thermal comfort and building indoor thermal environment, according to Salvati et al. [22]

At the building scale, increasing solar reflectance in the building envelope is shown to have beneficial effects on indoor thermal comfort, because the decrease in surface temperature implies a reduction in T_{mrt} indoor. However, the building scale considerations are partial when the building itself is surrounded by other surfaces (other buildings), and more complex physical processes occur. In fact, in an urban setting, increasing the reflectance of building facades can produce a negative effect on indoor thermal comfort because the reflected energy is mainly directed toward other buildings rather than towards the sky. Since the effect of using cool materials is directly related to the specific urban morphology, the net impact of reflective materials on outdoor and indoor microclimates and thermal comfort is still unclear.

What is known is that some conditions have a positive impact on UCA and air temperature, meaning they overall mitigate the UHI effect, but at the same time the effects on outdoor thermal comfort is detrimental. This happens, for example, when the reflectivity of pavement is increased. Moreover, an increase in the reflectance of the facade produces a considerably small reduction in $T_{\mathbf{mrt}}$ and has a negligible impact on air temperature, meaning that thermal comfort has a limited improvement. Oppositely, reducing the facade reflectance has a beneficial effects on thermal comfort. The best solution from the cases analyzed in the research by Salvati et al. [22] is the combination of high solar reflectance road and low solar reflectance on facades. By combining these two reflectances, there is a significant increase in UCA but the pedestrian comfort is not negatively impacted.

The change in solar reflectance of surfaces affects the indoor thermal environments of buildings because it modifies two boundary conditions: the external surface temperature and the incident radiation on the facade. Considering a single building, the increase of solar reflectance of the outer wall implicates a reduction of surface temperature, with positive impact on the indoor thermal comfort. However, at the street level, increasing solar reflectance of facades and pavements of an urban canyon increase the total incident radiation on the facades. However, it is important to mention that if the walls are insulated the indoor of the building will be less affected by the external surface temperature [22]. In summary, the overall effect of varying the solar reflectance of a building is complex to understand and is case specific, due to its high correlation with the urban canyon geometry.

Insulation

In the Mediterranean area, both active and passive retrofit strategies are commonly assessed. Passive strategies are implemented 31.5% more frequently than active ones, due to the reduced costs for users. The most commonly adopted passive retrofit strategies include glazing replacement, addition of thermal insulation and shading systems [40].

Most studies on insulation are energy saving oriented, often relying on large building samples, and tend to overlook other - sometimes conflicting - issues such as thermal comfort [41]. When retrofitting, insulation can be positioned either externally or internally, leading to different thermal performances. There is extensive literature on the effects of insulation on indoor thermal comfort, with particular attention in this work to studies focusing on summer conditions and extreme heat events.

It is well established that insulation improves energy efficiency in winter, and under certain conditions also in summer. However, as temperature rises, summers get warmer, and heatwaves are more frequent and intense, some studies noticed that insulation can lead to overheating in buildings under specific circumstances. A study conducted by Fang et al. [42] concluded that insulation could increase the cooling load of a building during summer. Buildings with high insulation levels are more at risk of overheating during summer [43]. In particular, the literature agrees that internal insulation is the configuration most prone to overheating, as shown by Stazi et al. [41] in a comparative analysis of various insulation configurations and types. Overall, external insulation enhances the thermal performance of buildings in both summer and winter.

A study conducted by Basaly et al. [43] investigated the risk of overheating of different retrofitting scenarios for actual and future weather. They concluded that to prevent overheating and enhance thermal comfort, external insulation was performing better than internal insulation. Similar results were obtained by Kossecka and Kosny [44], who analyzes six different wall configurations and concluded that external insulated walls have the best annual performance out of the tested scenarios, for the considered climate.

1.4. Identified Gaps in the Literature

The literature review above has offered a thorough overview of the ongoing research on facade retrofitting strategies. The research is carried in parallel on two binaries: the first one is to mitigate the Urban Heat Island effect on the outside of the building and the second one is to have a thermal comfortable indoor, with particular consideration to energy consumption. The retrofitting strategies proposed in the literature to mitigate and adapt to UHI effect are often related to pedestrian comfort and rarely investigate how the indoor environment change, changing the outdoor conditions. To link these two branches of research, the role of the facade wall system is critical. Hence, there is a need for future research on the potential impacts of facade retrofitting strategies on both indoor and outdoor environments accounting for UHI effect, and for a conceptual structure for retrofitting planning. One of the reasons of the research gap in studies correlating indoor and outdoor thermal environments is the lack of a common index used in indoor and outdoor thermal comfort studies [20].

2
Methodology

2.1. Workflow

Figure 2.1 shows the workflow adopted in this thesis. On the left column of the figure there is the workflow, composed of research actions which are needed to answer the research questions. On the right column of the figure, there are the research questions. Each step of the workflow is connected to the subsequent one, and by completing all the steps, the main research question is answered.

The workflow is organized in a chronological way from the top to the bottom. The process starts with a literature study, to then continue with the parameter selection and the scenario planning. From the scenario planning, the facade variation can be modeled for both indoor and outdoor. The definition of the study area is also a starting point of the workflow, which leads to the baseline simulations, through data collection. The outdoor simulations are done once the urban canyon is modeled, and with it also the facade variations. Once the outdoor simulations are done, the results are extracted and used as input for the indoor simulations. When also the indoor simulations are done, the results can be post-processed, evaluated and discussed.

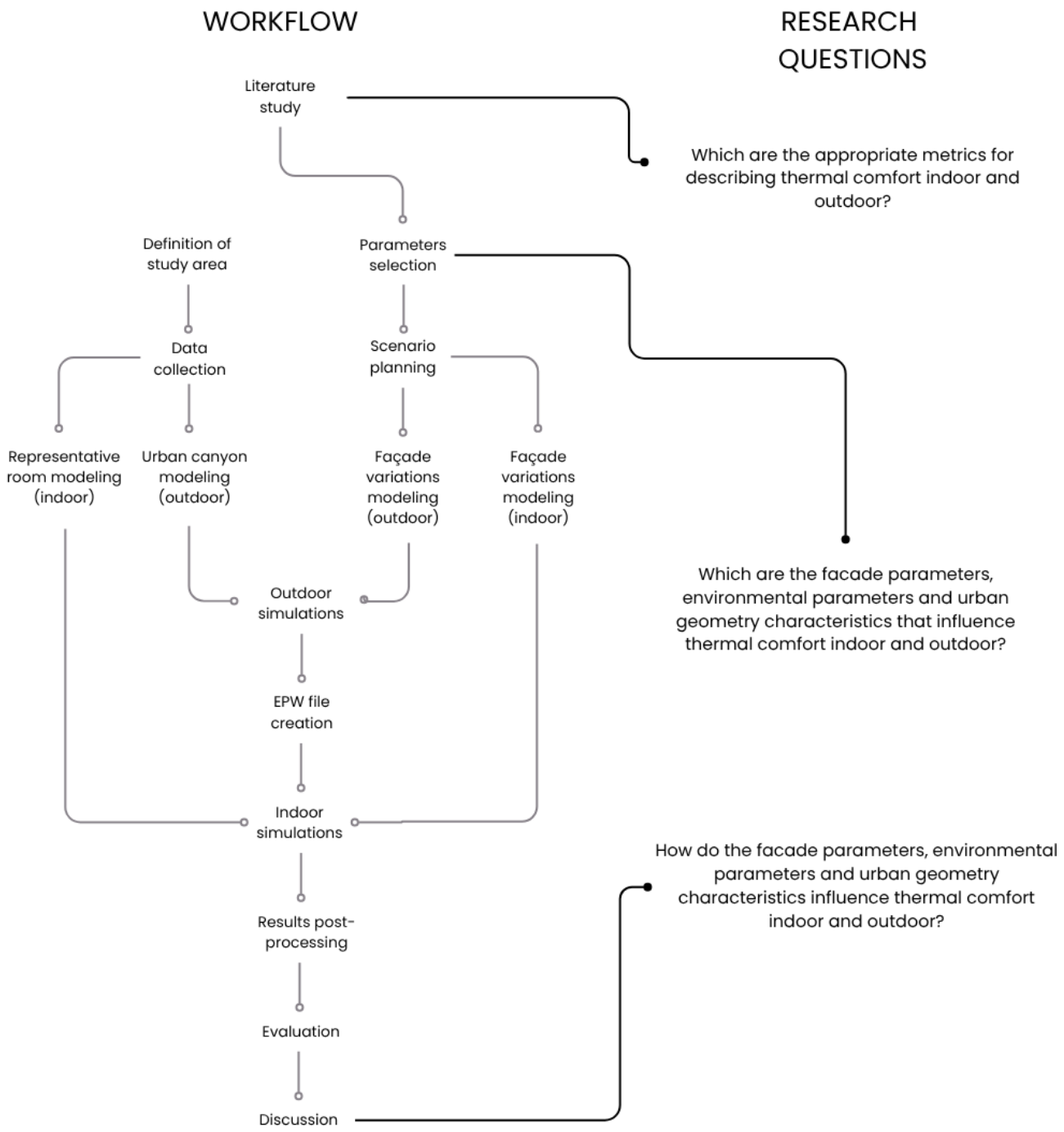

Figure 2.1: Workflow of the Thesis

3

Thermal comfort metrics

In this chapter the research question *" What are the appropriate metrics for describing thermal comfort indoor and outdoor?"* will be answered. A systematic literature review is conducted to understand the most used thermal comfort metrics and indices, what model they employ, what assumptions they rely on and what limitations have to be considered. The outcome of this chapter is the choice of the thermal comfort indices that will be used in this research.

3.1. Thermal comfort

3.1.1. Outdoor considerations on thermal comfort

Compared to indoor thermal comfort, outdoor thermal comfort is still challenging to be quantitatively described by researchers. This is due to the complexity of outdoor environments [16] and to the fact that people are directly exposed to local microclimate conditions [21].

The study conducted by Binarti et al. [17] is a review on outdoor thermal comfort indices for hot-humid regions. Hot and humid are key characteristics of humid tropical climates, but they can also be found in humid sub-tropical climates during summer. These two climates represent the climate of a large area of the world, in which more than 33% of the world's population lives. According to the study, the cities that are in these climates suffer the heat island effect twice as much as the others. These climates correspond to the following Koppen's climate classes: Cfa, Cwa, Af, Am, Aw.

According to Koppen's climate classification, Milan is classified as Cfa [45]. Therefore, in this research, since Milan summer conditions are analyzed, the considerations on hot-humid regions of the study of Binarti et al. [17] will be considered.

At the time when the review [17] was written (2020), about 162 human thermal comfort indices were produced, trying to best describe the thermal sensation. Some researchers highlighted the importance of developing regional outdoor thermal comfort indices (OTCI), because the validation for most comfort indices was made for European / American subjects living in cold climate. When the validation of the indices was made for people who lived in warmer areas, there was a disparity in the results [46]. However, a region-specific development of OTCI would not guarantee the required accuracy because many other factors play a role in it.

The study from Binarti et al. [17] reviewed the most frequently used outdoor thermal comfort indices for hot-humid regions in various studies, published in reputable peer-reviewed journals not older than 2007, and most of the papers were using the Physiological Equivalent Temperature (PET). Some of the reasons behind the choice of using PET mentioned in these studies are the availability of PET in various free software packages, and his inclusion in VDI (German Association of Engineers) guideline 3787.

Relatively few studies have been done on outdoor thermal comfort compared to those on indoor thermal comfort, due to the complexity of the former. Theoretically, the indices developed for the indoor environment can also be applied outdoor. However, the main challenge in using these indices in outdoor settings is that the climatic variables can differ significantly from the controlled indoor conditions under which they were developed [47].

One of the reasons for the research gap in studies correlating indoor and outdoor thermal environments is the lack of a common index used in indoor and outdoor thermal comfort studies [20]. An overview of the most used indices for thermal comfort, the models they employ and their application is provided in the following section.

3.1.2. Thermal comfort models and indices

Equivalent temperature is the most used type of model for thermal comfort and many popular indices are equivalent temperatures: PET, UTCI, SET*, and OUT_SET*. The equivalent temperature is defined as the air temperature of a typical indoor room in which a person would have the same physiological responses as in the real environment.

The primary distinction between the different equivalent temperatures lies in the human heat transfer model employed to calculate the physiological response [48]. These models, known as Human Thermoregulatory Models (HTM), simulate the heat exchange between the body and its surroundings and are used in many mechanism-based thermal comfort indices.

HTM are divided in (controlled) passive systems and (controlling) active systems. In the passive systems the human body is simulated, and the heat exchange between the human body and its environment is modeled, considering conduction, convection, radiation and evaporation. In the active systems, the human body's thermoregulatory mechanisms that are involved in keeping the thermal balance of the body are modeled. The HTM are classified based on how the human body is divided (nodes or elements) and how the temperature of the body parts are calculated. The human body in these models is divided into elements and the higher the number of elements, the higher the accuracy [17].

Fanger's model and the Predicted Mean Vote

Fanger's model is a one-node HTM. Since it is derived statistically, it is considered an empirical model. The Predicted Mean Vote (PMV) is a thermal index that employs Fanger's model.

Fanger developed a set of equations which were able to predict how many people in a room would be thermally dissatisfied [15]. He then conducted experimental studies in climate chambers with 1396 people, and the comfort equations were expanded to the Predicted Mean Vote (PMV) index. The PMV is an index that predicts the mean response of a large group of people in a scale that goes from -3 (cold) to +3 (hot). According to Fanger, a body is in steady-state thermal comfort if: (i) the body is in heat balance, (ii) mean skin temperature and sweat rate (which influence the heat balance) are within a certain range, (iii) no local discomfort exists [16]. Fanger's conceptual heat balance equation is:

$$H - E_d - E_{\text{sw}} - E_{\text{re}} - L = K = R + C \tag{3.1}$$

Where H is the internal heat production in the human body, E_d is the heat loss by water vapor diffusion through skin, E_{sw} is the heat loss by evaporation of sweat from skin surface, E_{re} is the latent respiration heat loss, L is the dry respiration heat loss, K is the heat transfer from skin to outer surface of clothing, R is the heat transfer by radiation from clothing surface and C is the heat transfer by convection from clothing surface + others. Each of these terms can be calculated from the six basic parameters [23].

The PMV is a widely used index for indoor thermal comfort and has appeared in the ASHRAE 55 standard since the 1992 edition [20].

In Fanger's model both the heat balance theories and the physiology of thermoregulation are employed to determine which range of temperature is considered comfortable. When the heat balance is maintained, a neutral thermal sensation could be achieved [18]. This model relates the thermal sensation of people to the unbalance in the comfort equation. However, a neutral sensation does not mean thermal satisfaction [15]. It is agreed by researchers that the PMV index perform better in environments controlled by AC systems, where the thermal neutrality can be created by artificial mechanisms. This makes the PMV index inadequate for naturally ventilated (NV) spaces and outdoor environments. The PMV is described by the following formula, which is determined from the heat balance equations [49]:

$$PMV = [0.303e^{(-2.1M)} + 0.028][(M - W) - H - E_c - C_{res} - E_{res}] \tag{3.2}$$

Where M is the metabolic rate in (W/m^2), W is the effective mechanical power in (W/m^2), H is the sensitive heat losses, E_c is the heat exchange by evaporation on the skin, C_{res} is the heat exchange by convection in breathing and E_{res} is the evaporative heat exchange in breathing.

In Equation 3.2 the terms H, E_c, C_{res}, and H_{res} are calculated from the following equations:

$$H = 3.96 \cdot 10^{-8} \cdot f_{cl} \cdot \left[(t_{cl} + 273)^4 - (t_r + 273)^4\right] - f_{cl} \cdot h_c \cdot (t_{cl} - t_a) \tag{3.3}$$

$$E_c = 3.05 \cdot 10^{-3} \cdot [5733 - 6.99 \cdot (M - W) - p_a - 0.42 \cdot ((M - W) - 58.15)] \tag{3.4}$$

$$C_{res} = 0.0014 \cdot M \cdot (34 - t_a) \tag{3.5}$$

$$E_{res} = 1.7 \cdot 10^{-5} \cdot M \cdot (5867 - p_a) \tag{3.6}$$

Where f_{cl} is the clothing surface area factor, t_a is the air temperature in (°C), p_a is the water vapor partial pressure in (Pa) and t_{cl} is the clothing surface temperature in (°C). The term of the clothing surface temperature is unknown a priori, and has to be calculated by an iterative process.

From the PMV Fanger elaborated an equation that predicts the percentage of people dissatisfied in a thermal environment. The equation for the Predicted Percentage of Dissatisfied (PPD) is the following 3.7:

$$PPD = 100 - 95e^{(-0.03353PMV^4 + 0.2179PMV^2)} \quad [\%] \tag{3.7}$$

Figure (3.1) shows the PPD plotted against the PVM.

It can be noted that even when the PMV is 0, there is still a 5% of dissatisfied.

Fanger's model has its limitation. Beside being accurate just for specific ranges of metabolism, clothing resistance, air temperature indoors, mean radiant temperature, air velocity and partial water vapor; there are other influential factors for thermal comfort which are not taken into account, such as: age, gender, illness, habits, climate or acclimation [15]. Moreover, it is suitable just for homogeneous, steady-state and uniform thermal environments, which are close to thermal neutrality [17].

One of the main Fanger's model's limitation is that it does not account for adaptation. If the ability to adapt to the environment is considered, the people's vote would change because they would accept environmental conditions outside of the comfortable range [15].

"If a change occurs as to produce discomfort, people react in ways which tend to restore their comfort." [50]

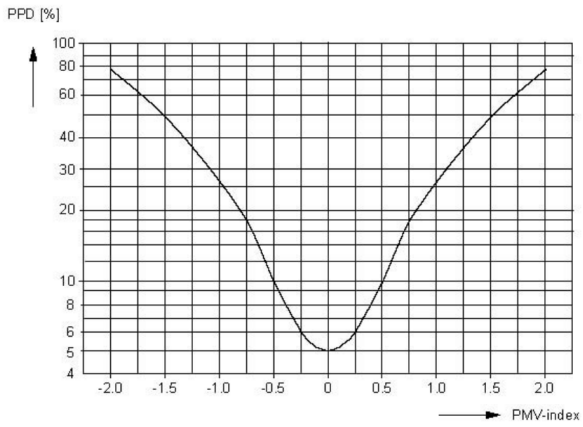

Figure 3.1: Predicted Percentage of people dissatisfied (PPD) against Predicted mean Vote (PMV) [15]

The adaptive approach uses statistical analysis on field surveys [16]. The aim of adaptive approaches is to observe the real acceptability of thermal environment. The adjustments that people can do are divided in three categories [51] :

- Behavior adaptation,
- Physiological adaptation,
- Psychological adaptation

Gagge's model and the Standard Effective Temperature

The one-node models are too simplistic when it comes to considering asymmetric boundary conditions and transient environment. This is why models with more than one node were developed. Gaggae's model is the most well-known two-node model. It models the human body as two different concentric nodes, the central one is the core node, and the external one is the skin node. It uses two different energy balance equations for each of the nodes. The Standard Effective Temperature (SET*) was developed using this model. Figure 3.2 shows a two-node model schematic diagram

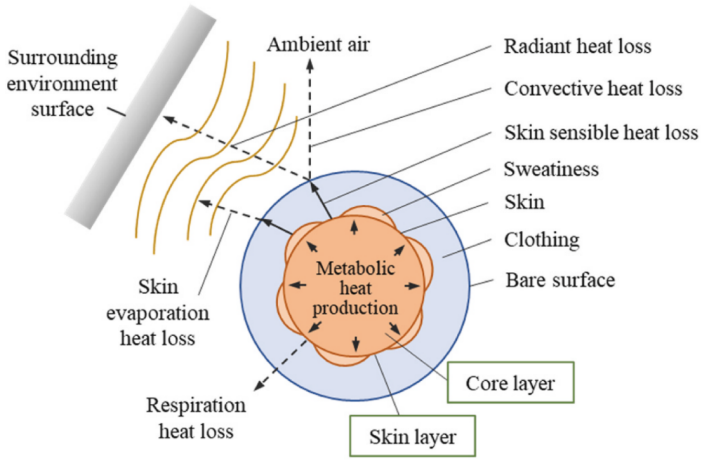

Figure 3.2: Two-node model schematic diagram by Ji et al. [52]

The heat balance equation for the core layer and the skin layer are the following [52]. Core layer:

$$M + \Delta M - W = C_{\text{res}} + E_{\text{res}} + (K + \rho_{bl} m_{bl} c_{bl})\,(T_{cr} - T_{sk}) + \frac{m_{cr}}{A_d} c_{cr} \frac{dT_{cr}}{d\tau} \tag{3.8}$$

Skin layer:

$$(K + \rho_{bl} m_{bl} c_{bl})\,(T_{cr} - T_{sk}) = Q_{sk} + \frac{m_{sk}}{A_d} c_{sk} \frac{dT_{sk}}{d\tau} \tag{3.9}$$

Where M, ΔM are the metabolic rate of human body and the metabolic rate increased by shivering in (W/m^2); W is the external work done by human body in (W/m^2); C_{res}, E_{res} are the respiratory sensible heat loss and latent heat loss in (W/m^2); K is the heat transfer coefficient from the core layer to the skin layer in $(W/(m^2°C))$; ρ_{bl} is the blood density in (kg/L); m_{bl} is the blood flow in $(L/(m^2 s))$; c_{bl}, c_{cr}, c_{sk} are the specific heat capacities of blood, core layer and skin layer in $(J/(kg°C))$; T_{cr}, T_{sk} are the core and skin temperature in $(°C)$; m_{cr}, m_{sk} are the mass of core layer and skin layer in (kg); A_d is the body surface area in m^2; is the time in (s); Q_{sk} is the skin heat loss in (W/m^2) [52].

The three parameters of the real environment Q_{sk}, T_{sk} and w can be obtained from the previous equations that describes the two-node model. A third equation in defined (Equation 3.10), based on the hypothesis that people would have the same Q_{sk}, T_{sk} and w in the SET standard environment and in the real environment. If these three values are the same, then the people have the same thermal sensation.

$$Q_{sk} = h_w\,(T_{sk} - T_o) + w h_e\,(P_{sk} - P_a) = h_{ws}\,(T_{sk} - \mathrm{SET}) + w h_{es}\,(P_{sk} - 0.5\,P_{sSET}) \tag{3.10}$$

Where h_w is the comprehensive heat transfer coefficient of convection and radiation in $(W/(m^2°C))$, wh_e is the comprehensive evaporation heat transfer coefficient in $(W/m^2 Pa)$, T_o is the operating temperature in $(°C)$, P_{sk} is the vapor pressure on the skin surface in (Pa), P_a s the saturated vapor pressure corresponding to the air temperature of T_a in $(°C)$, h_{ws} is the comprehensive heat transfer coefficient of the standard environment in $(W/(m^2°C))$, wh_{es} is the comprehensive evaporative heat transfer coefficient of the standard environment in $(W/(m^2 Pa))$, SET is the equivalent air temperature in $(°C)$, $0.5\,P_{sSET}$ is the steam pressure corresponding to SET and 50% relative humidity [53].

When the SET index was proposed, there was not a unified definition and description of it. For this reason, there is some confusion in the understanding of the SET standard environment condition. Ji et al. [52] summarized in Figure 3.3 the definitions found in some references, such as ASHRAE standard, ASHRAE handbook and Gagge's articles.

SET involves a steady-state clothing adaptation [54]. The clothing insulation in the standard environment depends upon activity level and follows the equation [23]:

$$I_{\mathrm{cls}} = 1.33/(Met - Wk + 0.74) - 0.095 \tag{3.11}$$

Where I_{cls} is the clothing insulation in the standard environment (Clo), Met is the metabolic rate and Wk is the mechanical work.

When considering convective and radiant heat exchange, SET* has a limited performance, making it an appropriate index only for indoor conditions [17]. Additionally, it applies physical parameters measured in stable conditions, which is not always a reasonable consideration when studying outdoor environments. In fact, OUT_SET* was later on developed for outdoor use, which implemented the radiative exchange in the model.

However, SET* is now the most appropriate thermal index for outdoor and indoor comparison because it has been widely used in literature for both thermal environments. SET* is the only thermal index that is commonly used in outdoors and indoors. A review from Potchter et al. [55] found that in warm and hot outdoor conditions SET* is an appropriate index. Even if it is widely used for both environments, it is important to note than SET* is an objective human thermal index. This means that to compare it with the thermal sensation, regression has to be applied. Other studies, like the one conducted by Jing et al. [56], found that when SET* was used in an outdoor environment, it constantly underestimated the thermal sensation, suggesting that the index was not fully capturing the thermal dynamics of the settings.

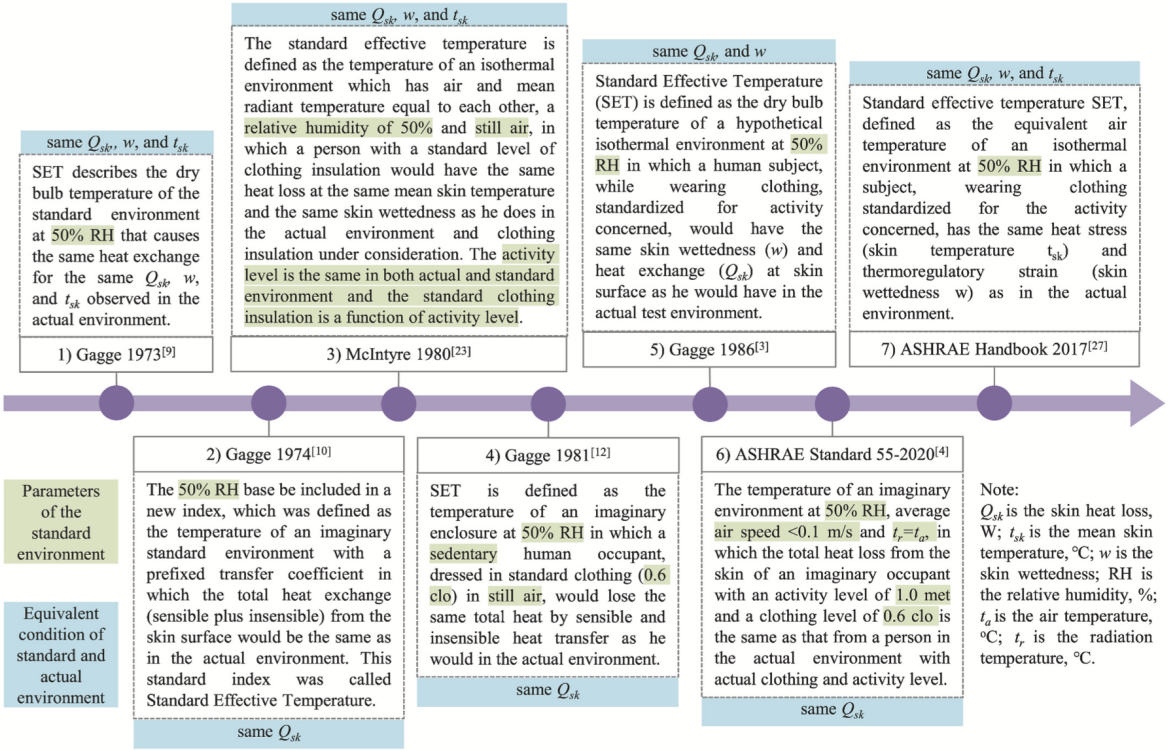

Figure 3.3: The evolution and difference of SET definition [52]

Munich Energy-Balance Model for individuals and the Physiological Equivalent Temperature

With similar theoretical background of Gaggae's model, Munich Energy-Balance Model for individuals (MEMI) was developed. The Physiological Equivalent Temperature (PET) is a real climatic index [57] which takes into account all basic thermoregulatory processes and is based on a thermophysiological heat balance model, the MEMI developed by Höppe. It is defined as "the equivalent air temperature at which, in a typical indoor condition heat balance of the human body exists (work metabolism 80 W of light activity, and clothing of 0.9 clo)" [58]. Even if PET is an index developed on virtual indoor conditions, it is used also in real outdoor conditions [47]. Its thermal scale can vary in relation to the climate and region, which is one of the reason that led researchers to chose this index over others [17].

The MEMI models the human metabolism as two concentric cylinders, the inner one representing the core, and the outer one representing the skin layer. The heat transfer from the core cylinder to the skin one occurs in parallel via conduction. It can be represented with an equivalent electrical scheme, as shown in Figure 3.4, according to Walther et al. [59].

According to Walther et al. [59], the method for solving the PET equation described in the VDI norm is presented in this section.

The model is described by three equations. Equation 3.12 balances the heat flux through clothing with the convection and radiation losses at the clothing surface.

$$\frac{T_{\mathrm{sk}} - T_{\mathrm{cl}}}{R_{\mathrm{cl}}} = h_c \frac{A_{\mathrm{cl}}}{A}(T_{\mathrm{cl}} - T_a) + \sigma \varepsilon_{\mathrm{cl}} f_{\mathrm{eff}} \frac{A_{\mathrm{cl}}}{A}\left(T_{\mathrm{cl}}^4 - T_{\mathrm{mrt}}^4\right) \tag{3.12}$$

Where T_{sk} is the skin temperature in (°C), T_{cl} is the clothing temperature in (°C), R_{cl} is the clothing

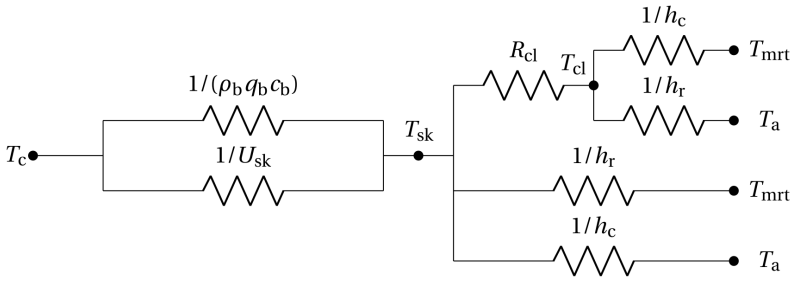

Figure 3.4: Equivalent electrical scheme for the steady-state heat transfer from core to skin; according to Walther et al. [59].

heat transfer resistance in (K/W), h_c is the convective heat transfer coefficient in (W/m^2K), A_{cl} is the clothed surface of the body in (m^2), A is the body surface after Dubois in (m^2), T_a is the temperature of ambient air in $(°C)$, σ is Boltzmann's constant in (W/m^2K^4), ϵ_{cl} is the emissivity of the clothes, f_{eff} is the factor for the effective surface subject to radiation and T_{mrt} is the mean radiant temperature [52] [60].

Equation 3.13 establishes a balance at the core node, equating the sum of metabolic rate and respiratory losses to the heat flux transferred from core to skin via conduction and blood flow through the skin layer.

$$M + Q_{\text{resp}} = (T_c - T_{\text{sk}}) \times \left(U_{sk} + \rho_b c_b \times \frac{q_b^{\text{set}} + C_d (T_c - T_c^{\text{set}})}{1 + C_s (T_{\text{sk}}^{\text{set}} - T_{\text{sk}})} \right) \tag{3.13}$$

Where M is the metabolic heat rate in (W/m^2), Q_{resp} is the sum of the heat exchanges by breathing in (W/m^2), T_c is the core temperature in $(°C)$, U_{sk} is the skin heat transfer coefficient in (W/m^2K), ρ_b is the blood density in (kg/m), c_b is the specific heat capacity of blood in (J/kgK), q_b^{set} is the set blood flow rate from blood to skin in (L/m^2h), C_d is the dilatation coefficient in (L/m^2hK), T_c^{set} is the core set temperature in $(°C)$, C_s is the striction coefficient in $(1/K)$ and $T_{\text{sk}}^{\text{set}}$ is the skin set temperature in $(°C)$.

The third equation 3.14 formulates a global steady-state balance on the body, considering metabolic activity, convection, radiation, sweating, diffusion losses and respiratory losses.

$$M + C + R + E_{\text{sw}} + E_{\text{diff}} + Q_{\text{resp}} = 0 \tag{3.14}$$

Where $C$and R are the convection and radiation on both the clothed and bare parts of the body, E_{sw} is the heat loss by sweating in (W/m^2) and E_{diff} is the heat loss by diffusion in (W/m^2).

Once the values of T_c and T_{sk} for the given environment are known, the model iteratively adjusts the air and clothing temperatures until Equation 3.14 reaches zero, yielding the PET as the resulting air temperature.

To reduce numerical complexity, Höppe's original code neglects the dependency between core and skin temperature with their environment. Specifically, environmental influence is considered only through the calculation of T_{sk}.

Several studies demonstrated the fitness of PET for hot-humid regions. The reason for this could be that it considers standard clothing and activity level, which is similar to the real conditions in these areas. It is indeed the most frequently used index in hot-humid regions [17]. Other reasons that led researchers to use PET are because it is one of the recommended indices in new German guidelines for urban and regional planners (VDI, 1998) and because it is available in a free software package [47]. PET assumes constant values for clothing and activity [57]. This could be a limitation of the

index, since it has to be adjusted to these subjective characteristics, but it is also a strength, since it guarantees the index to be independent of individual behavior and makes it more universal than other indices. A limitation of PET is that the variation in air humidity and clothing insulation have a small influence on the index. To overcome this limitation, the modified physiological equivalent temperature (mPET) was developed [61].

Fiala's model and the Universal Climate Index

Multi-nodes models were developed, with the aim of increasing their accuracy. Fiala's model is a multi-node model. In this model, heat exchange equations and blood circulation calculations are solved by using finite-difference method or Crank-Nicholson approach. In particular, the Fiala model is a 343-node multi-segment dynamic HTM.

The Universal Thermal Climate Index (UTCI) is an outdoor thermal comfort metric developed using Fiala's model, designed to encompass the human body's multivariate dynamic response to outdoor climatic conditions. The index uses a self-adaptive clothing model and an integrated physiological response [48]. The UTCI is defined as "the air temperature (Ta) of the reference condition causing the same model response as the actual condition" [62]. It can be expressed as the air temperature summed to an offset, which depends on the mean radiant temperature, the wind speed, and humidity:

$$\mathrm{UTCI}(T_a, T_r, v_a, p_a) = T_a + \mathrm{Offset}(T_a, T_r, v_a, p_a) \tag{3.15}$$

where T_a is the air temperature, T_r is the mean radiant temperature, v_a is the wind speed and p_a the water vapor pressure.

Figure 3.5 shows the derivation of UTCI for an actual climate condition, according to Bröde et al. [62].

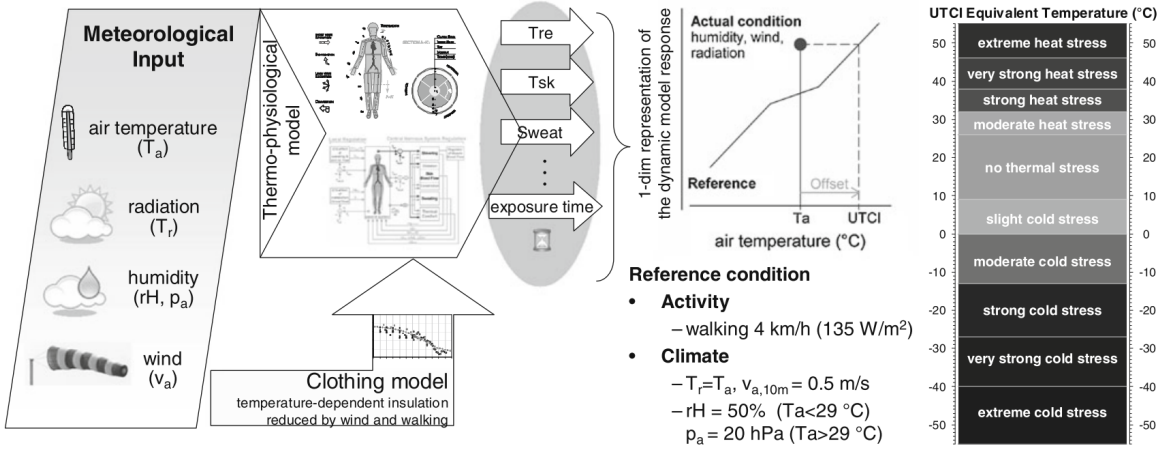

Figure 3.5: Concept of UTCI derived as equivalent temperature from the dynamic multivariate response of the thermophysiological UTCI-Fiala model (Fiala et al. [63]), which was coupled with a clothing model (Havenith et al. [64]) [62]

As shoown in Fiure 3.5, the UTCI values are obtained by combining Fiala's thermophysiological model and an adaptive cloting model. The actual conditions are then compared to the reference conditions, and the UTCI is obtained. The reference conditions are defined so that they can be representative for most scenarios and relevant across the climate zones where the UTCI is intended to be used. For this reason, the rate of metabolic heat production in the reference system is fixed at 2.3 MET ($135 W/m^2$), which correspond to a person walking with a speed of 4 km/h.
A key limitation of this index is that it has a restricted application to some extreme conditions [65]. Additionally, its validity can not be expanded in sports scenarios, as its assumptions on activity and clothing do not properly represent physically active individuals [66].

3.1.3. Comparison between thermal comfort indices

The physiologically equivalent temperature (PET), predicted mean vote (PMV), universal thermal climate index (UTCI), and standard effective temperature (SET*) are the four most commonly used thermal comfort indices [48]. Whether they can be used for outdoor or indoor comfort or both, depends on the way they were developed and on the physics behind the models that they employ. Table 3.1 shows the classification of thermal perception and physiological stress levels according to PMV, SET, PET, and UTCI indices.

Thermal perception	**Grade of physical stress**	**PMV (-)**	**SET* (°C)**	**PET (°C)**	**UTCI (°C)**
Very cold	Extreme cold stress	−4	< 10	< 4	< −27
Cold	Strong cold stress	−3	10–14.5	4–8	−27–−13
Cool	Moderate cold stress	−2	14.5–17.5	8–13	−13–0
Slightly cool	Slight cold stress	−1	17.5–22.2	13–18	0–9
Comfortable	No thermal stress	0	22.2–25.6	18–23	9–26
Slightly warm	Slight heat stress	1	25.6–30.0	23–29	26–32
Warm	Moderate heat stress	2	30.0–34.5	29–35	32–38
Hot	Strong heat stress	3	34.5–37.5	35–41	38–46
Very hot	Extreme heat stress	4	> 37.5	> 41	> 46

Table 3.1: Thermal perception and corresponding stress levels according to PMV, SET*, PET, and UTCI.

Table 3.2 shows a comparison between the main indices, where T_a stands for air temperature, T_r is the mean radiant temperature, RH the relative humidity and v the air velocity, according to Ji et al.[52], Höppe [57], Yau et al. [67], Binarti et al. [17].

Table 3.2: Comparison of PMV, SET*, PET, and UTCI

		PMV (-)	**SET* (°C)**	**PET (°C)**	**UTCI (°C)**
Model	**Approach**	Empirical	Rational	Rational	Rational
	Type	Based on thermal sensation votes of a group of people	Two-node model	Two-node model	Multi-node model
	Heat transfer	Static – steady-state	Static – steady-state	Static – steady-state	Dynamic – steady-state and transient
Physical variables		Ta, RH, Tr, v	Ta, RH, Tr, v	Ta, RH, Tr, v	Ta, RH, Tr, v
Personal variables		M and Icl	M and Icl adjusted by metabolic rate	Standardized sedentary activity (80 W; 0.9 clo)	M = 135 W/m² (walking speed 1.1 m/s); Icl automatically adjusted by Ta

	PMV (-)	SET* (°C)	PET (°C)	UTCI (°C)
Assumptions	Studies show that the PMV model underestimates thermal sensations due to steady-state assumptions made during laboratory experiments. Moreover, metabolic rate and clothing insulation values are derived from limited samples of people in controlled environments, leading to inaccuracies. Psychological and behavioral adaptations are not considered.	Assumes that the human body experiences the same thermal sensation when skin heat loss, skin temperature, and skin wetness remain constant. Ignores the influence of respiratory heat dissipation, which becomes significant at high metabolic rates. The correlation between heat loss and thermal sensation lacks systematic experimental validation.	Assumes steady-state conditions and uses fixed personal parameters: constant values for clothing and activity.	Implies the comparison with a standardized reference scenario that assumes a person walking at a fixed speed and metabolic rate. The clothing insulation is handled through an adaptive model based on ambient air temperature. Exposure duration is assumed to be two hours.
Limitations	Applies accurately only within specific metabolic ranges, clothing insulation, indoor air temperatures, mean radiant temperature, air velocity, and partial water vapor pressure. Other key factors affecting thermal comfort—such as age, gender, health status, habits, and acclimatization—are not included. Suitable only for homogeneous, steady-state, and uniform thermal environments close to neutrality.	Limited performance under changing convective and radiant heat transfer. Tends to overestimate skin temperature and underestimate skin wetness.	Weak sensitivity to variations in air humidity and clothing behavior, reducing its sensitivity in scenarios where these parameters are important. Fixed representation of activity and clothing.	it does not allow direct modifications to the metabolic rate or clothing insulation beyond its predefined adaptive functions. Furthermore, its performance in extreme climates may be compromised due to the simplified representation of individual variability and the fixed activity level.
Advantages	Simple to apply and interpret.	Allows direct use of observed values for clothing insulation and metabolic rate, adjusting clothing insulation to match activity levels.	Calculates all thermoregulatory processes. Capable of predicting real skin and core temperatures, sweat rates, and skin wetness.	Calculates all thermoregulatory processes and is highly sensitive to changes in air velocity and mean radiant temperature over time.

The four analyzed indices have similar physical background; they are all equivalent temperatures, all based on a Human Thermoregulatory Model. However, they rely on different assumptions, which brings the comparison to another level of complexity.

One could argue that a straightforward comparison of equivalent temperatures may overlook the variability of six key factors — air temperature, mean radiant temperature, air speed, relative humidity, metabolic rate, and clothing insulation — that directly influence thermal sensation and comfort [20]. For a direct comparison between indoor and outdoor equivalent temperatures, the sensitivity of each parameter used in the calculations would need to be the same, but this assumption is questionable due to the different thermal dynamics in indoor and outdoor environments.

Some studies propose SET* as the index that could bridge between the indoor thermal environments and the outdoor ones, but other researchers highlighted the drawbacks encountered when SET* was applied for outdoor settings.

3.2. Indices choice

The objective of this part of the thesis was to explore to what extent it is possible to compare indoor and outdoor thermal comfort studies. Four thermal comfort indices were examined, along with their assumptions, derivations, and limitations: the Predicted Mean Vote, the Standard Effective Temperature, The Physiological Equivalent Temperature and the Universal Thermal Comfort Index.

These were selected as they are among the most widely used indices in thermal comfort research.

Each index was analyzed individually, then it was investigated whether the literature had ever proposed using a single index for both indoor and outdoor thermal environments. SET* emerged as the only index frequently adopted in both contexts, appearing in several studies as a potential bridge between indoor and outdoor thermal environments. A review on SET* confirmed its suitability in warm and hot outdoor conditions. However, other studies reported that SET* tends to underestimate thermal sensation in outdoor environments.

Based on these findings, it is concluded that SET* is a good candidate for indoor-outdoor comparison, but that a multi-metric approach is ultimately necessary to grasp the full complexity of outdoor thermal comfort.

PET was selected as the reference outdoor index to be compared with SET*. This decision was based on evidence showing PET's accuracy in hot-humid regions, such as Milan during summer. This is likely because PET assumes standardized clothing and activity levels, which reflect the actual outdoor conditions in this study area.
It is important, however, to remain aware of the different assumptions behind these indices, in order to understand the limitations of this comparison. The differences are here listed, according to Walther et al. [59]:

- SET is defined as the air temperature in the standardized reference environment that would lead to the same skin temperature and degree of skin moisture as observed under the real environmental conditions. On the other hand, PET represents the air temperature in a comparable reference setting that reproduces the same combination of skin temperature and core temperature as that measured in the actual environment.

- In the standard reference environment, PET assumes a clothing insulation value of 0.9 [clo], whereas for SET, the clothing insulation is defined according to the activity level.

- SET is calculated with a transient calculation process, whereas PET can be determined under both steady-state and variable metabolic conditions [60].

Given the specific context of the present study, certain differences can be reasonably overlooked. The second difference listed above may be disregarded if normal light activity is studied. The third difference outlined above does not apply to this thesis, as both PET and SET* — given the tools employed for their computation in the present study — are determined under steady-state or steady-state equivalent conditions.

4

Parameters selection

This chapter presents a comprehensive literature review aimed at addressing the following research question: *"Which are the facade parameters, environmental parameters and urban geometry characteristics that influence thermal comfort indoor and outdoor?"*. An RC thermal model was made to fully understand all the parameters that play a role in the heat transfer through a facade. At the end of this chapter, relevant parameters are selected and a scenario planning for the simulations is provided.

4.1. Heat transfer through walls

Heat transfer through walls and ceilings of a house is a transient heat transfer problem, as outdoor conditions change constantly. The conditions inside a house are not so steady either. Therefore, it is almost impossible to perform a heat transfer analysis of a house accurately. This is why the problem is assumed to be steady-state. The heat transfer mechanisms through walls of a building is also assumed to be one directional, as the thermal gradient is significantly larger in one direction. Fourier's law of heat conduction for one-dimensional heat conduction is:

$$\dot{Q}_{cond} = -kA\frac{dT}{dx} \tag{4.1}$$

The rate of change of the energy content in a large plane wall is given from the rate of heat conduction at x, minus the rate of heat conduction at $x + \Delta x$ plus the rate of heat generation inside the wall. For this problem we assume no heat generation. In formulas, that is:

$$\dot{Q}_x - \dot{Q}_{x+\Delta x} = \frac{\Delta E_{element}}{\Delta t} \tag{4.2}$$

The rate of change of the energy content of the wall can be re-wrote as:

$$\Delta E_{element} = E_{t+\Delta t} - E_t = mc(T_{t+\Delta t} - T_t) = \rho cA\Delta x(T_{t+\Delta t} - T_t) \tag{4.3}$$

Substituting in equation 4.2:

$$\dot{Q}_x - \dot{Q}_{x+\Delta x} = \rho cA\frac{T_{t+\Delta t} - T_t}{\Delta t} \tag{4.4}$$

Dividing by $A\Delta x$:

$$-\frac{1}{A}\frac{\dot{Q}_x - \dot{Q}_{x+\Delta x}}{\Delta x} = \rho c\frac{T_{t+\Delta t} - T_t}{\Delta t} \tag{4.5}$$

Taking the limits for $\Delta x \to 0$ and $\Delta t \to 0$ and substituting with Fourier's law (equation 4.1):

$$\frac{\partial}{\partial x}(k\frac{\partial T}{\partial x}) = \rho c\frac{\partial T}{\partial t} \tag{4.6}$$

Assuming the conductivity to be constant, it can be taken out of the derivative. The equation becomes:

$$\frac{\partial^2 T}{\partial x^2} = \frac{1}{\alpha}\frac{\partial T}{\partial t} \tag{4.7}$$

Where α is the thermal diffusivity, assumed as $\alpha = \frac{k}{\rho c}$.

At the beginning of the derivation, the assumption of steady-state was done, meaning that there is not change of temperature in time (i.e. $\frac{\partial T}{\partial t} = 0$). The simplified one-dimensional heat conduction equation for steady-state conditions becomes:

$$\frac{\partial^2 T}{\partial x^2} = 0 \tag{4.8}$$

This simplified heat conduction equation was developed using energy balance on a differential element inside the medium and no information are given on the conditions on the surface by the equation itself [68]. Being equation 4.8 a second order differential equation, to have a unique solution two more mathematical expressions need to be known. These are the boundary and initial conditions and express the conditions at the boundaries of the problem. Boundary conditions can be specified temperatures at the boundary or specified heat fluxes.

Convection represents a heat flux boundary condition derived from the surface energy balance, where the heat conducted through the surface in a given direction equals the convective heat flux at the surface in that direction. Similarly, radiation can serve as a heat flux boundary condition: in the absence of convection, the heat conducted at the surface in a given direction is balanced by the radiative exchange in the same direction. In real cases, both convection and radiation happen, and the general rule follows an energy balance as well. It can be expressed as: the heat transfer to the surface in all modes is equal to the heat transfer from the surface in all modes.

As demonstrated before, $\dot{Q}_{in} - \dot{Q}_{out} = 0$ for steady-state, meaning that $\dot{Q}_{cond,wall}$ is constant. Taking Fourier's law (equation 4.1) if the thermal conductivity k is assumed constant, A is constant and $\dot{Q}_{cond,wall}$ is constant, this means that also $\frac{dT}{dx}$ is constant. This implies a linear variation of T in x. In steady-state conditions, in a one-dimensional problem, the temperature varies linearly in space. If the integral of Fourier's law is taken:

$$\int_{x=0}^{L} \dot{Q}_{cond,wall} dx = -\int_{T=T_1}^{T_2} kA dT \tag{4.9}$$

$$\dot{Q}_{cond,wall} = kA\frac{T_1 - T_2}{L} \tag{4.10}$$

$$\dot{Q}_{cond,wall} = \frac{T_1 - T_2}{R_{wall}} \tag{4.11}$$

Where R_{wall} is the conduction resistance defined as $R_{wall} = \frac{L}{kA}$.

Equation 4.11 represents the rate of heat conduction through a plane wall, which is proportional to the thermal conductivity, the wall area, and the temperature difference, while is inversely proportional to the wall thickness [68]. This equation is analogous to the equation for electric current flow I, expressed as:

$$I = \frac{V_1 - V_2}{R_e} \tag{4.12}$$

Where $R_e = \frac{L}{\sigma_e}$ is the electrical conductivity and $V_1 - V_2$ is the voltage difference across the resistance. Thus, the rate of heat transfer through a layer corresponds to the electric current, the thermal resistance corresponds to electrical resistance, and the temperature difference corresponds to voltage difference across the layer [69].

Convection resistance

Considering Newton's law of cooling for convection heat transfer rate $\dot{Q}_{conv} = hA_s(T_s - T_\infty)$, it can be rearranged as:

$$\dot{Q}_{conv} = \frac{T_s - T_\infty}{R_{conv}} \tag{4.13}$$

where

$$R_{conv} = \frac{1}{h_{conv}A_s} \tag{4.14}$$

is the thermal resistance of the surface against heat convection, or convection resistance. The parameter h_{conv} is called the convection heat transfer coefficient, and in this chapter this terminology will be used:

$$h_{conv}A_S = h_c \tag{4.15}$$

Radiation resistance

In real cases, the surface is in contact with the air, meaning that there will be radiative effects of significative importance. The rate of radiation heat transfer of a surface can be expressed as:

$$\dot{Q}_{rad} = \epsilon\sigma A_s(T_s^4 - T_{surr}^4) = h_{rad}A_s(T_s - T_{surr} = \frac{T_s - T_{surr}}{R_{rad}}) \tag{4.16}$$

where

$$R_{rad} = \frac{1}{h_{rad}A_s} \tag{4.17}$$

is the thermal resistance of a surface against radiation, or the radiation resistance. The radiation heat transfer coefficient is defined as:

$$h_{rad} = \epsilon\sigma(T_s^2 + T_{surr}^2)(T_s + T_{surr}) \tag{4.18}$$

In this chapter, this terminology will be used:

$$h_{rad}A_s = h_r \tag{4.19}$$

The definition of a radiation heat transfer coefficient and a convection heat transfer coefficient is convenient to express both in terms of a temperature difference. However, while the radiation heat transfer coefficient is highly influenced by the temperature, the convection heat transfer coefficient is usually not. In real cases, convection and radiation occur simultaneously at the surface and they both determine the total heat transfer at the surface. The convection and radiation resistances are parallel to each other.

4.1.1. Thermal Model

To represent the heat transfer mechanisms through the facade and to comprehensively account for the variables involved, an RC thermal model is developed (Figure 4.1). It is composed of: nodes, resistances, capacitances and external inputs. The nodes (i.e. boundary conditions) are: T_{sky}, $T_{air,ext}$, $T_{s,ext}$, T_1, $T_{s,int}$ and T_z. T_{sky} represents the effective temperature of the sky, used in the model for longwave exchange with the sky. $T_{air,ext}$ is the outdoor air temperature, also used as an approximation for the temperature of the surrounding surfaces. $T_{s,ext}$ is the temperature at the external surface of the facade. T_1 is the temperature at the boundary between the cladding and the wall core. $T_{s,int}$ is the temperature at the internal surface of the facade. T_z is the indoor air temperature, or zonal temperature, inside the room. The resistances are of four types: $1/h_r$, $1/h_c$, R, $1/U_{win}$. The convective thermal resistance (i.e. $1/h_c$) is characterized by h_c, the convective heat transfer coefficient. It describes how easily heat is transferred from a surface to the surrounding air when

there is a temperature difference. The linearized radiative thermal resistance (i.e. $1/h_r$) depends on h_r which is the radiative heat transfer coefficient. The coefficient is described by equation 4.18 and represents the easiness of the heat transfer from a surface to air via radiation. R is the thermal resistance of wall layers. It depends on the material's thermal conductivity and thickness. The last resistance is $1/U_{win}$, which is the resistance of the window. U_{win} is the U-value and describes the rate of transfer of heat through the glazing. A lower U-value means better insulation. The capacitances (i.e. $C_{s,ext}$, C_1, $C_{s,int}$, C_z) represent energy storage (i.e. heat accumulation) points in the model. There is a capacitance for every internal node of the model, because it is where heat accumulates. It depends on the density of the material, its specific heat, its thickness and area. A higher C means greater thermal inertia. The external inputs of this model are: Q_{sol}, Q_g, Q_{int}, Q_{sens}. Q_{sol} is the solar heat gain, which is just a portion of the total incoming solar radiation. Q_g is the g-value, which is the sum of the direct transmission and the secondary radiation passing through the glazing. Q_{int} is the internal heat gains due to occupants, appliances, lighting. Q_{sens} is the sensible heat, and represent the convective portion of the internal heat gain that directly heats the indoor air.

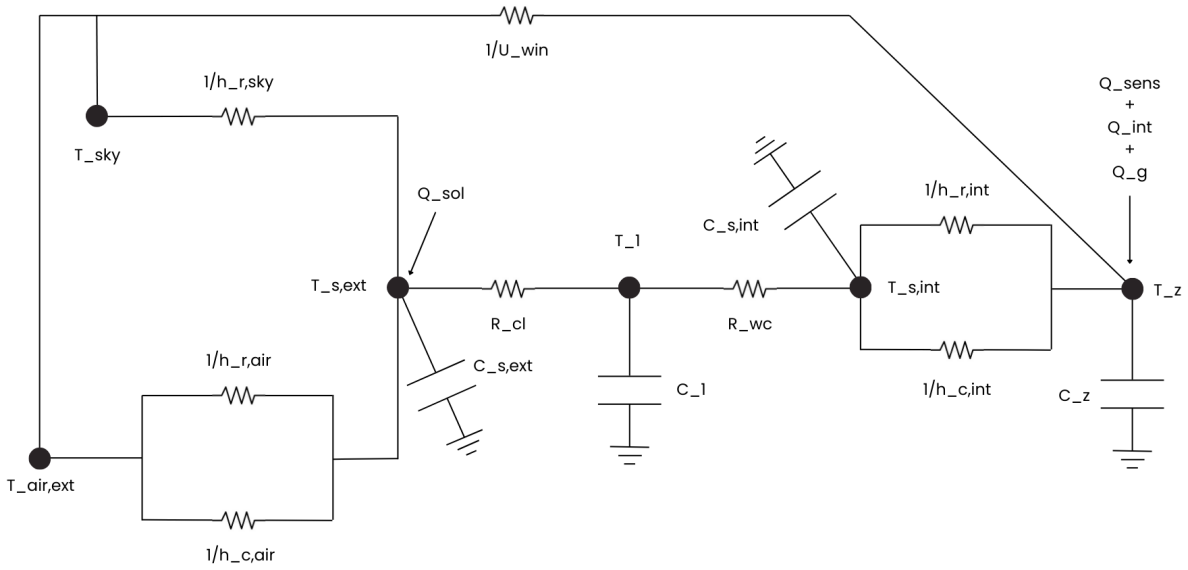

Figure 4.1: RC thermal model

In Table 4.1 the input and elements of the model are grouped. Their formulas are shown, and environmental parameters, facade parameters and urban characteristics that influence them are mentioned.

Table 4.1: Thermal RC model inputs and elements, formulas, and influencing parameters

Model Inputs and Elements	Name	Formula	Environmenta Parameters	Façade Parameters	Urban Characteristics	Model Role
Q_sol	Solar heat gains	$Q = n \cdot G_{tot}$, with $n = \alpha$ (opaque) or τ (glazing)	G_{tot} (solar radiation)	Absorptance α, Transmittance τ, Reflectance ρ	SVF, orientation, tilt, H/W ratio	Heat flux (input)
Q_g	G-value	$Q_g = g \cdot G_{tot} \cdot A_{win}$	G_{tot}	G-value g, window area A_{win}	SVF, orientation, tilt, H/W ratio	Heat flux (input)
h_conv,i	Convective heat transfer coefficient	$Q = h_{conv} \cdot (T_{surf} - T_{air})$	Wind speed, $T_{air,ext}$, T_z	Surface roughness	Surface orientation, H/W ratio	Thermal resistance
h_rad,i,i	Radiation heat transfer coefficient	$Q = h_{rad} \cdot (T_{env} - T_{surf})$	T_{sky}, $T_{air,ext}$, T_z	Emissivity ε	SVF, H/W ratio, surface orientation	Thermal resistance
R_i	Wall thermal resistance	$R = \delta / k$	—	Wall thickness δ, conductivity k	—	Thermal resistance
$1/U_{win}$	Window thermal resistance	$Q = (T_{ext,win} - T_z)/(1/U_{win})$	—	U-value of glazing	—	Thermal resistance
C_i	Thermal capacity	$C = \rho \cdot c \cdot \delta \cdot A$	—	Density ρ, specific heat c, thickness δ	—	Thermal capacitance
T_i	Temperature	—	—	—	—	Temperature node (boundary condition)

In the next sections, the facade parameters and urban characteristics that were identified as influential for the heat transfer mechanism will be explained in detail.

4.1.2. Façade parameters

From the thermal model, facade parameters that play a role in the heat transfer through walls are identified. They will be discussed in this section with regard to their impact on thermal comfort.

It is widely recognized that surface properties of facades impact thermal performance of buildings and play a role in pedestrian comfort [70]. Figure 4.2 represents a scheme of the energy budget of the building facade. I_s represents the short-wave incident radiation, α is the facade reflectance, Φ_H is the convective heat exchange between the air and the facade, Φ_L is the long-wave radiation exchange and Φ_{st} is the heat storage [71].

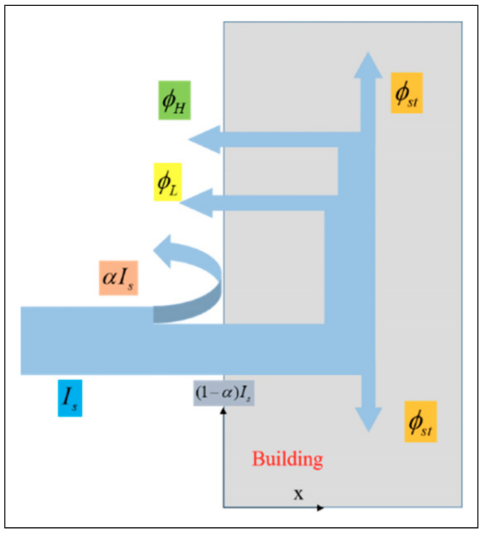

Figure 4.2: Facade energy budget (according to [71])

Reflectance and albedo

In this section, with the term *reflectance* is meant wavelength-specific reflection properties of materials, while the word *albedo* describes the overall reflective behavior of surfaces across the solar spectrum.

Studies have shown that a reflective facade reduces the solar heat gain, but increases the surrounding outdoor air temperature [8]. A study conducted by Tabatabaei et al. [12] investigated the thermal performance of twenty samples of facade materials and concluded that materials with higher reflectance are shown to have higher Mean Radiant Temperature in the surrounding outdoor air. There is a direct relationship between albedo and thermal comfort: high albedo facades decrease outdoor thermal comfort in summer and improve it in winter [19]. Also reflection directional characteristics of facades has been studied, but they were found to have little effect on the outdoor thermal environment [9]. In summary, the use of high albedo facade materials have a double effect: on one hand, it lower the indoor Operational Temperature (OT), on the other hand it increases the Mean Radiant Temperature (T_{mrt}), adversely affecting pedestrian comfort [2].

Darker colored facade have a high absorption [14], which causes the increase of the external surface and air temperature. Conversely, bright colored facade have lower external surface and air temperature [8] [12]. The study conducted by Ata Chokhachian et al. [19] demonstrates that dark materials end up in less Mean Radiant Temperature values than brighter ones. The comparison of the T_{mrt} is made with two test points located at pedestrian height in the canyon. This happens because more heat is absorbed, therefore there is less heat reflected back into the canyon.

Emissivity

Emissivity represents the ability of a material to absorb and release long-wave radiation[71]. Researchers have observed that a facade with lower emissivity corresponds to a lower T_{mrt}, which means a better outdoor thermal comfort [12]. The high emissivity is favorable to lower the surface temperature during night-time [8]. While reflectance predominantly influences facade performance during daytime, emissivity becomes the more critical factor during nocturnal hours [71]. Some typical emissivity values for facade materials according to Albatici et al. [72] are displayed in Table 4.2.

Thermal mass

Thermal mass (TM [J/K]) is defined as "the ability of a building component to store heat while experiencing a temperature change" [73]. The thermal mass of an element depends on its volume

Table 4.2: Thermal emissivity of some building materials [72]

Material	Emissivity (ϵ)
Fiber-reinforced concrete	0.94 - 0.95
Plasterboard	0.92 - 0.93
Brick	0.93 - 0.95
Aluminum	0.2 - 0.4
Steel	0.4 - 0.6

and its volumetric heat capacity (VHC) [73]. It can be described as:

$$TM = V \cdot VHC \tag{4.20}$$

The VHC $[J/m^3K]$ is the ability of a volume of material to store internal energy under a given temperature difference. It can be derived by multiplying the density ρ $[kg/m^3]$ of an element by its specific heat c $[J/kgK]$.

$$VHC = \rho \cdot c \tag{4.21}$$

Studies have shown that heavyweight (HW) materials (e.g. concrete, asphalt) and lightweight (LW) materials (e.g. sandwich walls) have a different thermal performance because of their diverse thermal mass. Thermal mass is defined as the capacity of a material to absorb, store (ΔQ_S) and release heat. A high thermal mass means a big delay in heat transfer and lower speed of the heat flux to go from the outside to the inside [12] (and viceversa). Heavyweight materials' facade help stabilizing the indoor temperature, because they store heat during the day and release it in the afternoon period [8]. However, when releasing heat, the envelope materials modify local ambient air [25] increasing the UHI phenomenon.

Surface temperature

Surface temperature is a key factor in the present research. The surface transfers heat by convection to the surrounding air and by conduction to the inside of the building. When considering surface temperature, it is important to distinguish between the external surface temperature and the internal surface temperature. Researchers have compared the air temperature and the external surface temperature and have found a direct relationship [12]. A cooler surface temperature could reduce heat reflection to the nearby environments, providing a better outdoor thermal comfort [74]. The most influential factors of facade materials that impact external surface temperature are found to be: solar reflection, emissivity and heat capacity [12]. The results of conducted studies show that W/E canyons present higher external surface temperatures than S/N ones Camporeale and Mercader-Moyano [25].

4.1.3. Urban morphology and geometry

Built environments are known as climate modifiers, because urban morphology influences microclimate parameters such as: direct and indirect solar radiation, air temperature, Mean Radiant Temperature, relative humidity and wind speed and direction [19]. Therefore, in the assessment of pedestrian comfort, considering the spatial arrangements of buildings and landscapes is essential. The *urban canyon* is defined by Oke as the "basic geometric unit which can be reasonably approximated by two-dimensional cross-sections, neglecting street junctions, and assumes that buildings along the canyon axis are semi-infinite in length." [13].

Aspect ratio and sky view factor

The aspect ratio is defined as "the ratio between the average height (H) of the canyon walls and the canyon width (W)" [3]. A higher aspect ratio corresponds to a lower daytime air temperature and a higher nighttime air temperature [13]. This happens because during the day a high H/W ratio means higher shading, therefore less solar radiation entering the canyon. While, during the night-time, a higher H/W ratio corresponds to a slower cooling of the canyon because the heat remains "trapped" inside it.

The Sky View Factor (SVF) is defined as “the ratio of the amount of the sky which can be seen from a given point on a surface to that potentially available" [3]. The obstacles that obstruct the sky sight are buildings and vegetation. SVF and H/W ratio are directly related [13]. Low SVF traps inside the canyon long-wave radiation and decelerates the cooling of the street canyon during night-time.

Street orientation

The street orientation is a fundamental parameter when studying outdoor thermal comfort because the orientation of a canyon defines the solar access inside it and the wind speed. The E / W canyons are found to be the most problematic for pedestrian thermal comfort [13].

4.2. From parameters selection to scenario planning

This section outlines the parameters chosen for analysis in the present study. The relationship between these parameters and the indoor and outdoor environment will be further analyzed in the next chapters. A structured workflow for the simulations will be established.

The thermal model adopted in this chapter to describe the thermal behavior of a facade consists of: nodes, resistances, capacitances and external inputs. All these elements form an energy balance system, whose behavior is influenced by three factors:

- The structure of the model
- The values of the model’s elements (nodes, resistances, capacities)
- The values of the inputs of the model

With model structure is intended the way in which the elements are organized and connected. For example, for a cavity wall, an extra air layer has to be inserted in the wall composition, thus altering the model’s structure and its thermal behavior over time. The values of the model elements refer to the material properties of every component such as thermal resistance, thermal capacity, surface emissivity, and reflectance.

The parameters involved in the model can be grouped as follows:

- **Environmental parameters**
  - $T_{\text{air, ext}}$: external air temperature
  - T_{sky}: sky temperature
  - Q_{sol}: solar heat gain
  - v: wind speed
- **Façade parameters**
  - R: thermal resistance of each layer
  - C: thermal capacitance of each layer
  - ε: surface emissivity
  - ρ: solar reflectance
  - α: solar absorptance
- **Urban geometry characteristics**

- H/W ratio: aspect ratio
- SVF: sky view factor
- Orientation

4.2.1. Scenario planning

The aim of this section is to define a limited and clear set of parameters whose impact will be studied. The tested parameters are limited in order to have semi-controlled simulations and to better assess the effect of every parameter. From the list of parameters presented in the section above, just a subset was selected for the simulation scenarios. The selection was guided by two main criteria: (i) relevance to retrofit strategy, (ii) feasibility of change implementation in the thermal model and in ENVI-met. The elements that will vary across the simulation scenarios can be grouped into:

1. Model parameters:

- Aspect ratio (H/W)
- Reflectance (ρ) and emissivity (ε)

2. Model configurations:

- Insulation position

In order to isolate and evaluate the influence of specific facade and urban geometry parameters on thermal comfort, a matrix of simulation scenarios is defined based on two different urban geometry (H/w ratio) and five different configurations (i.e. external insulation, internal insulation, cool facade, and combined scenarios). The simulation matrix is shown in Table 4.3.

Table 4.3: Simulation matrix combining facade strategies with two urban geometry configurations.

Facade Strategy	**Urban Case A** (Large H/W)	**Urban Case B** (Small H/W)
Cool Facade	A1	B1
External insulation	A2	B2
Internal insulation	A3	B3
Cool Facade + External insulation	A4	B4
Cool Facade + Internal insulation	A5	B5

5

Case study

In this chapter, the Acquabella district will be analyzed and a focus area within the neighborhood will be selected. Once the street canyon of interest is found, the buildings in the street will be studied and clustered. This step is essential to optimize the simulation time, and to do informed simplifications when needed in the models.

5.1. Introduction

The Acquabella district is a neighborhood located in the east side of Milan, Italy. Milan is one of the most densely populated metropolitan areas in Europe, facing challenges related to rapid urbanization and heat island effect. The primary stakeholders of this research are the residents of the district, who are directly affected by the thermal comfort of their district, especially pedestrian comfort, and are interested in developing and proposing strategies to improve living conditions in the district. The particularities of the case that are relevant for the research project are the urban morphology and architectural features that characterize Acquabella district, but also the initiative, interest and participation of the residents in projects that aim to better the district's quality of life. The simulations will be done in a selected area of the district, making the case study not only a relevant example for the thesis project, but a practical application of façade-focused strategies for improving indoor and outdoor comfort. The academic relevance of the case is providing a real life case to work on to contribute on the ongoing research of adaptation strategies to heatwaves and façade retrofitting for thermal comfort.

5.2. Site analysis

This section applies the Local Climate Zone (LCZ) classification to the Acquabella district. The use of LCZs provides a standardized framework that ensures comparability across studies and geographic contexts, supporting the systematic integration of urban climate data into planning and design processes.

Local Climate Zone

The Local Climate Zone (LCZ) have been adopted as a description of global urban areas into recognisable types. There is a distinction between 10 urban land-use classes (LCZ1-10) and 7 rural classes (LCZA-G). Having a clear classification gives consistency between studies, and even regions. In addition, it provides urban weather models with greater surface accuracy and it facilitates the integration of urban climate knowledge with urban planning. However, the LCZ has some drawbacks. It is still quite generic and there is no information on specialized topography, climatology, building materials etc. There are no clear limits of each class: it is not clear when one LCZ ends, therefore classes can blend into each other. There could be internal variability in one zone which is not clear how to address [3].

The *World Urban Database and Access Portal Tools* (WUDAPT) provides open access to the LCZ maps generated by users using the LCZ Generator. For every map, a certain overall accuracy ($0 \leq OA \leq 1$) is displayed. According to Bechtel et al. [75], the accuracy of the LCZ maps generated via WUDAPT is obtained via an automated cross-validation approach, that uses 25 bootstraps. A random sampling scheme is applied to estimate accuracy from a given sample. From this data sample, 70% of the Training Area (TA) polygons are used for the training and the remaining 30% for the testing. The process is repeated 25 times, where the sample is re-organized into training and testing. However, a high accuracy does not necessarily mean that the map is correct. This can be attributed to one or more of the following reasons:

- The accuracy assessment is only performed on the pixel that are contained in the TA polygons, meaning that outside of the TA the accuracy is not guaranteed;
- TA polygons can be inaccurate due to human error;
- Inadequate differentiation of LCZ types in the training sample can result in an artificially high OA.

According to Demuzere et al. [76] other accuracy measures are used in addition to the OA:

- OA_u: overall accuracy for the urban LCZ classes only;
- OA_{bu}: overall accuracy for the built versus natural LCZ classes only;
- OA_w: weighted accuracy;
- $F1$: class-wise metric, which is a harmonic mean of the user's and producer's accuracy.

There are 10 available LCZ maps for the city of Milan. The Overall Accuracies range from 0.35 to 0.72. The three maps with the higher OA will be compared to investigate the LCZ classification of the Acqubella district.

The LCZ map for the city of Milan with the highest OA is the map generated by Haotian Wu the 7/12/2021, which has an OA of 0.72. According to Figure A.1 and Figure A.7, the LCZ of the Acquabella district is LCZ 3. The second analyzed LCZ map is the map generated the 19/12/2023 by an unknown user. The OA of the map is 0.71 and according to it (Figure A.3) the LCZ of the district is 3 and 5. The third analyzed LCZ map is the map generated the 11/12/2021 by Haotian Wu. The OA of the map is 0.69 and according to it (Figure A.5) the district Acquabella is LCZ 3. Local Climate Zone 3 correspond to compact lowrise, while Local Climate Zone 5 to open midrise [77]. A comparative analysis of the accuracies of the three LCZ maps is conducted to determine the most reliable one for reference.

	date	author	OA	OA_u	OA_{bu}	OA_w
Map 1	07/12/2021	Haotian Wu	0.72	0.77	0.91	0.92
Map 2	19/12/2023	-	0.71	0.67	0.99	0.94
Map 3	11/12/2021	Haotian Wu	0.69	0.74	0.89	0.90

Table 5.1: Accuracy metrics for the different maps

From the results it seems like map 1 and 3 have a higher accuracy in describing the urban classes (OA_u), while map 2 describes better the differences between the natural and built classes (OA_{bu}). The weighted accuracy OA_w is obtained by applying weights to the confusion matrix and accounts for dissimilarities between LCZ types. In calculations, it penalizes confusion more in dissimilar types than on similar types [76]. In this analysis, OA_u is likely more relevant than the other metrics, being the uncertainty in classifying Acquabella between class 3 and class 3 and 5, which are urban classes. However, also the F1 metrics have to be compared, as they provide insight into the accuracies of each LCZ class.

The F-score is the (weighted) harmonic average of precision and recall, where precision is defined as the probability that an object is relevant given that it is returned by the system, while the recall

is the probability that a relevant object is returned [78]. In this case, the F1 metric represents the accuracy of every single LCZ class separately, considering the user's and producer's accuracy. The F1 metric boxplots are provided in the factsheets of the maps, and are shown in Figure A.2 for map 1, Figure A.4 for map 2 and Figure A.6 for map 3. Comparing the boxplot visualizations, it is clear that the map with the highest F1-score for class 3 and 5 is the second map. The F-score of the other two maps for the relevant classes of this study are not even comparable with the F-score of map 2. For this reason, in this research the second map will be consider the relevant one for the Acquabella district in Milan.

In conclusion, the Acquabella district in Milan can be classified as Local Climate Zone 3 and Local Climate Zone 5, which represent, respectively, compact lowrise and open midrise.

5.3. Selection of the study area

For this research, a focus area within the district has to be determined, due to the limited computational time of the project.

Thanks to dr. Colaninno who provided the UTCI maps of the district for July 22, 2022, it was possible to conduct an analysis of the thermal performance of different streets during a the hottest day of a heatwave. A total of 24 hourly maps were available for that day. Two criteria were applied to identify the most critical street canyon:

- Streets that exhibit the highest UTCI values across the entire dataset;
- Streets that exceed a selected UTCI threshold for the longest duration throughout the day.

The outcomes of each criterion will be presented in this section, and the final selection of the focus area will be made based on a comparison of the results.

Peak UTCI values

To identify the street canyons that exhibit the highest values of UTCI across the entire dataset, the map with the highest peak (i.e. 14:00) was selected and the analysis was conducted only on that map. The latter is shown in Figure 5.1.

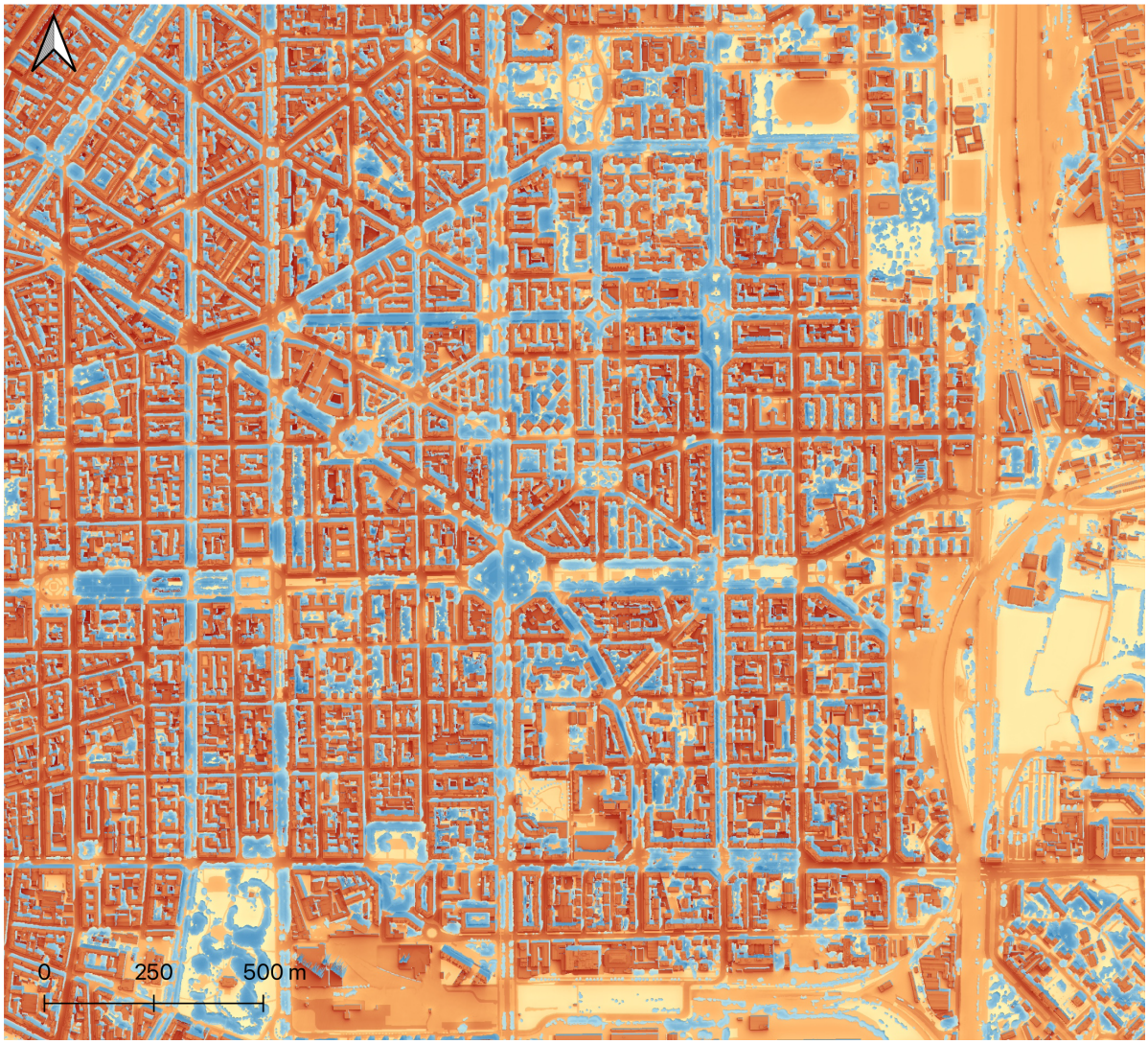

Figure 5.1: Acquabella UTCI map for the 22nd of July 2022 at 14:00

OpenStreetMap was used to import the streets of the area in QGIS. A zonal statistic analysis was conducted filtering the streets just for: 'footway', 'pedestrian', 'cycleway' and 'residential', since the main goal is to analyze pedestrian comfort. Other streets like 'highway' or 'service' were excluded from the analysis. For the analysis a buffer distance of 10m was considered, so that both the lanes and the pathways of the streets were considered. The results show that in certain areas the UTCI values are greater than 40°C. The results for the zonal statistic analysis were filtered and the segments with a mean UTCI value above 44°C were filtered. These segments can be seen highlighted in green in Figure 5.2.

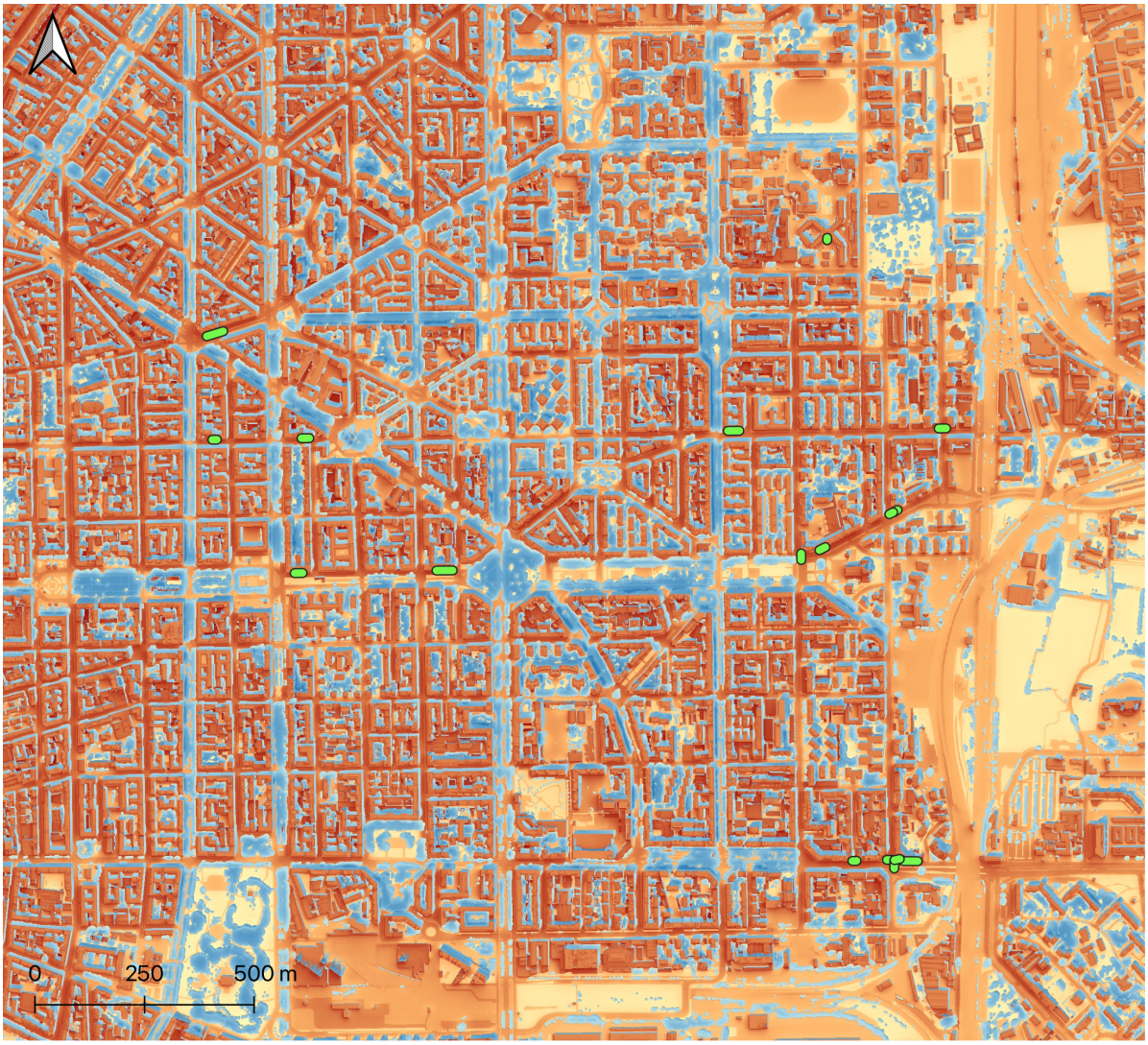

Figure 5.2: Highlighted segments with UTCI > 44°C

The segments of streets which present peak UTCI values correspond to: via Gustavo Modena, Corso Plebisciti, via Giovanni Antonio Amadeo and via Ferdinando Marescalchi.

Hourly exceedance of UTCI threshold

To identify the street canyons that exceed a selected UTCI threshold for the longest duration throughout the day, two different threshold were chosen: UTCI = 32°C and UTCI = 38°C. These two temperatures represent a threshold value in the stress category for the UTCI: from 32°C onward the stress category is "strong heat stress" and from 38°C onward the UTCI falls into the category of "very strong heat stress". To identify the worst street canyons, binary rasters were generated in QGIS for each hour of the day, where cells with UTCI higher than the threshold were assigned a value of 1, and 0 elsewhere. The hourly rasters were then summed to produce a cumulative raster representing the number of hours above the threshold throughout the day. This process was repeated for the two threshold values. A zonal statistics analysis was then performed, calculating the mean value for each street segment. These mean values indicate the number of hours, on average, during which each street segment experiences UTCI values above the selected threshold. The maximum mean value observed for UTCI > 32°C was 13 hours, while for UTCI > 38°C it was 8.9 hours. Figure 5.3 highlights the street segments with an average UTCI > 32°C for 12.9 hours or more.

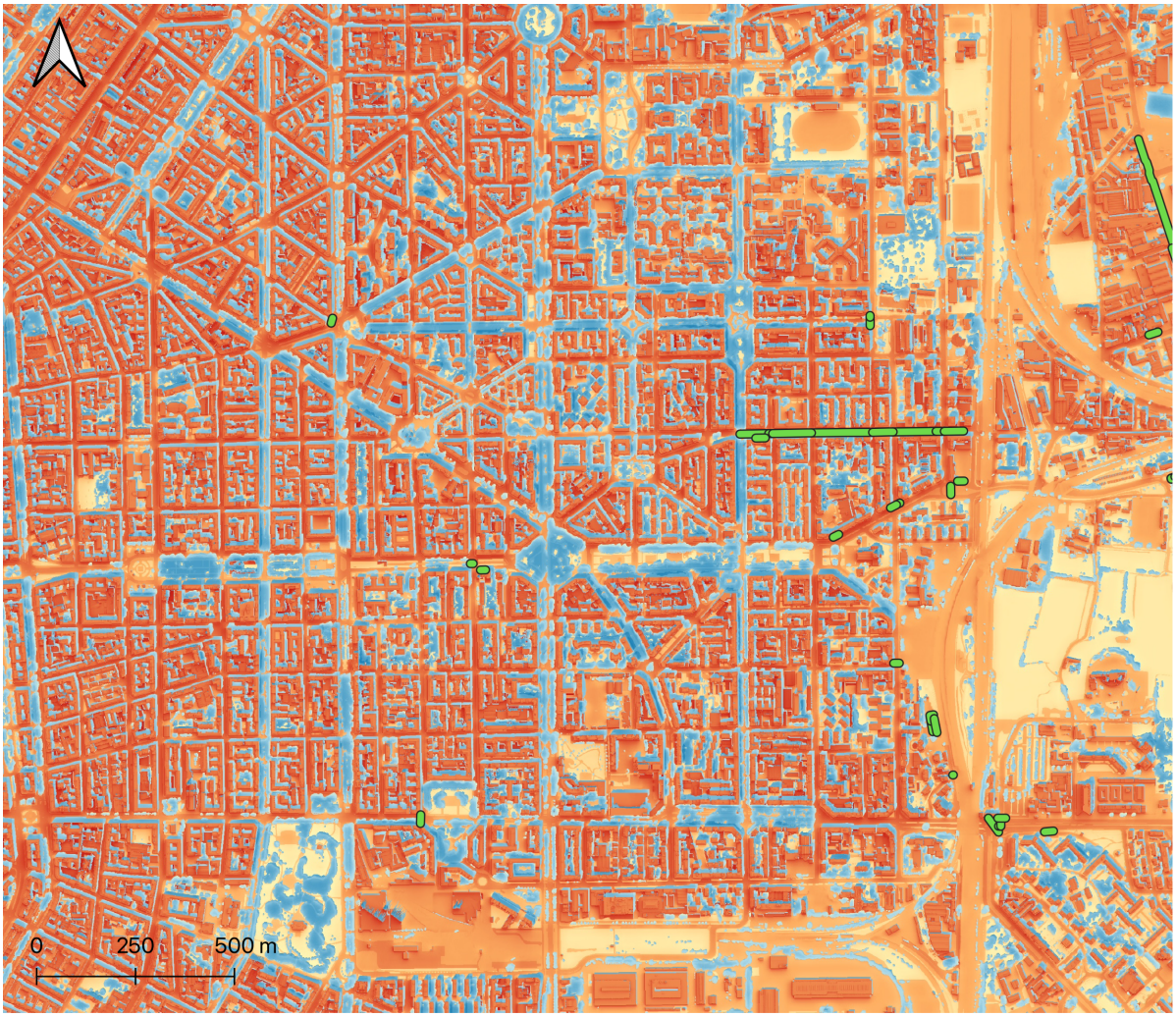

Figure 5.3: UTCI above 32°C

Figure 5.4 highlights the street segments with an average UTCI > 38°C for 8.2 hours or more.

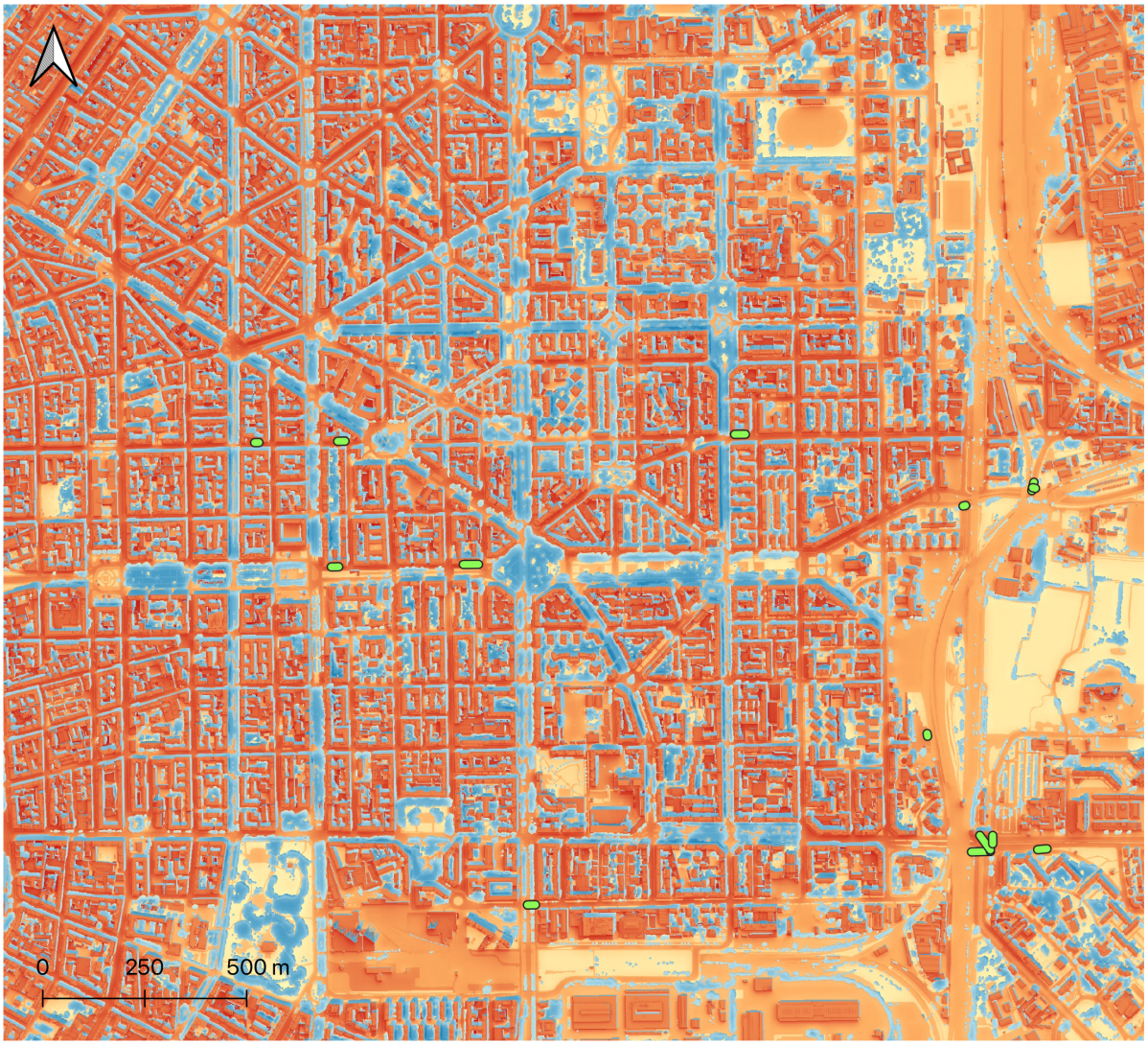

Figure 5.4: UTCI above 38°C

It is concluded, comparing all the UTCI maps, that there are evident critical areas in the district. In particular, via Giovanni Antonio Amadeo appears to be the most urgent area to focus on.

5.4. Building clustering

In this section, criteria for clustering buildings are defined in order to optimize the modeling process, enable informed simplifications where appropriate, and reduce the number of variables in the simulations, thereby facilitating a controlled-variable experimental setup.

The TABULA (Typology Approach for BUiLding stock energy Assessment) research project has classified the italian national building typology according to the following categories [79]:

- Region / climatic zone
- Construction period classes
- Building size classes

Italy is divided in climatic zones and Milan correspond to the climatic zone E, which is the "average climatic area". For every climatic area eight classes which defines the construction period are defined. Every class represents a specific time period which reflects dimensional and construction

typologies, which are also relevant from the energetic point of view. The construction period classes are the following:

- Class 1: until 1900
- Class 2: from 1901 to 1920
- Class 3: from 1921 to 1945
- Class 4: from 1946 to 1960
- Class 5: from 1961 to 1975
- Class 6: from 1976 to 1990
- Class 7: from 1991 to 2005
- Class 8: from 2005 onward

Each construction period class is represented by building size classes, which categorize buildings based on their dimensions and geometry. The building size classes are as follow:

- Single-family house, characterized by a single housing unit, on one or two floors, either detached or adjacent to another building;
- Terraced house, consisting of a single housing unit, on one or two floors, adjacent to other housing units
- Multi-family building, a small building characterized by a limited number of housing units (from 2 to 5 floors and up to 15 apartments, or from 2 to 4 floors and from 16 to 20 apartments);
- Apartment block, a large building characterized by a higher number of housing units.

There are three different methodological approaches to define building typologies, according to the Fascicolo sulla Tipologia Edilizia Italiana by Corrado et al. [79]. The first approach is the real example building (ReEx). This approach is based on the choice made based on experience. The building typology is selected in a specific climatic context as the most representative of dimensions or of a construction period. This first approach is used when reliable statistical data are missing. The second approach identifies the building typologies (called real average building, ReAV) through a statistical analysis. The available data are collected and analyzed. Then a building is selected so that it has geometric and construction characteristics which coincide with the mean of the analyzed sample. The third approach defines the building typologies as "archetypes". The building typologies are here called synthetical average building o theoretical building (SyAv). The archetype is defined as "a statistical composite of the features found within a category of buildings in the stock". The archetype is not a real building but a virtual one characterized by a set of properties statistically identified within a building.

This study adopts the real example building (ReEx) approach. Figure 5.5 shows the footprint of the buildings in the selected study area, and their categorization based on facade characteristics. Each building is assigned a letter based on observable differences in facade materials.

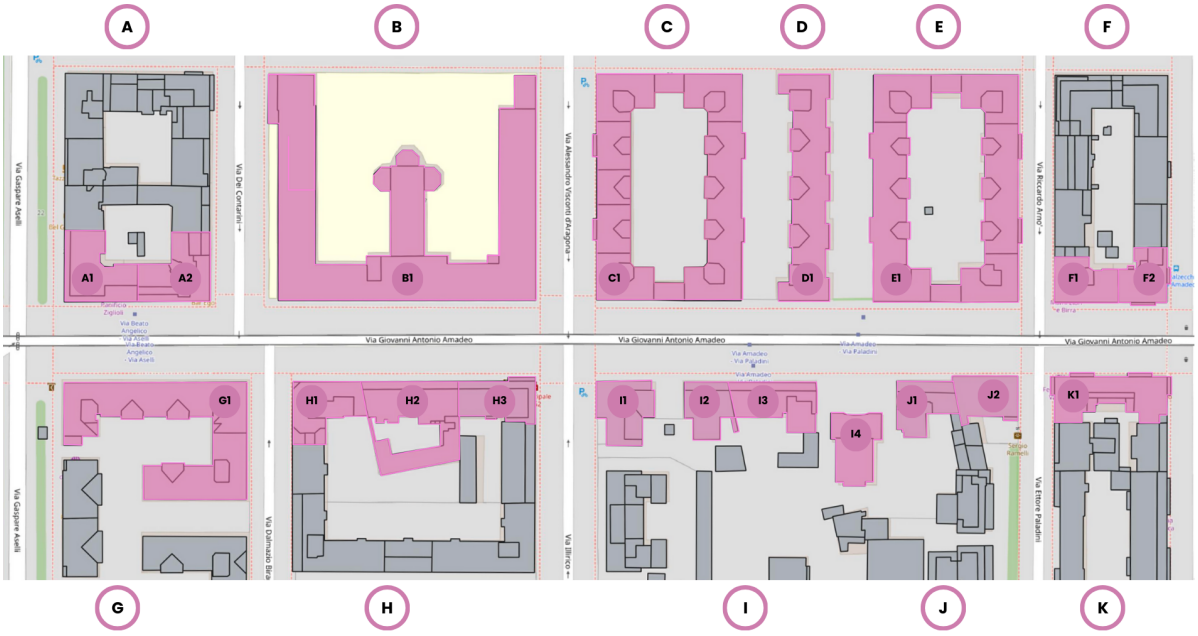

Figure 5.5: Selected buildings

Table 5.2 summarizes the main characteristics of the buildings. Building heights and number of floors were obtained through direct visual inspection and measurements conducted via Google Earth. Construction years were derived from the 1946 urban census. The census was carried out in the post-war period, following the bombings that damaged several buildings across the city, and served as a preliminary study for the approval of the 1953 urban master plan. These records are accessible through the Milan Municipality Geoportale [80], and are also compiled in the volume "Milano 1946. Alle origini della ricostruzione" by Pertot and Ramella [81]. In these sheets there are detailed information on the buildings built before 1946, and a precise construction date is available. For buildings constructed after 1946, the construction period was estimated by comparing historical urban maps available on the Milan Municipality Geoportale.[80]. The historical maps are available for the following years: 1930, 1946, 1956, 1965, 1972, 1990, 2006, 2012. The criteria used to assign a certain construction period to a building was that if a building was absent in the 1946 map but present in the 1956 one, the assigned construction range was $1946 < y < 1956$. A summary with all the historical maps is available in the Appendix A.9.

Corrado et al. [79] propose a classification of Italian buildings based on construction period, referred to as "construction class". Each building was assigned a construction class based on its actual or estimated construction year. Each construction class corresponds to a specific construction typology: solid brick masonry for Class 3 (1921–1945) and hollow-core wall with perforated bricks for Class 4 (1946–1960). Associated U-values are also defined in the reference document by Corrado et al. [79].

Block	Code	Floors [-]	Height [m]	Constr. year	Class	Constr. type	U-value [W/m^2K]
A	A1	7	24.39	1934	3	Solid brick masonry	1.14
	A2	7	24.39	1946<y<1956	4	Hollow-core wall with perforated bricks (30 cm), low insulation	1.15
B	B1	4	16.20	1940	3	Solid brick masonry	1.14
C	C1	5	18.33	1930	3	Solid brick masonry	1.14
D	D1	4	15.94	1930	3	Solid brick masonry	1.14
E	E1	5	19.50	1930	3	Solid brick masonry	1.14
F	F1	5	18.94	1930<y<1946	3	Solid brick masonry	1.14
	F2	5	18.94	1930<y<1946	3	Solid brick masonry	1.14
G	G1	6	22.30	1928	3	Solid brick masonry	1.14
H	H1	6	22.06	1936	3	Solid brick masonry	1.14
	H2	7	23.49	1956<y<1965	4	Hollow-core wall with perforated bricks, low insulation	1.15
	H3	8	26.30	1946<y<1956	4	Hollow-core wall with perforated bricks, low insulation	1.15
I	I1	7	24.44	1956<y<1965	4	Hollow-core wall with perforated bricks, low insulation	1.15
	I2	9	29.58	1956<y<1965	4	Hollow-core wall with perforated bricks, low insulation	1.15
	I3	7	23.19	1956<y<1965	4	Hollow-core wall with perforated bricks, low insulation	1.15
	I4	9	29.89	1956<y<1965	4	Hollow-core wall with perforated bricks, low insulation	1.15
J	J1	7	23.34	1956<y<1965	4	Hollow-core wall with perforated bricks, low insulation	1.15
	J2	5	18.25	1956<y<1965	4	Hollow-core wall with perforated bricks, low insulation	1.15
K	K1	7	23.21	1946<y<1956	4	Hollow-core wall with perforated bricks, low insulation	1.15

Table 5.2: Summary of the main characteristics of the buildings modelled in ENVI-met.

To simplify simulation procedures, buildings were clustered into representative archetypes. Four different archetypes were defined, based on the construction typology and on observable differences in facade materiality. Each facade was divided into two levels: upper and lower, to account for differences in material finishes.

The archetype 3A, whose characteristics are shown in Table 5.3, is the archetype assigned to buildings: A1, B1, C1, D1, E1, and G1.

Facade level	Wall system	Finish
Upper facade	Solid brick masonry (50 cm)	Light brown plaster
Lower facade	Solid brick masonry (50 cm)	Light-colored plaster

Table 5.3: Description of Archetype 3A: A1, B1, C1, D1, E1, G1.

Archetype 4A, described in Table 5.4, characterizes buildings: A2, F2, H3, J2 and K1.

Facade level	Wall system	Finish
Upper facade	Hollow-core wall with perforated bricks (30 cm)	Light brown/orange plaster
Lower facade	Hollow-core wall with perforated bricks (30 cm)	Grey plaster

Table 5.4: Description of Archetype 4A: A2, F2, H3, J2, K1.

Table 5.5 describes the characteristics of archetype 4B, which is assigned to buildings: F1, H2, I3, I4 and J1.

Facade level	Wall system	Finish
Upper facade	Hollow-core wall with perforated bricks (30 cm)	Red-brown brick
Lower facade	Hollow-core wall with perforated bricks (30 cm)	Marble – off-white

Table 5.5: Description of Archetype 4B: F1, H2, I3, I4, J1.

Finally, archetype 4C (detailed in Table 5.6) characterizes buildings: I1 and I2.

Facade level	Wall system	Finish
Upper facade	Hollow-core wall with perforated bricks (30 cm)	White plaster
Lower facade	Hollow-core wall with perforated bricks (30 cm)	Grey marble

Table 5.6: Description of Archetype 4C: I1, I2.

6

Simulation and scenario testing

This chapter presents the modeling approach, including the configuration of all simulation models and the description of the scenarios' implementation. Two tools were used to assess indoor and outdoor thermal comfort: Envi-met for outdoor simulations and EnergyPlus for indoor simulations. The model for outdoor simulations consists of a street canyon, while the model for indoor simulation in a numerical test cell. The next paragraphs outline the simulations' tools, the modeling assumptions and the simulation processes.

6.1. Envi-met software and modeling set-up

Envi-met is a microenvironmental numerical simulation software [39]. It offers an analysis of the heat and energy fluxes at any point within the model domain, determining the air temperature, the mean radiant temperature, relative humidity and air velocity. This software was selected to assess the outdoor thermal comfort because it is integrates fluid dynamics with thermodynamics, plant physiology and soil science, capturing the complexity and interactions of the urban setting. Envi-met simulations need model data and weather data. The scope of this thesis project was to evaluate the facade performance on indoor and outdoor thermal comfort during a heatwave, so in the next section the individuation of the critic day in which the simulations were made is explained. After the critic day was highlighted, the input file could be created.

6.1.1. Climatic analysis and individuation of the critic day

According to Copernicus Climate Change Service [82], during summer 2022 extensive areas across Europe saw large heat stress anomalies. A large part of southern and western Europe experienced more than five days of 'very strong heat stress' during the summer. Figure 6.1 shows the number of days that experienced strong heat stress. According to Figure 6.1, Milan had around 70 days of strong heat stress (i.e. UTCI > 32°C) from the beginning of June 2022 to the end of August 2022.

To find a representative simulation day, summer period of 2022 in Milan was explored. Temperature data were collected from the Rete Regionale di Rilevamento Meteorologico of ARPA (Agenzia Regionale per la Protezione dell'Ambiente) [83], which are freely available on their website if requested. The temperature dataset are available in Celsius degrees. The data were collected in the weather station of via Juvara, which is in close proximity to the Acquabella district (the distance from the weather station in via Juvara and via Giovanni Antonio Amadeo is approximately 1km).

The daily temperature data for the months of June, July and August were analyzed and the maximum temperature per month was computed. The maximum temperature for the month of June is 34.6°C, for the month of July is 37.3°C and for the month of August is 36.5°C. The month of July is therefore selected as the most critical month for Milan in 2022. The hourly data for July 2022 were then analyzed and the daily maximum temperatures for July wre plotted. They are shown in

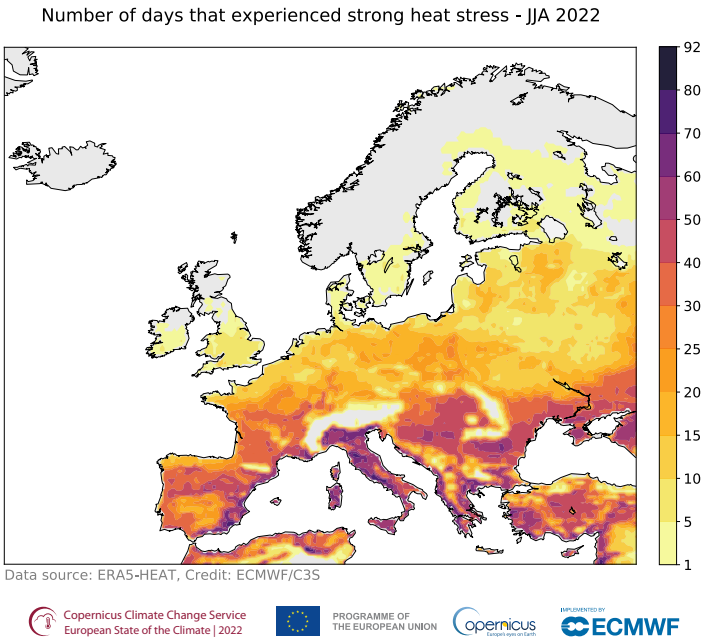

Figure 6.1: Number of days that experienced 'strong heat stress' (UTCI between 32 and 38°C) during June, July and August 2022. Data source: ERA5-HEAT. Credit: C3S/ECMWF [82].

Figure 6.2.

The hottest day for July 2022 was found to be the 22nd of the month, with a maximum temperature of 37.3°C. This day is selected to be the simulation day. The calculations' code can be found in Appendix B.

6.1.2. Input data

The input file for the Envi-met simulations was created by assembling meteorological data for the selected period and formatting them into a forcing file (.FOX). The simulated period is two days (i.e. 48 hours), from the 21st of July 2022 to the 22nd of July 2022. An EPW file was manually created by inserting the collected data into an already existing EPW file. The available data were collected and inserted in the file, while the not available ones were filled with standard values (i.e. 9999, 0). The data were collected from two sources: Agenzia regionale per la protezione dell'ambiente della Lombardia (ARPA) [83] and Copernicus Atmosphere Monitoring Service (CAMS) [84].

ARPA Lombardia - Agenzia regionale per la protezione dell'ambiente della Lombardia - is a company that supports local institutions on the prevention and protection of the environment in a variety of activities: from combating air and noise pollution to protecting surface and groundwater, from monitoring electromagnetic fields to investigating soil contamination and remediation processes. ARPA collects and elaborates the necessary data to supports the political decision of Regione Lombardia and other public entities. In the ARPA database the following data can be requested through a form: hydrometric level, snow height, precipitation, temperature, relative humidity, global radiation, wind speed and direction and wind gust speed and direction. In particular, the data used for the EPW file were: temperature, relative humidity, global radiation and wind speed and direction.

CAMS is one of six services form Copernicus, the European Union's Earth observation program. Copernicus offers information services based on satellite Earth observation, in situ (non-satellite) data and modeling. CAMS is implemented by the European Center for Medium-Range Weather Forecasts (ECMWF) on behalf of the European Commission. CAMS provides time series of global,

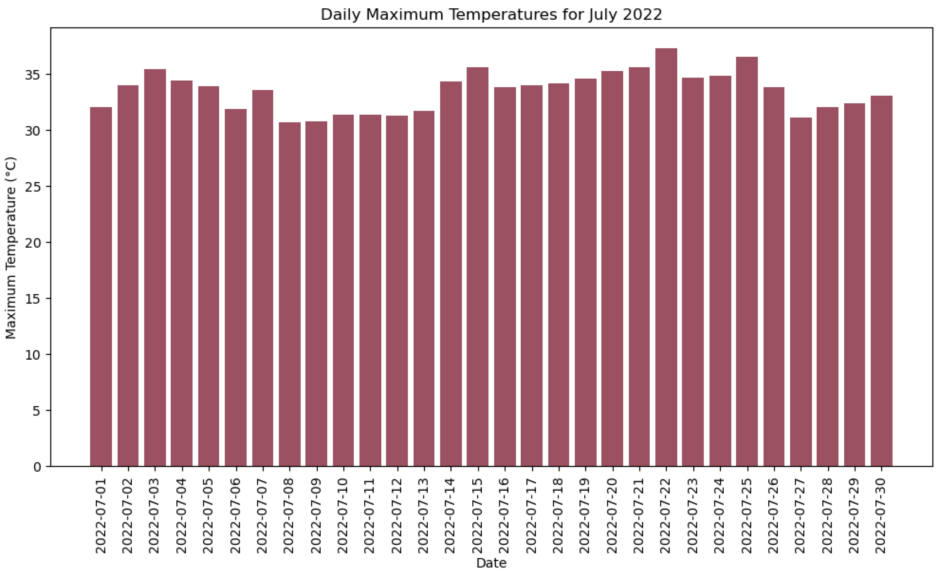

Figure 6.2: Daily maximum temperatures for July 2022

direct, and diffuse irradiation on horizontal surfaces, and direct normal irradiation for both observed (i.e. with the actual clod conditions) and clear-sky conditions [84]. CAMS data were used to gather radiation data (specifically direct normal radiation and diffuse horizontal radiation) to fill the EPW file with. The data were requested 120 meters above sea level, which corresponds to the elevation of Milan.

The Forcing Manager on Envi-met enables to create one's own specific Full Forcing files [85]. Forcing is a type of lateral boundary condition, and there are two possibilities on Envi-met: simple forcing and full forcing. For this project full forcing was used, even if some values were not fully forced. The precipitation was not fully forced and was set to zero. The wind speed was not fully forced and a constant value of the mean speed of the 22nd of July was used. The wind direction was also not fully forced and a constant direction was forced instead, to avoid numerical instabilities. In order to understand which was the predominant wind direction of the 22nd of July 2022 a wind rose was made. It is illustrated in Figure A.8.

The Forcing Manager automatically reads the file format (EPW) and converts it into a forcing file (FOX) usable in the simulation process. Once created, the Forcing File can then be used as meteorological input data for Envi-met simulations.

6.1.3. Model Details

Two primary baseline models were developed: Baseline Model 1 (shown in Figure 6.3) and Baseline Model 2 (visualized in Figure 6.4). The two models have the same exact buildings and building's materiality, the only difference between the two is in the H/W ratio of the street canyon. The model of the Baseline 1 has a larger H/W ratio, while the model of the Baseline 2 has a smaller one. This results for the model of the Baseline 2 in a bigger computation domain. The details of the model for the Baseline 1 are summarized in Table 6.1, and those of the model for the Baseline 2 are reported in Table 6.2.

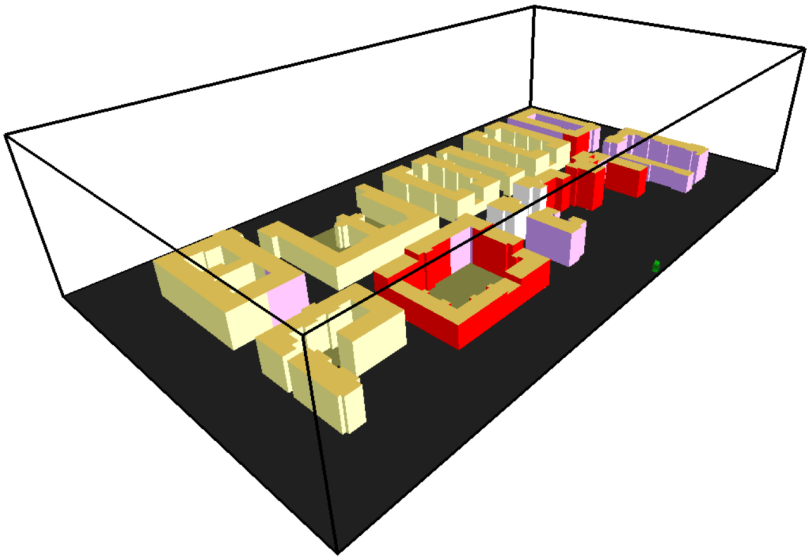

Figure 6.3: Baseline Model 1

Table 6.1: Details and settings of the model (Baseline 1)

Parameter	**Value**
Software and version	ENVI-met V5.6.1 Winter23
Computation domain	450 x 250 x 60m (x, y, z)
Basic cell size	2 x 2 x 2m (dx, dy, dz)
Near-ground grid cells	Divided into 5 sub-cells
Simulation site	Milan, Italy, 45.47338330056684, 9.22039057076111

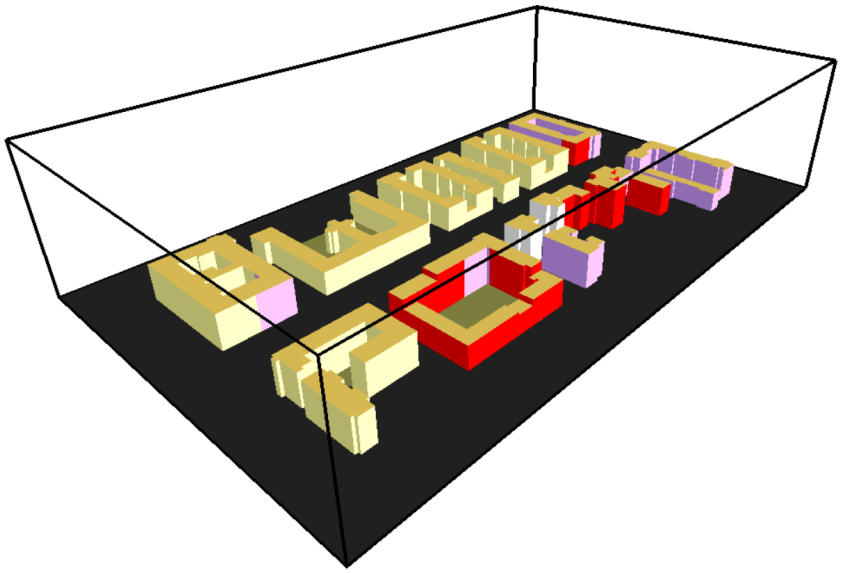

Figure 6.4: Baseline Model 2

Table 6.2: Details and settings of the model (Baseline 2)

Parameter	Value
Software and version	ENVI-met V5.6.1 Winter23
Computation domain	450 x 270 x 60m (x, y, z)
Basic cell size	2 x 2 x 2m (dx, dy, dz)
Near-ground grid cells	Divided into 5 sub-cells
Simulation site	Milan, Italy, 45.47338330056684, 9.22039057076111

6.1.4. Model Setup

The creation of building models in ENVI-met Spaces follows a structured process. First, the building footprints of Via Giovanni Antonio Amadeo were imported from Milan Geoportale [80] and compared with other maps for accuracy. Then an AutoCAD file was created with the footprint of just the selected buildings. The file was exported in .dxf format and subsequently converted in a .bmp file. Scaling was crucial during this process to guarantee accuracy, and a scale of 1:1 was kept during all the steps. The .bmp file was imported in ENVI-met Spaces, and the dimensions and proportions were coherent with the assigned grid. The model was built on the building footprint, assigning to each building its own height. The heights were found using Google Earth and approximated rounding for a whole number. The buildings were then numbered assigning different numbers if there were different heights or different facade materials within the same building.

Each building was assigned with a wall material according to the archetypes described in section 5.4. For the roofs, all the buildings were assigned with the default roofing tiles material in ENVI-met DataBase manager library, which is identified with the code [0200RI]. The properties of the roofing tile are shown in Table 6.3.

Parameter	Default roofing tile
Default thickness [m]	0.05
Absorption [-]	0.70
Transmission [-]	0.00
Reflection [-]	0.30
Emissivity [-]	0.93
Specific heat [J/kg·K]	800
Thermal conductivity [W/m·K]	0.84
Density [kg/m³]	1900

Table 6.3: Physical, thermal, and optical properties of the default roofing tile in ENVI-met [0200RI]

In Table 6.4 the thermal, optical and physical properties of the facade materials that were used are shown. The values displayed in Table 6.4 are assumptions based on literature.

Material	Color	Thermal properties		Optical properties			Physical properties	
		Thermal Conductivity [W/m·K]	Specific heat [J/kg·K]	Absorption	Reflectance	Albedo	Emissivity	Density [kg/m³]
Stucco	Bright	1.5	720	0.65	0.45	0.66	0.94	2180
	Grey	1.5	720	0.65	0.30	0.30	0.94	2180
Plaster	Bright	1.5	1000	0.35	0.45	0.45	0.86	1300
	Dark	1.5	1000	0.50	0.25	0.25	0.86	1300
Marble	Bright	2.2	880	0.55	0.45	0.59	0.90	2600
	Grey	2.2	880	0.65	0.35	0.40	0.90	2600
Concrete	Bright	0.85	840	0.30	0.70	0.70	0.90	2050
	Grey	0.85	890	0.80	0.20	0.30	0.90	2050
Brick	Red	1.31	800	0.70	0.30	0.39	0.95	1500
Ceramic	Bright	0.80	840	0.55	0.45	0.70	0.95	1700

Table 6.4: Thermal, optical and physical properties of facade finishing materials.

Table 6.5 shows the values inserted in ENVI-met DataBase manager for the two wall systems: heavyweight masonry and hollow-core wall with perforated bricks. The values displayed in Table 6.5 are assumptions based on literature, but both the wall systems parameters respect the U-value value that is know, based on Fascicolo sulla Tipologia Edilizia Italiana by Corrado et al. [79].

Parameter	Masonry: heavyweight	Hollow-core wall with perforated bricks
Default thickness [m]	0.50	0.30
Absorption [-]	0.65	0.65
Transmission [-]	0.00	0.00
Reflection [-]	0.35	0.35
Emissivity [-]	0.90	0.85
Specific heat [J/kg·K]	840	800
Thermal conductivity [W/m·K]	0.57	0.345
Density [kg/m³]	1850	800

Table 6.5: Physical, thermal, and optical properties of the two wall types used in ENVI-met.

For the soil configuration, the default asphalt material from the ENVI-met Database Manager was

assigned to the areas surrounding the buildings. Within the building perimeters, where courtyards or internal open-air spaces were present, the default ENVI-met ground material (lime0000) was applied. This choice was made to reduce variability in the simulation scenarios.

Considerations and simplifications

The model was simplified to reduce complexity and prevent excessively long simulations. It is important to note that all the values inserted in the ENVI-met DataBase manager, are not directly calculated but are based on assumptions from the literature. In the previous section, the buildings were grouped based on their facade material, which was divided into an upper and a lower facade level. However, in the model just the upper facade material was applied to the entire facade for each building. This choice was made for simplicity because the model was in 2.5D. Assigning different facade materials to the same wall would have required converting the model to 3D, and the simulation process would have taken longer. However, this remains a reasonable approximation, since in most cases the lower facade included commercial entrances, gates, or was partially covered by shopfronts and building entrances, rather than being a continuous surface of the same material. Moreover, the heights of the buildings are approximated, since ENVI-met could not take decimal numbers. Lastly, complex geometries of building envelopes were also simplified, and balconies were excluded from the model.

6.1.5. Scenarios Setup

As explained in section 4.2.1, 10 different scenarios were made, along with the two baseline simulations. The scenarios consisted in the application of a cool coating to the facade, the addition of an insulation layer (external and internal), and a combination of the cool coatings with the different insulation configurations.

For the cool facade scenario, the external layers of the facade of all buildings were changed to a cool coating. Regarding the cool coating's properties, only the optical characteristics were modified from those of standard plaster, which seemed a reasonable assumption based on the review on cool coatings of Pisello et al. [86] and on the research of Donthu et al. [87]. The properties assigned for the cool coating are summarized in Table 6.6.

Parameter	Cool coating
Default thickness [m]	0.01
Absorption [-]	0.20
Transmission [-]	0.00
Reflection [-]	0.80
Emissivity [-]	0.90
Specific heat [J/kg·K]	1000
Thermal conductivity [W/m·K]	1.50
Density [kg/m^3]	1300

Table 6.6: Physical, thermal, and optical properties of the cool coating

For the insulation scenarios, the wall layers of all buildings were modified. The insulation used in the wall layers is not the default one in the ENVI-met DataBase manager. This choice was made because the default Envi-met insulation had a relatively low R value compared to the insulation materials that are commonly used. The insulation parameters were defined according to the literature and are shown in Table 6.7.

Parameter	Default insulation
Default thickness [m]	0.1
Absorption [-]	0.50
Transmission [-]	0.00
Reflection [-]	0.50
Emissivity [-]	0.90
Specific heat [J/kg·K]	1500
Thermal conductivity [W/m·K]	0.035
Density [kg/m³]	400

Table 6.7: Physical, thermal, and optical properties of the default insulation in ENVI-met [0200IN]

In the scenarios with internal insulation, the insulation layer was placed as the innermost layer, from outside to inside. In the scenarios with external insulation, it was positioned between the finishing layer and the wall-system layer. For the combined scenarios, what is described in the paragraphs above still applies.

6.2. From outdoor simulations to indoor simulations

How can the results from outdoor simulations be integrated into indoor simulations?

This is a key aspect of the present research, as the microclimate conditions modeled with ENVI-met directly influence indoor thermal comfort. To ensure continuity between the simulations and to effectively use ENVI-met outputs as input data for EnergyPlus, a series of processing steps were implemented.

The EPW file used for the indoor simulations was formed through this process: a Typical Meteorological Year (TMY) file was used as the starting file. The month of July was substituted with real data from a weather station, and the values for the 22nd of July were substituted from Envi-met simulations. The climatic data for July 2022 were collected from ARPA, from the weather station of Milano Juvara, which is approximately 1 km from the analyzed street. In particular, the following data were collected: Dry Bulb Temperature, Relative Humidity, Global Horizontal Radiation, Direct Normal Radiation, Diffuse Horizontal Radiation, Wind Direction, Wind Speed.

The results from the Envi-met simulations for every scenario were exported as .csv files for specific points. The same point was used for the data extraction of every simulation. Those results were inserted in the EPW file for the 22nd of July only. In particular, the following results were extracted: Potential Air Temperature, Relative Humidity, Wind Speed, Wind Direction.

The graphs below (Figure 6.5) show the curves of the Dry Bulb Temperature and of the Relative Humidity, for the EPW created for the Baseline 1. The code for the implementation of this file can be found in the Appendix B, where just the EPW file for the Baseline 1 is shown, as all the other EPW files were created with the same script. The blue line represent the data exported from Envi-met, while the gray dashed line represent the the data from the original EPW (which were taken from a near-by weather station located at a distance of 1km). It is interesting to note how the curves from ENVI-met have a higher amplitude. This can be explained by the fact that the weather station data represent mean conditions on an open area. ENVI-met, on the contrary, simulates the local microclimate in specific points. The local microclimate is affected by the surrounding buildings, shadows, heat accumulation, reduced ventilation, etc., which leads to higher maximum values and lower minimum ones (i.e. bigger thermal excursion).

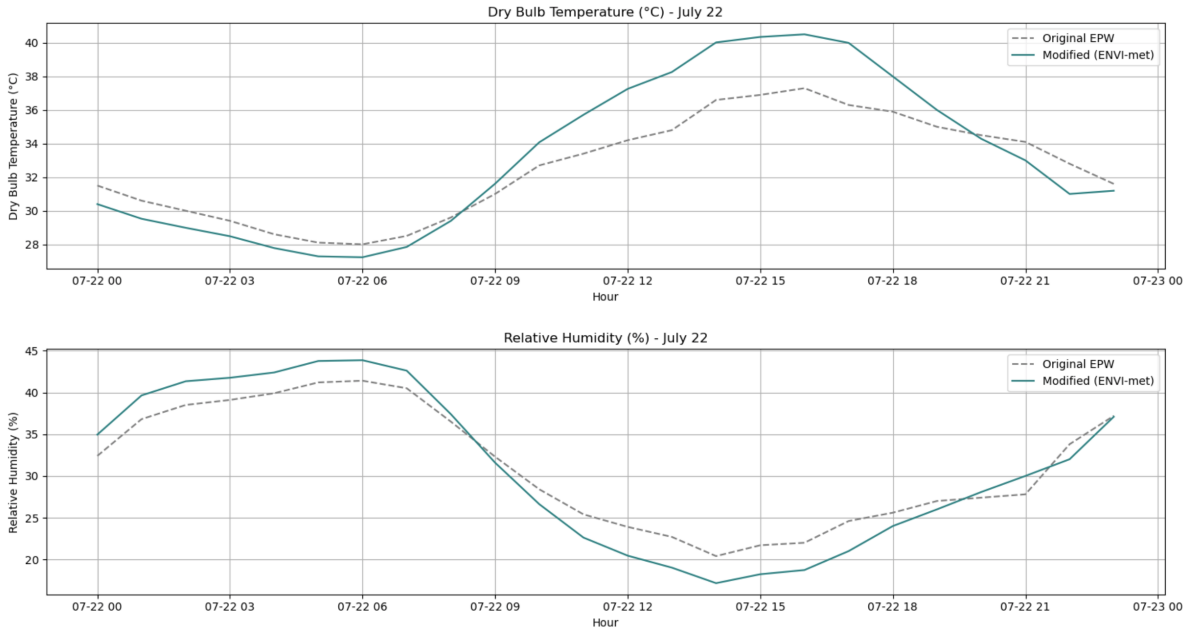

Figure 6.5: Dry bulb temperature and relative humidity - EPW files

The graphs below (Figure 6.6) show the different behavior of the wind direction and wind speed in the original EPW file and in the one modified with the Envi-met data. The values from the ENVI-met results for the wind speed and wind direction appeares as straight lines. This is because the data have a really low standard deviation. This can be explained as in the ENVI-met simulations, the values for wind direction and wind speed were not fully forced, but a mean was applied for the wind speed (v=1.6m/s) and a wind rose was done to establish the average wind direction (160°C). This choice was made due to the numerical instability of ENVI-met under changing wind data. In order to keep consistency between the outdoor and the indoor simulations, the wind data from ENVI-met will be used, even if they are highly simplifying the real wind pattern.

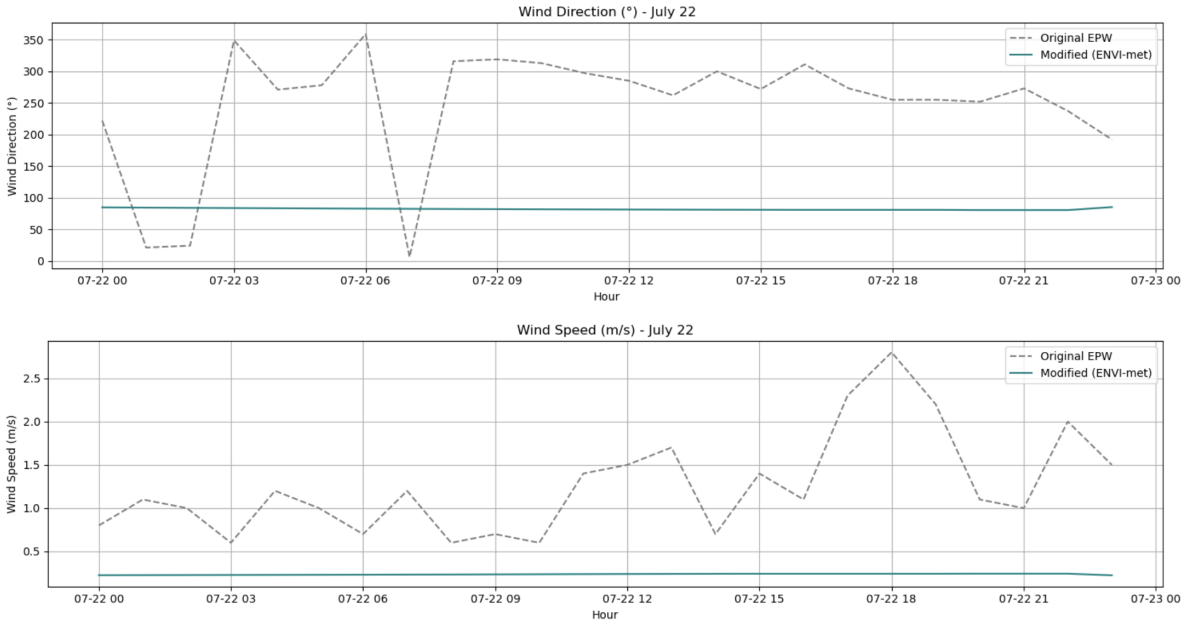

Figure 6.6: Wind speed and wind direction - EPW files

6.3. EnergyPlus software and modeling set-up

EnergyPlus is a building energy simulation program used to model energy consumption and water use in buildings [60]. It was adopted as it provides, among all its features, the following aspects were of particular interest for the present study:

- Heat balance-based solutions of radiant and convective effects,
- Combines heat and mass transfer modeling that considers air movement between zones.

There are two different input files that are needed to perform an EnergyPlus simulation: the EPW file (weather data), and the IDF file (building model description file). Together, these two files are used to perform simulations. In the previous section (6.2), it was extensively explained how the EPW files were built. Every simulation performed in EnergyPlus had its own EPW file, created from the corresponding outdoor simulation results.

6.3.1. Model Setup - IDF file

A specific building (identified with the code C1) was selected for the indoor simulations. The building was selected based on its location, which is in the middle of the modeled street canyon. The effect of the scenarios on the indoor thermal comfort was analyzed by modeling with EnergyPlus a representative room (i.e. a test cell) of building C1 on a middle floor.

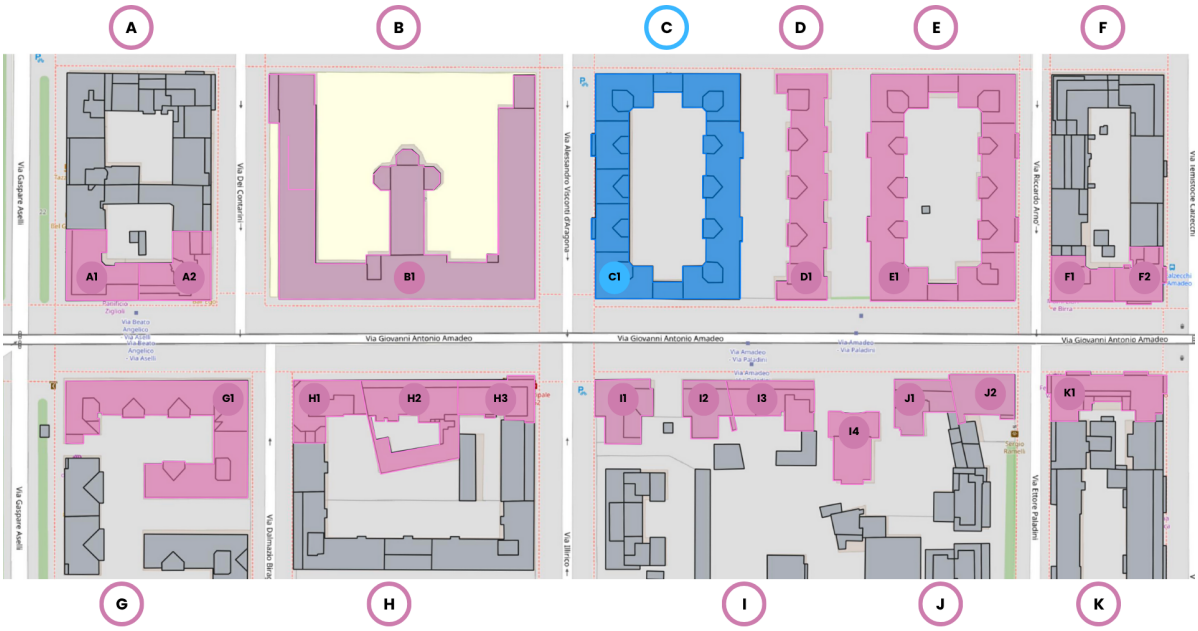

Figure 6.7: Building C1 is selected for indoor simulations

The rationale for using a numerical test cell instead of modeling an entire apartment — or a more realistic scenario — is provided in the next section 6.3.2. In the following paragraph, the numerical test cell is described.

The geometry of the model is a cubic room (4m x 4m x 4m), with four walls, one floor and a ceiling. The south wall is the one that is exposed to the outdoor environment, while the other walls (as well as the floor and the ceiling) are modeled as adiabatic surfaces. The south wall has a window, characterized by a window-to-wall ratio of 20%. The model has a natural fixed ventilation of $0.3 m^3/s$ from 21:00 to 07:00, as to represent the window to be opened only at night (i.e. night ventilation).

Every scenario was modeled with a different IDF file. The only variable that was changed from the various files was the south wall materiality, according to the scenario the model was representing. For the materiality of the south wall of the EnergyPlus model, the same thicknesses and relevant parameters used in Envi-met were used. The U-value and g-value of the window was assigned according to the Building Typology Brochure – Italy [79]: $U = 4,90 W/(m^2 K)$, $g = 0.85$.

6.3.2. Model Rationale and Validation

In this section, the EnergyPlus model rationale and validation are presented.

Modeling rationale

To investigate the effects of different facade systems on indoor thermal comfort, a simplified modeling strategy was adopted. A numerical test cell model was used to reduce the number of variables involved in the simulations and to ensure that the outcomes primarily reflected changes in the facade system. For this reason, no people, equipment or lighting were included in the model.

What is commonly intended as a test cell is a small-scale single-zone physical room, built to investigate the thermal behavior of specific building and facade parts, components, or technologies. In literature test cells are becoming popular to assess the effects of new technologies on the building envelope. For instance, the research conducted by León-Rodríguez et al. [88] consisted in evaluating the effect of retrofitting strategies on facade by using test cells as an experimental method. Test cells were used so that the facade effect could be isolated from the user's influence. The study concluded that the use of test cells is an effective method to evaluate and compare the effects of the various facade retrofitting.

In the present study a test cell was not physically built, but it was instead modeled in EnergyPlus. No experimental data were collected in this work. However, a study conducted by Mateus et al. [89] demonstrated that for simplified configurations such as test cells, the simulation results obtained with EnergyPlus were aligned well with the experimental ones. In particular, their study aimed to validate EnergyPlus thermal simulation of a test cell with experimental data from a physical test cell. Validation of simulation tools like EnergyPlus is an open discussion due to the complexity of the models and the differences between every case. Typically, the validation is done for the case-specific model, which gives little information on the expected error that the tool could give in that context. Their study focused on a double skin naturally ventilated test cell. The simulation results aligned well with the experiments.

The current study aims to isolate the effects of the facade (i.e. the south wall) on the indoor environment, and for this reason the other walls (i.e. the floor, ceiling, north wall, east wall, west wall) were modeled as adiabatic. In real conditions, the internal walls, the ceiling and the floor exchange heat with the adjacent areas, contributing to lower the temperature of the room. For this reason, the outcomes of the simulations are expected to have higher temperatures - and lower differences in temperature - compared to similar experiments conducted in the literature.

The model includes natural night ventilation. This choice appeared to be the best one, for the scope of the research, between multiple ventilation options that were considered. HVAC systems were not included a priori in this model, as the dimensioning of them would have been out of the scope. Natural ventilation was selected as an alternative. The options were to have natural ventilation all day long, night ventilation or none ventilation at all. In the first case, with natural ventilation throughout the entire day, the data were always stable, but the differences between the diverse facade scenarios were minimal, due to the fact that the main variable affecting the indoor air temperature was the outside air temperature. By not including ventilation at all, there were various numerical instabilities, and some temperatures were reaching infinite values, due to the fact that the room had no ways to dissipate the stored heat. However, the differences between the various facade systems were notable. The more reasonable option to have realistic results without numerical instabilities, and to still capture the differences between the various facade systems,

was to have natural night ventilation. The window was modeled open from 21:00 to 07:00. Small numerical instabilities are still present in the model. In particular, at 07:00 and at 21:00 the room changes from constant ventilation to no ventilation at all, and viceversa, involving large and abrupt transfers of air volumes. It is worth noting that, besides modeling reasons, natural night ventilation is frequently employed in practice during hot summers when HVAC is not present, as a passive cooling strategy.

Model validation

Although no experimental analysis and validation was carried out in the present study, the model and the adopted approach can be considered reliable for the scope of the research, which is assessing the influence of the different facade retrofitting strategies on the indoor thermal comfort. To do so, a numerical test cell was modeled as a simplified and idealized configuration, where user's influence were overlooked. This assessment was done under specific ventilation and boundary conditions.

Previous studies in the literature, as the one conducted by Mateus et al. [89], found that simplified numerical models developed with EnergyPlus could simulate with good accuracy the results obtained from a physical test cell, even with naturally ventilated conditions. Given that the present model exhibits similar simplifications — such as the use of natural ventilation, the absence of internal equipment and users and the focus on facade effects — the simulation results presented in this work can be considered representative for the comparative analysis of facade retrofitting scenarios under controlled conditions. The results are validated in the discussion section by comparing them with experimental results found in literature.

7
Evaluation

This chapter presents the results of the simulations, which are divided into two main sections: outdoor and indoor evaluations. The outdoor thermal comfort evaluation is based on Envi-met simulations, and focuses on how the different scenarios affect the Physiological Equivalent Temperature. The indoor analysis is performed through EnergyPlus and investigate the impact of different facade systems on the Standard Effective Temperature. The objective of this chapter is to compare each scenario against the baseline conditions in order to assess the benefits or drawbacks they have on indoor and outdoor thermal comfort.

7.1. Outdoor Thermal Comfort Evaluation

The results of the outdoor simulations are presented in this section. Each retrofitting scenario is compared to the baseline condition, with the objective of understanding the effects on outdoor thermal comfort The outcomes are visualized through comparison maps.

The retrofitting strategies investigated in this study can be schematized as:

- Cool Facade
- External Insulation
- Internal Insulation
- Cool Facade + External Insulation
- Cool Facade + Internal Insulation

Cool Facade

The Cool Facade Scenario consists of applying cool coatings (i.e. coatings with high reflectance and high emissivity) to the Baseline conditions. As with the other scenarios, this one was applied in both the Baseline 1 (i.e. the street canyon with the larger H/W ratio) and in Baseline 2 (i.e. the street canyon with the smaller H/W ratio). To understand the effect of this retrofitting strategy on outdoor thermal comfort, the results obtained from the ENVI-met simulations for the Scenario and the Baseline conditions were compared. This is done by creating a comparison map. In particular, the comparison focuses on the spatial distribution of the Physiological Equivalent Temperature across the street canyon.

Figure 7.1 shows the aforementioned comparison map, plotted for the 22nd of July 2022 at 16:00. The minimum $\Delta(PET)$ observed in the canyon is -17.96K, showing that there is significant difference in PET between the Baseline conditions and the Cool Facade Scenario. The maximum $\Delta(PET)$ registered is 0.48K. The map clearly shows that the Cool Facade Scenario has an overall highly detrimental effect on outdoor thermal comfort, with the most adverse effects occurring in specific parts of the canyon. These areas include courtyards and narrower streets.

Figure 7.1: Comparison between Baseline 1 and Scenario Cool Facade 1

A similar comparison was performed for the Baseline Simulation 2, assessing the Cool Facade Scenario against the Baseline Simulation 2 for the 22nd of July 2022 at 16:00. The minimum absolute difference in PET observed is -17.65K, indicating again the detrimental effect on outdoor thermal comfort of the Cool Facade Scenario. From the comparison map shown in Figure 7.2, a similar trend to that of the Baseline 1 (i.e. larger H/W) is observed. What differs from that case is that the street canyon between the buildings appears to be less impacted by the PET rise compared to the Baseline 1.

Figure 7.2: Comparison between Baseline 2 and Scenario Cool Facade 2

External Insulation

The External Insulation Scenario consists of adding a layer of external insulation to the Baseline conditions. This scenario was applied in both the Baseline 1 (i.e. the street canyon with the smaller H/W ratio) and in Baseline 2 (i.e. the street canyon with the larger H/W ratio). To provide an overview of how the additional layer of external insulation changes the outdoor thermal comfort, comparison maps were generated, showing the absolute difference in Physiological Equivalent Temperature.

The comparison map presented in Figure 7.3 shows the absolute difference in PET at 16:00 of the

22nd of July 2022 between the External Insulation Scenario against the Baseline 1. The minimum absolute difference in PET is -8.14K and the minimum is 1.26K. Most of the areas in the map have a $\Delta(PET)$ of around -1.5K. This scenario is worse for the outdoor thermal comfort compared to the Baseline, although to a lesser extent than the Cool Facade Scenario. However, a similar trend is observed: the courtyards are the areas most affected by this intervention.

Figure 7.3: Comparison between Baseline 1 and Scenario External Insulation 1

Similar results were obtained by comparing the Baseline 2 against the External Insulation Scenario. The comparison map is provided in Figure 7.4. With a minimum absolute difference in PET of -8.24K, and a maximum of 0.74K, the trend is very similar to what is discussed above for the first case (i.e. larger H/W).

Figure 7.4: Comparison between Baseline 2 and Scenario External Insulation 2

Internal Insulation

The Internal Insulation Scenario comprises of adding a layer of internal insulation to the Baseline conditions. This scenario was applied in both the Baseline 1 (i.e. the street canyon with the smaller H/W ratio) and in Baseline 2 (i.e. the street canyon with the larger H/W ratio). To provide an overview on the effects of adding this additional layer to the baseline, a comparison map was

generated, where the absolute difference of the Physiological Equivalent Temperature is displayed all over the street canyon.

The comparison map displayed in Figure 7.5 shows the absolute difference in PET at 16:00 of the 22nd of July 2022 between the Internal Insulation Scenario and the Baseline 1. The minimum absolute difference in PET is -0.13K and the minimum is 1.81K. Overall, this scenario leads to a slight improvement in outdoor thermal comfort—particularly in the courtyards—although its overall impact remains negligible.

Figure 7.5: Comparison between Baseline 1 and Scenario Internal Insulation 1

Figure 7.6 displays the comparison map between the Baseline 2 and the Internal Insulation Scenario. Whereas the External Insulation scenario showed hardly any difference between different street canyons (i.e. Baseline 1 and 2), for the Internal Insulation case it is observed that the effects on outdoor thermal comfort are less evident with a smaller aspect ratio. Furthermore, the comparison map highlights the courtyards as critical zones of interest.

Figure 7.6: Comparison between Baseline 2 and Scenario Internal Insulation 2

Cool Facade + External Insulation

The combined Cool Facade and External Insulation scenario consists of applying a cool coating (i.e., a coating with high reflectance and high emissivity) together with an additional layer of external insulation to the Baseline. This scenario was applied in both the Baseline 1 (i.e. the street canyon with the larger H/W ratio) and in Baseline 2 (i.e. the street canyon with the smaller H/W ratio). In order to assess the impact of this combined scenario, comparison maps of the absolute difference in PET with the Baseline were generated.

The comparison map illustrated in Figure 7.7 shows the absolute difference in PET between the Baseline 1 and the combined Scenario Cool Facade + External Insulation for the 22nd of July 2022 at 16:00. The minimum absolute difference in PET is -19.99K, and the maximum absolute difference is 0.78K. The minimum absolute difference in PET is two degree lower that the one for the Cool Facade Scenario, meaning that the already detrimental conditions on outdoor thermal comfort of that scenario, are even worst in this scenario, almost reaching a $\Delta(PET)$ of 20K. As in previous cases, it is noteworthy that the courtyards and narrow areas behave differently than the wider ones.

Figure 7.7: Comparison between Baseline 1 and Scenario Cool Facade 1 + External Insulation 1

The comparison map displayed in Figure 7.8 shows the absolute difference in PET between the Baseline 2 and the combined Scenario Cool Facade + External Insulation for the 22nd of July 2022 at 16:00. The minimum absolute difference in PET is -19.77K, and the maximum absolute difference is 0.98K. The trend is really similar for what is discussed above for the smaller canyon (i.e. Baseline 1).

Figure 7.8: Comparison between Baseline 2 and Scenario Cool Facade 2 + External Insulation 2

Cool Facade + Internal Insulation

The combined scenario of Cool Facade and Internal Insulation involves applying a cool coating (i.e., a coating with high reflectance and high emissivity) along with the addition of an internal insulation layer to the Baseline configuration. This scenario was applied in both the Baseline 1 (i.e. the street canyon with the larger H/W ratio) and in Baseline 2 (i.e. the street canyon with the smaller H/W ratio). Comparison maps were generated to assess the impact of this combined scenario.

The comparison map illustrated in Figure 7.9 shows the absolute difference in PET between the Baseline 1 and the combined Scenario Cool Facade + Internal Insulation for the 22nd of July 2022 at 16:00. The minimum absolute difference in PET is -16.86K, and the maximum absolute difference is 0.57K. The courtyards behavior is considerably different than the surrounding wider areas.

Figure 7.9: Comparison between Baseline 1 and Scenario Cool Facade 1 + Internal Insulation 1

Figure 7.10 is a comparison map highlighting the absolute difference in PET between the Baseline 2 and the combined Scenario Cool Facade + Internal Insulation for the 22nd of July 2022 at 16:00. The minimum absolute difference in PET is -16.73K, and the maximum absolute difference is 0.64K. The trend is closely aligned with what is discussed above for the smaller canyon (i.e. Baseline 1).

Figure 7.10: Comparison between Baseline 2 and Scenario Cool Facade 2 + Internal Insulation 2

7.2. Indoor Thermal Comfort Evaluation

The results of the indoor simulations are presented in this section. Each retrofitting scenario is compared to the baseline condition, with the objective of understanding the effects on indoor thermal comfort The results are displayed in the form of graphs.

The external Surface Temperature behavior for each scenario is shown in Figure 7.11). The overall trend of the graph shows a peak during the hottest hours of the day, and a minimum during night-time, in line with the solar radiation pattern. While the shape of the curves remains consistent across all scenarios, their amplitudes vary. The Baseline condition is represented by the dark green continuous line. The Cool Facade Scenario is illustrated by the dashed light green line. In the hottest hours of the day, the difference between the Baseline and the Cool Facade Scenario is more than 5°C, while during the night the difference is minimal. The External Insulation Scenario, represented by the pointed red line, shows the highest peaks between all curves, reaching up to more than 50°C. In the hottest time of the day, the difference in temperature between the External Insulation Scenario and the Baseline arrives to circa 7°C. The Internal Insulation Scenario shows a negligible difference in external surface temperature compared to the Baseline. The combined Scenario Cool Facade + External insulation is illustrated by a dash-dot blue line. Its behavior is worst during the hottest hours of the day, but better during the cooler ones. The combined Scenario Cool Facade + Internal Insulation is visualized by the dashed yellow line. This curve is the lowest during the hottest time of the day, but does not cool down as other scenarios during night-time.

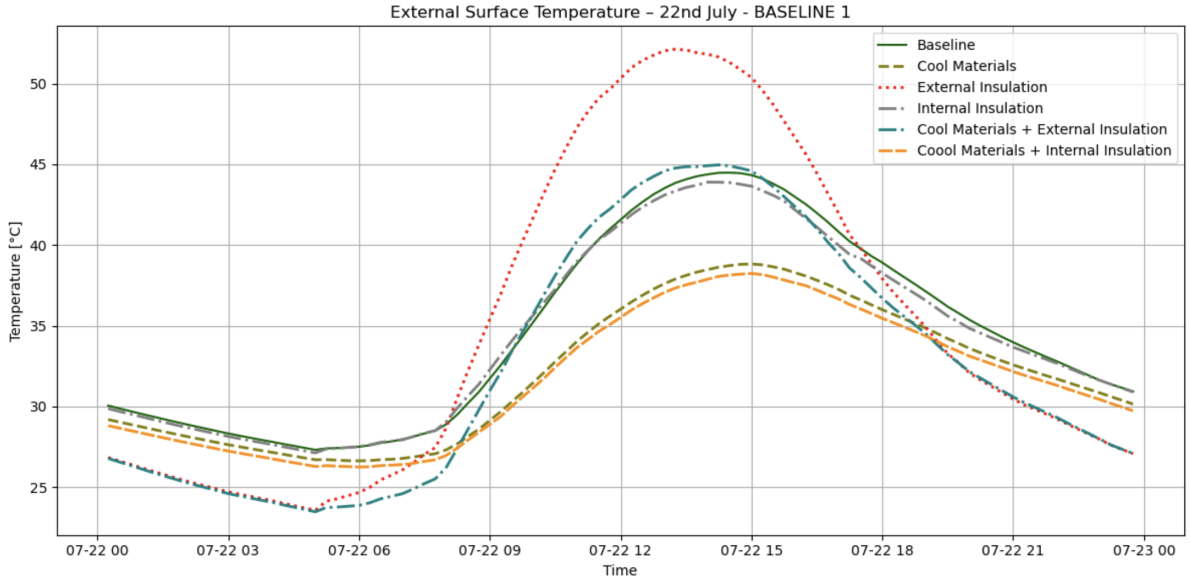

Figure 7.11: External Surface Temperature - Indoor Simulations

Figure 7.12 shows the internal Surface Temperature for the various scenarios. The internal Surface Temperature of the Cool Facade Scenario (i.e. the dashed green light line) is consistently lower than the Baseline (i.e. the continuous dark green line) by 0.5°C through the whole day. The internal Surface Temperature of the External Insulation Scenario (i.e. the pointed red line) is consistently lower than the Baseline by 0.25°C through the whole day. The Scenario Cool Facade + Internal Insulation, represented by the dashed yellow line, appears to be the worst scenario, as it reaches high temperatures during day-time, but during night-time it does not cool down as the Internal Insulation Scenario. For the Scenarios Internal Insulation, and Cool Facade + Internal Insulation, during the hottest hours of the day, the internal surface temperature is higher of about 1.5°C compared to the Baseline.

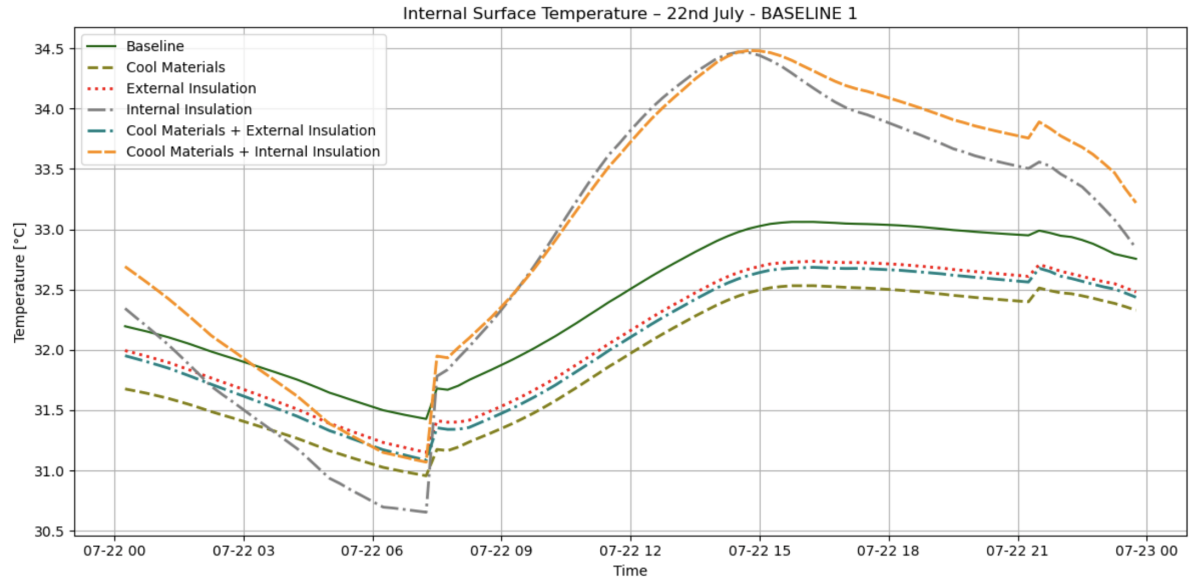

Figure 7.12: Internal Surface Temperature - Indoor Simulations

The Air Temperature comparison between the different scenarios is displayed in Figure 7.13. The Air Temperature of the Cool Facade Scenario is consistently lower than the Air Temperature of the Baseline, by 0.3°C circa. The External Insulation Scenario, and the combined one Cool Facade +

External Insulation give negligible results. The Internal Insulation Scenario is significantly worst than the Baseline conditions, in terms of warmer Air Temperature inside, of about 0.5°C in the hotter hours of the day.

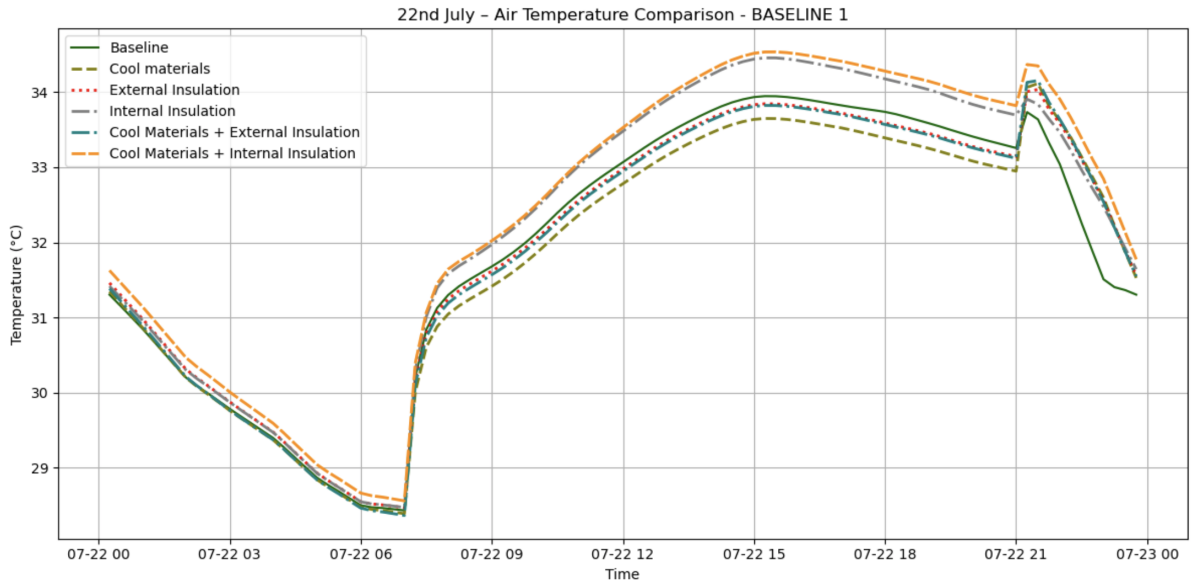

Figure 7.13: Air Temperature Comparison - Indoor Simulations

Figure 7.14 presents the Standard Effective Temperature (SET) values obtained for each scenario. The Scenario that exhibits the the lowest SET is the Cool Facade one, with a decrease of 0.25°C in SET for the warmer hours of the day. The Internal Insulation scenario and the combined Scenario Cool Facade + Internal Insulation have a negative impact on SET, resulting in higher SET values of about 0.3°C for the hottest hours of the day.

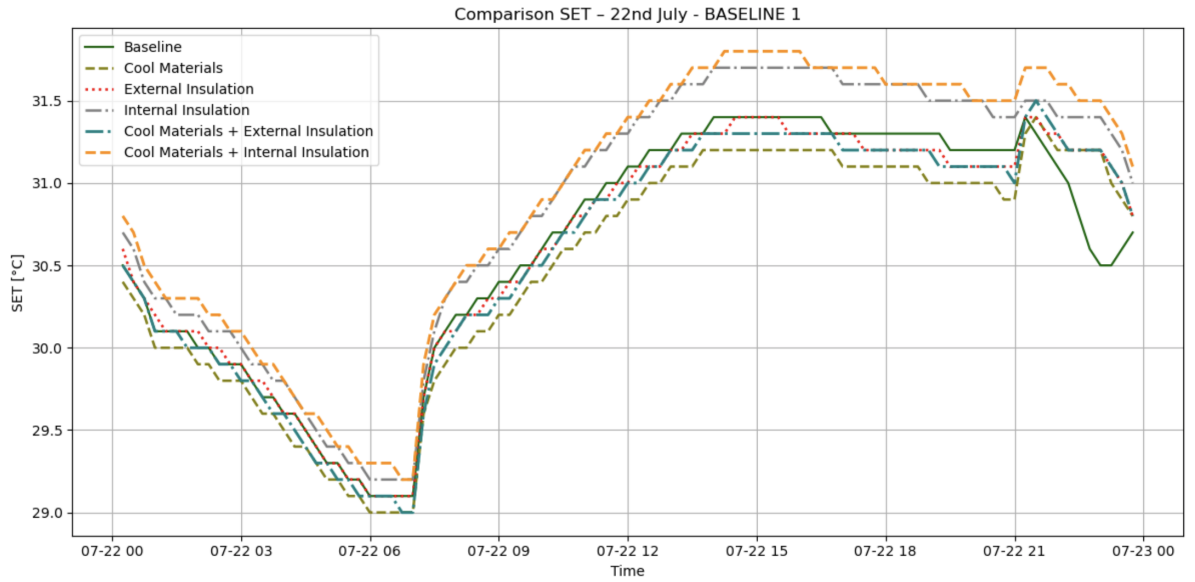

Figure 7.14: SET Comparison - Indoor Simulations

7.3. Baseline Comparison

To assess the influence of different aspect ratios on outdoor thermal comfort, a representative point located at the center of each street canyon was selected. The corresponding Mean Radiant

Temperature, Air Temperature, Wind Speed, and PET values at these points were computed and are presented in this section.

A comparison between the Mean Radiant Temperature (T_{mrt}) of the Baseline 1 and the T_{mrt} of Baseline 2 is shown in Figure 7.15. The T_{mrt} of Baseline 1 is higher than the T_{mrt} of the Baseline 2 during night-time, and lower during day-time. For the night-time trend, the beginning of the graph is considered (the night between the 21st and the 22nd of July) and not the end (the night between the 22nd and the 23rd of July), since the simulations were done starting the 21st of July in order to stabilize the model, while the last hours of the 22nd of July were the end of the simulations.

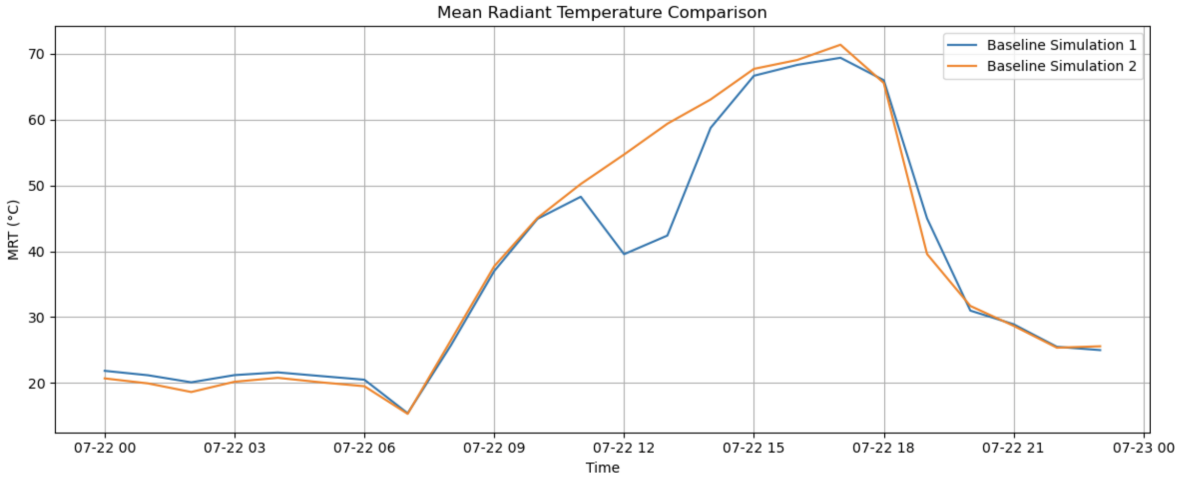

Figure 7.15: Mean Radiant Temperature Comparison

Figure 7.16 shows the Air Temperature comparison between the Baseline 1 and the Baseline 2. The air temperature is consistently lower for the Baseline 1 compared to the one of the Baseline 2, except for the afternoon hours.

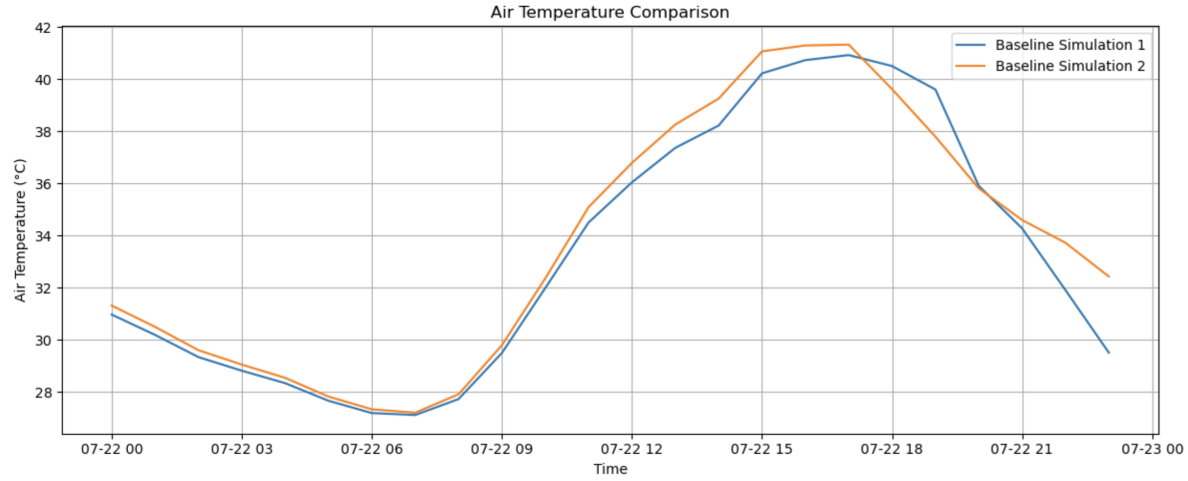

Figure 7.16: Air Temperature Comparison

Figure 7.17 shows the wind speed comparison for the same point for the two baseline simulations. The wind speed of the Baseline 2 (i.e. model with the smaller H/W ratio) is consistently higher than the wind speed of the Baseline 1 (i.e. model with the larger H/W ratio).

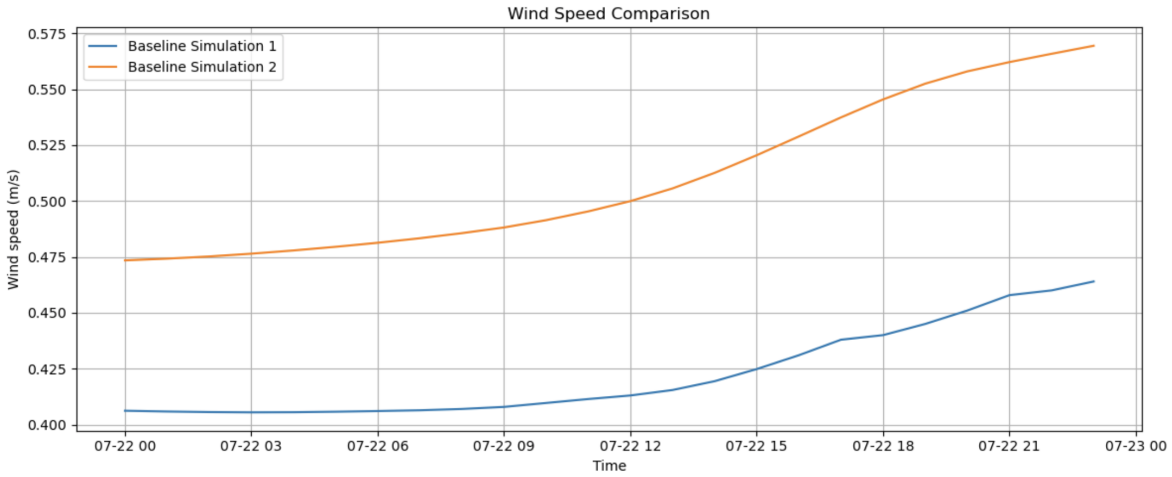

Figure 7.17: Wind Speed Comparison

Figure 7.18 shows a comparison between the PET of Baseline 1 and the PET of Baseline 2. Baseline 1 exhibits significantly lower PET values than Baseline 2 during the daytime. However, during nighttime hours, Baseline 1 performs worse. Baseline Simulation 2 shows a steeper nighttime decrease in PET values.

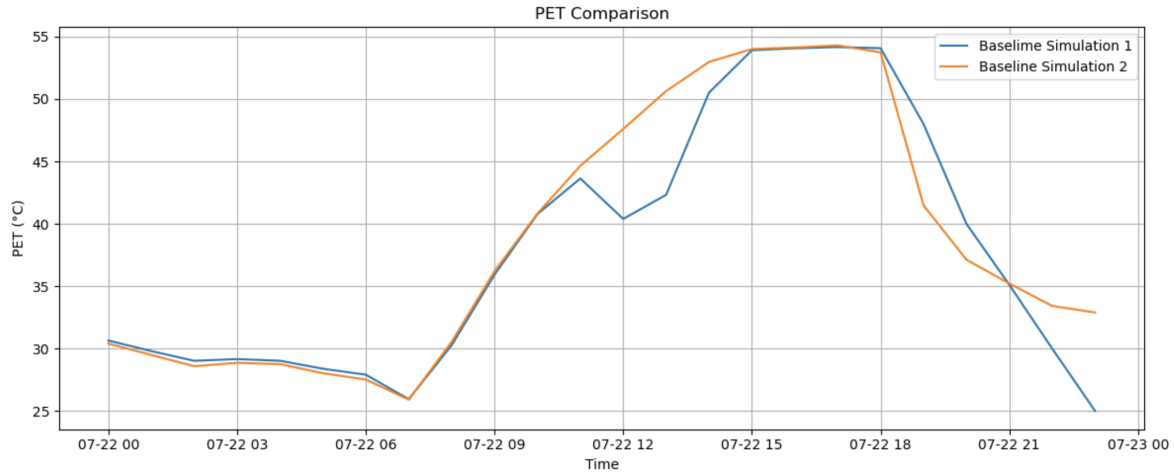

Figure 7.18: PET Comparison

The four box plots below illustrate the temperature differences (ΔT) between the baseline and each retrofitting scenario. The comparison is based on four variables: external surface temperature, internal surface temperature, indoor air temperature and SET.

$$\Delta T = T_{scenario} - T_{baseline} \tag{7.1}$$

By displaying the ΔT, when the box plots are above the zero line, it means that the scenario produces an increase in temperature, while when the box plots are under the zero line, it means that the scenario produces a drop in temperature. Summarizing, if:

- $\Delta T < 0$: the application of the retrofitting strategy produced a drop in temperature compared to the baseline;
- $\Delta T > 0$: the application of the retrofitting strategy increased the temperature compared to the baseline;
- $\Delta T \approx 0$: the application of the retrofitting strategy had a negligible effect.

The canyon with the larger H/W ratio is shown with the green box plots, while the canyon with the smaller H/W ratio is shown in orange. The box spans from the first to the third quartile (Q1–Q3), (i.e., the interquartile range (IQR)). The line inside the box plot is the median. The black point represents the mean value. The gray points are single observations. The main purpose of these plots is to highlight how each scenario performs differently depending on the baseline to which it is applied.

Figure 7.19 displays the difference between the external surface temperature of the various scenarios compared with the baseline. As illustrated in the graph, in the scenarios where a cool facade is present, the baseline with a smaller aspect ratio has a lower mean compared to the other baseline.

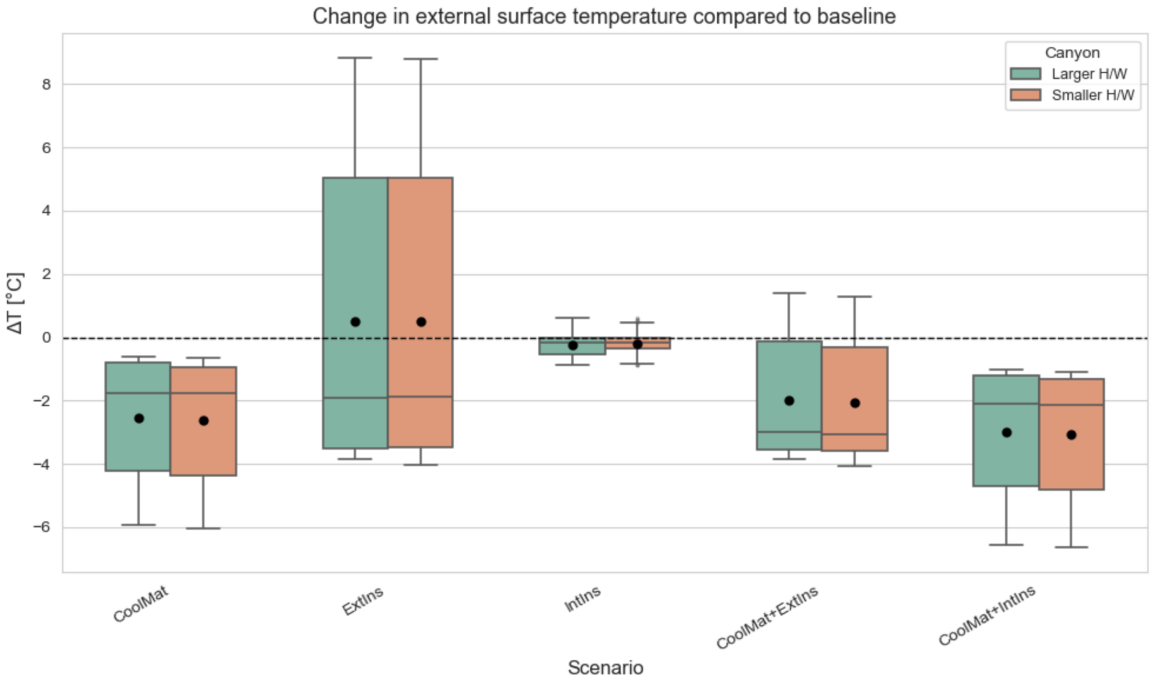

Figure 7.19: Change in external surface temperature compared to the Baseline 1 and 2

Figure 7.20 shows the difference between the internal surface temperature of the various scenarios compared with the baseline. Once again, the graph shows a lower mean value for the baseline with the smaller aspect ratio. On the contrary, the canyon with the larger aspect ratio exhibits a lower mean value for the internal insulation scenario.

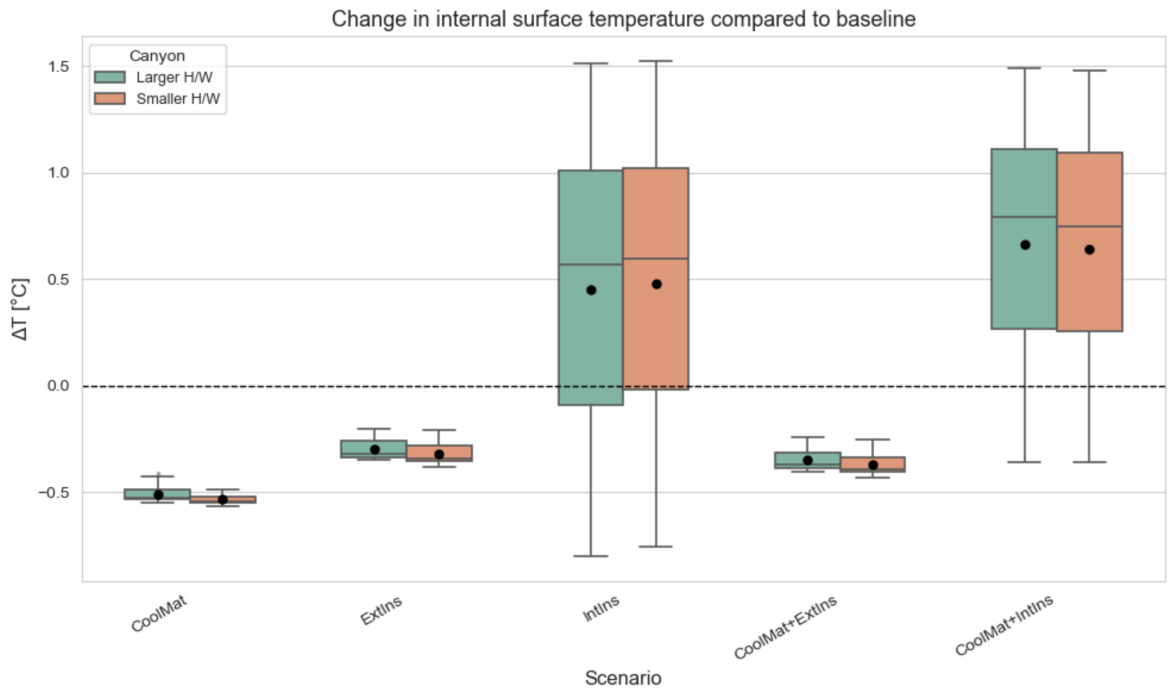

Figure 7.20: Change in internal surface temperature compared to the Baseline 1 and 2

Figure 7.21 shows the difference between the indoor air temperature of the various scenarios and the baseline. Across all scenarios, a consistent trend emerges: the mean values of ΔT are lower for the canyon with the smaller aspect ratio

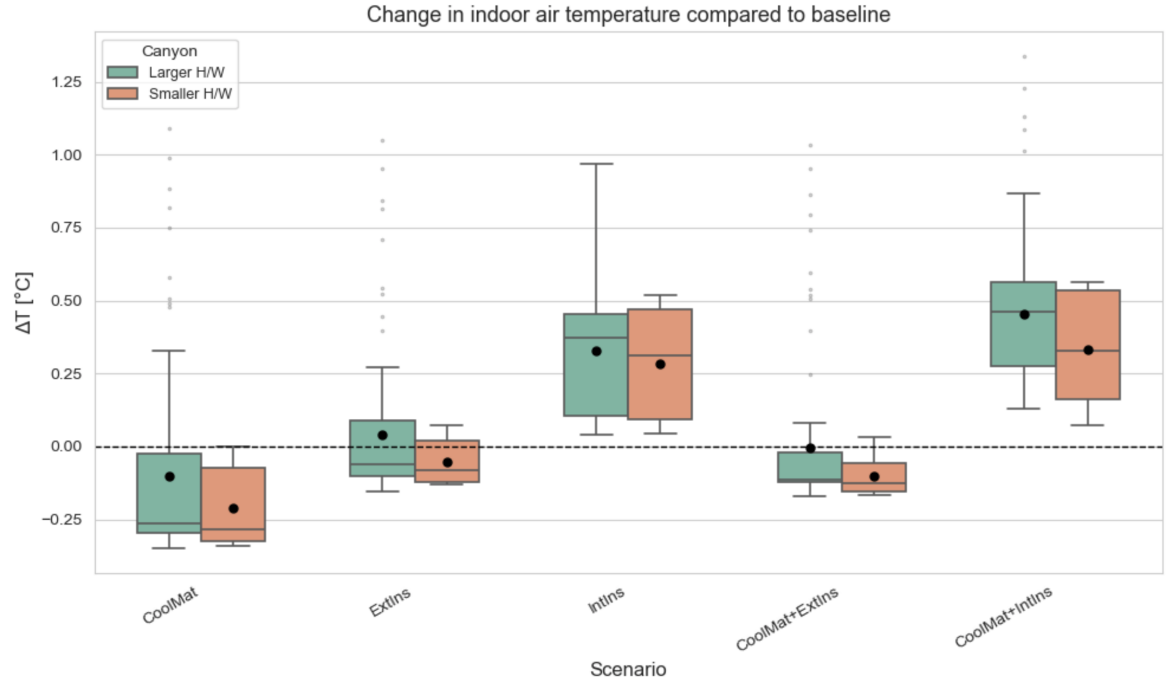

Figure 7.21: Change in indoor air temperature compared to the Baseline 1 and 2

Figure 7.22 shows the difference between the Standard Effective Temperature of the various scenarios with the baseline. According to the trend observed for the indoor air temperature, the mean values of ΔT are lower for the wider canyon (i.e. Baseline 2).

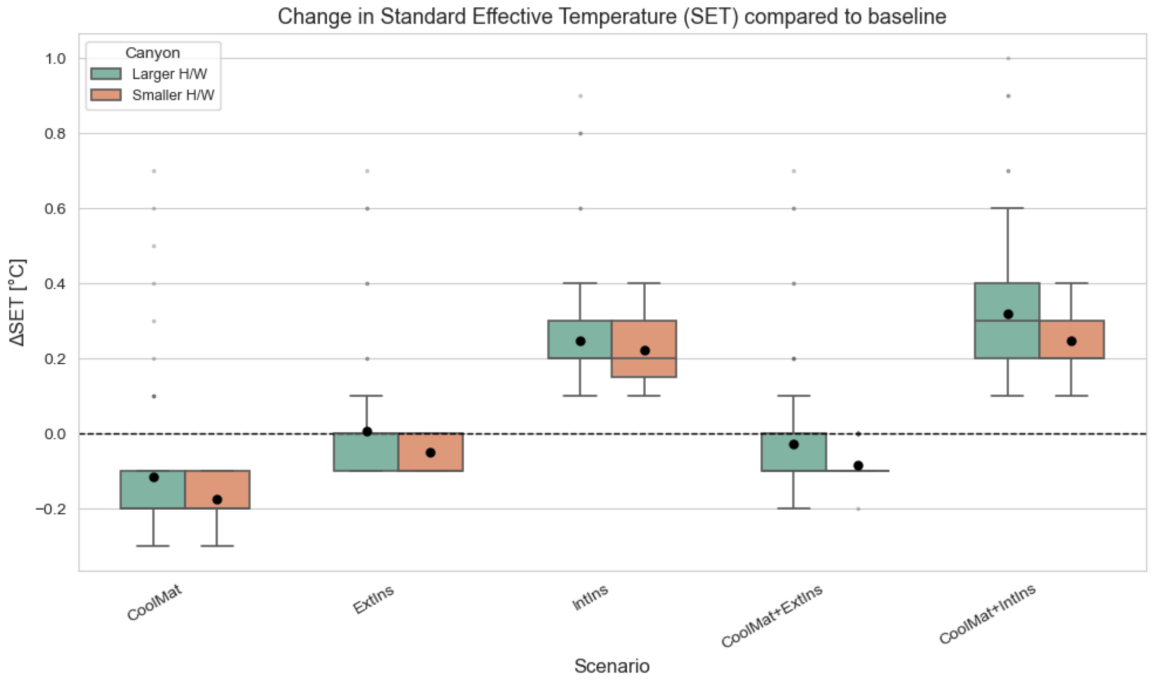

Figure 7.22: Change in SET compared to Baseline 1 and 2

8

Discussion

In this chapter, the results for both indoor and outdoor simulations are discussed, highlighting the interpretation, the implications, the limitations and recommendations. This chapter aims to answer the question: *How do the facade parameters, environmental parameters and urban geometry characteristics influence thermal comfort?*

8.1. Interpretation

This section provides a comprehensive interpretation of the simulation results presented in Chapter 7. The discussion is structured around four main parts: the effect of cool facades, the impact of insulation considering diverse configurations, and the influence of different aspect ratios on thermal comfort.

Cool Materials

The application of cool materials on buildings' facade is currently trending in research, as they have the potential to stabilize the air temperature indoor, and therefore reducing the cooling load of buildings during summer. Their effect on outdoor thermal comfort, however, is difficult to assess.

The outcomes of this research, illustrated in Chapter 7, indicate that applying cool coatings to the facade has a detrimental effect on outdoor thermal comfort. This is true for the entire canyon, but there are some areas whose PET is visibly more affected by the cool coatings. These areas are the courtyards. This happens because in the courtyards the reflection from a facade gets reflected again from the other adjacent facades, and the radiation gets trapped inside this mechanism, called inter-reflection. In fact, it can be seen from the comparison maps, that not only the courtyards' PET is more affected than the rest of the street from cool coatings, but also the narrower areas are more affected than the wider ones (e.g. the smaller streets between adjacent buildings compared to the wider main street). This phenomena is also observed by comparing the map for the Baseline 1 with the map of the Baseline 2. In the canyon with the larger aspect ratio, the PET increases more in the street, while in the wider canyon (i.e. smaller aspect ratio) the main street is not affected as much by the cool coatings. This happens because in the wider canyon, the distance between the buildings is enough for the radiation to escape back to the sky instead of being trapped inside the canyon.
The way cool facades affect indoor thermal comfort is clear from the simulations and coherent with what is expected, however almost negligible. Applying cool materials could lower the SET of about 0.25°C, but it can be discussed if such negligible improvement of the indoor conditions is worth the detrimental effects that cool materials have on outdoor thermal comfort.

The outcomes of the present study do not fully reflect what is often stated in studies on cool coatings. As an example, the review on cool coatings by Pisello [86] is reported. In the introduction of this study it is stated that *"cool coatings over building envelopes and urban pavements produce an improvement in indoor and outdoor thermal comfort conditions"* [86]. The papers cited to prove this

statement, however, do not take into consideration cool facades, but only cool roofs.

It is common in the existing literature on cool coatings, especially the studies conducted on energy efficiency, to draw the same conclusions on the outdoor behavior for cool roofs, cool facades and cool pavements, creating confusion and generalizing. This is a clear sign that research is still needed on the topic of cool coatings and their effect on outdoor thermal comfort. To generalize between cool roofs and facades, and assuming that they have the same effect on the microclimate, is not only misleading, but it is wrong. Indeed, the key distinction between the effects of cool roofs and cool facades on outdoor thermal comfort, lies in the inter-reflection between surfaces, which is also the driving factor of the results of the present work.

Another relevant study is that conducted by Taleghani et al. [90], which is often referred to in other studies as the demonstration that cool coatings improve outdoor thermal comfort. The objective of this study was to analyze how different cool facade orientations could affect outdoor thermal comfort. The conclusion of this research is that different orientations of cool facades produce different PET reductions. However, the phenomenon of the inter-reflection is not accounted for in this study, due to its methodology. The ENVI-met model created for this research consists of a perfectly symmetrical series of all identical buildings one next to each other, with various rows. Multiple scenarios were tested, where, one at a time, the facades with a certain orientation are assigned cool material properties (e.g. for the first scenario, all - and just - the north facades are cool facades). By doing so, because of the perfectly symmetrical model, for every scenario it never happens that one cool surface is exposed to another cool surface, therefore no inter-reflection occurs.

In conclusion, although several scientific studies state clearly that cool facades could improve - also - outdoor thermal comfort, all of them do not consider the entire complexity of the problem in their methodology or in their review.

Despite this, there are also studies who do consider the inter-reflections between surfaces, and whose results do confirm what is found in the present study. A relevant one is the one by Salvati et al. [22], which clearly states that increasing surface reflectance in urban canyons could lead to detrimental effects due to inter-reflections. In another study, conducted by Levinson [91], it is demonstrated that the effectiveness of cool facade in reducing the building cooling load is reduced in narrower urban canyons, which is aligned with the findings of the present research.

The net impact of cool coatings on thermal comfort is uncertain and difficult to assess due to the high dependence of the results on urban geometry. In this study, the detrimental effect of cool facade on outdoor thermal comfort is demonstrated through the outdoor simulations with Envi-met, and the phenomenon of the inter-reflections play a crucial role.

Insulation

Among passive retrofitting strategies, adding thermal insulation is one of the most employed in the Mediterranean area [40]. Generally, most studies on insulation as a retrofitting strategy are energy saving oriented, using large samples of buildings, and they often overlook other - sometimes - conflicting issues, as thermal comfort [41]. It is well established that adding insulation improves a building's energy efficiency in winter, and under some conditions also in summer. However, as temperature rises, summers get warmer, and heatwaves occur, some studies noticed that insulation may lead to overheating in buildings under certain conditions. A study conducted by Fang et al. [42] concluded that insulation could increase the cooling load of a building during summer.

In the present work, two insulation configurations were analyzed: namely, internal and external insulation. The two cases yielded markedly different outcomes.

The results obtained from the Envi-met simulations suggest that the effect of applying external insulation has a negative effect on outdoor thermal comfort, but it can overall be considered negligible. Similarly to the cool materials, the courtyards are the areas exhibiting the most significant

variations in PET. For the internal insulation case, the effect on outdoor thermal comfort is negligible and less evident compared to the external insulation. This result was expected, as the response of the internal insulation is mitigated by the thermal mass of the building. There is no existing literature on the effect that insulation has on outdoor thermal comfort, however, it can be concluded from the results of the current study that the effect is negligible for both cases.

The outcomes of the EnergyPlus simulations are more significant, and are consistent with the existing literature. They can be summarized as: while the application of external insulation leads to improvements in indoor air temperature and Standard Effective Temperature (SET), the use of internal insulation results in a general deterioration of thermal comfort. The existing literature agrees that under certain circumstances, internally insulated buildings could experience overheating during summer, as Stazi et al. [41] concluded by comparing various insulation configurations and types. The configuration with external insulation provided improved thermal performance in both summer and winter. There are many other studies that concluded that external insulation performs better than internal insulation in summer. Relevant studies include Kossecka and Kosny [44] and Basaly et al. [43].

In order to validate the EnergyPlus simulation results, this study compares them with experimental findings reported in previous literature. The study conducted by Larsen, Filippín, and Lesino [92] presents an experimental investigation on the monitoring two student housing units in Argentina during a summer week. The two units are identical in layout and orientation, with the only difference being the facade configuration: the reference unit consists in solid masonry, and the other unit presents insulation (EPS) in an external configuration. The data gathered involved external and internal superficial temperature, internal air temperature and thermal comfort metrics. This experiment was carried out under real-usage conditions, with people present, internal heat gains, and natural ventilation.

By contrast, in the present work, a simplified numerical model (i.e. a test cell) was modeled in EnergyPlus, with the objective of isolating the facade effects on the indoor environment. The model consists in a cube with just one wall exposed to the outdoor conditions, and the other surfaces (walls, roof, ceiling) are modeled as adiabatic. There are no internal heat gains, no users, and a constant natural night ventilation rate is applied.

The differences in the results obtained are consistent with the different modeling settings. In the study by Larsen, Filippín, and Lesino [92] the externally insulated wall led to a significant reduction in the temperature of the external surface (2–3°C) and also in the internal air temperature (up to 1.2°C). Similarly, in the present study, the internal air temperature of the external insulated case shows a decrease compared to the baseline. However, the magnitude of the decrease is considerably smaller (approximately 0.1°C). This discrepancy can be attributed to the fact that under real conditions, all walls present in a room participate in dissipating the heat inside the room. This does not happen in the model of the present work because three walls, the ceiling and the roof are modeled adiabatic. Moreover, in the experimental real case the adaptive behavior of the users could help with keeping the units cooler.

Unlike the study by Larsen, Filippín, and Lesino [92], the results of the present study show an increase in external surface temperature. It is important to mention that in the current work, the external insulation is in direct contact with the plaster, while in the comparison study, a ceramic brick layer is present at the outer side before the insulation. This additional mass contributes to moderating temperature fluctuations. Moreover, the current study is conducted under heatwave conditions, subjecting the building envelope to more extreme conditions compared to a normal summer day, which is the setting of the comparison study.

To further interpret these findings, another experimental study conducted by Chaumont et al. [93] is analyzed. In their research four roof configurations were tested, changing the position of the insulation (external or internal) and varying the reflectance of the surface (standard or cool roof). The roofs were built as real prototypes and were tested in a controlled simulated heatwave condition

in a climatic chamber with artificial solar radiation. During the test, internal and external surface temperatures were monitored as well as heat fluxes. The outcomes suggest that during strong irradiation, there is a significative increase in the external surface temperature.

Combined scenarios

Combined scenarios were tested to understand how the indoor and outdoor thermal comfort was changing under the coupled effect. The two configurations investigated were the combination of Cool Facade with External Insulation, and Cool Facade with Internal Insulation

Combining cool facade and external insulation gave expected results. From the outcomes of the Envi-met simulations, it is observed that the combined scenario leads to even poorer outdoor thermal comfort than the Cool Facade scenario alone, which was expected as the external insulation scenario was also worsening the PET compared to the baseline.

Focusing on the indoor settings, in term of external surface temperature, this scenario mirrors the performance of the external insulation case during night-time hours. This is explained by the fact that cool materials influence the heat transfer within the wall system primarily when exposed to solar radiation. Hence their effect is significant mainly during daytime hours. From sunrise to sunset, the cool materials have a clear effect on lowering the external surface temperature for this combined scenario. The internal surface temperature is also coherent with the expectations: the combined scenario has a lower temperature, giving that both Cool Facade and External Insulation separately had a lower temperature compared to the baseline. The indoor air temperature of the combined scenario has the same behavior as the external insulation case. This can be attributed to the fact that indoor air temperature is influenced by multiple variables, including radiation from internal surfaces. However, other factors — such as the wall system's ability to dissipate heat into the room — also play a significant role.

Combining Cool Facade and Internal Insulation gave more complex results. For outdoor simulations, the results are coherent from what was expected, as there is a slight improvement in outdoor thermal comfort compared to the cool facade scenario, and the internal insulation scenario alone had a slight improvement on outdoor thermal comfort compared to the baseline.

Focusing on the indoor simulations outcomes, the most surprising result is that this combined scenario (i.e. Cool Facade and Internal Insulation) is worse for indoor thermal comfort than the Internal Insulation scenario alone. These results are less straightforward and require more nuanced interpretation compared to those of the other combined scenario.

The internal surface temperature analysis indicates that during day-time the curve of the combined scenario has a smaller temperature jump at 07:00 compared to the Internal Insulation only. The reason this scenario exhibits the poorest performance among all is primarily attributable to its night-time behavior. During night-time, the room is not cooling down efficiently as it was with just the internal insulation - and without the cool materials. This is due to the fact that cool materials, besides having high reflectance, also exhibit high emissivity, implying that during night-time, the surrounding cool facades are releasing the heat that had been stored during the day. The challenge of integrating the aforementioned aspects with internal insulation lies in the fact that internal insulation has clear overheating issues, so, if more heat enters the system, the situation gets worse. This result is especially interesting and calls for deeper investigation.

The existing body of literature on this topic (i.e., combined scenarios) is limited; however, a few studies report outcomes that align with the findings of the present study. Chaumont et al. [93] studied four roof samples, one with external insulation, one with internal insulation, one with external insulation and a cool coating, and one with internal insulation and a cool coating. Their behavior was analyzed during a heatwave. They concluded that, in terms of outdoor air temperature, the behavior of the sample with external insulation and a cool coating was almost the same as the sample with just external insulation during night-time. While, for the internal insulated sample,

the night-time convective exchanged were slightly reduced, and the heat storage in the medium (i.e. concrete layer) was more than halved, which is consistent with the findings of the present study. From the results of the current study it was observed that, in terms of external surface temperature, the external insulated scenario was having the same behavior of the combined scenario cool facade + external insulation during night time, while the internal insulated scenario was having a slight reduction of temperature. Chaumont et al. [93] concluded that the sample that minimizes both the impact on the local microclimate and on the inside the building was the external insulation one with the addition of a cool coating. He also emphasized how, if surrounding buildings are present, the radiative roof might compromise the surrounding buildings, and the application of just the external insulation could be a valid alternative.

Aspect ratio

This section provides a comparative analysis of the results obtained for the two different canyons (.e. Baseline 1 and Baseline 2) aiming to highlight how different aspect ratios influence both indoor and outdoor thermal comfort.

A brief overview on the two baseline simulations is provided first. Baseline Simulation 1 is the model with the larger aspect ratio, meaning that the ratio between the height and the width of the canyon is higher. The Baseline Simulation 2 is the same exact model, with the same building's number and typology, but with a smaller aspect ratio. Given that the building height is the same in this analysis, Baseline 1 is the narrower street, while Baseline 2 the wider one.

To investigate the differences between the two cases, the behavior of the key variables influencing outdoor thermal comfort was analyzed with reference to a point located at the center of the street canyons.

The mean radiant temperature of Baseline 1 is lower than the mean radiant temperature of Baseline 2 during the day (Figure 7.15). During the night it is higher. This happens because during the day-time in the canyon with the larger H/W ratio, less radiation arrives inside of the canyon as there is more shading. However, during the night-time, the greater the aspect ratio of the canyon, the more the radiation gets trapped inside the canyon. The dump in the mean radiant temperature at 12:00 is due to the fact that for just two hours the selected point - for the Baseline 1 - is shaded by a taller building, but after two hours it is not shaded anymore. This does not happen in Baseline 2 due to the wider street. A similar behavior is observed for the PET curves. The wind speed is higher in Baseline 2, due to the smaller aspect ratio, as expected.

Having clarified the behavior of these variables at the center of the street canyon, a more rigorous analysis of the boxplot graphs (Figure 7.19, 7.20, 7.21, 7.22) can be conducted. These plots aim to highlight how different retrofitting scenarios perform under varying aspect ratio configurations. From the comparison of the SET it can be concluded that applying retrofitting strategies gives a better outcome (in terms of decrease of temperature compared to the baseline) for the wider canyons (i.e. smaller H/W ratio). This can be interpreted as a consequence of two main driving factors: the inter-reflections and the increased wind speed in Baseline 2. The Baseline 2, having a wider canyon, has an increased wind speed, which is a fundamental favorable aspect for thermal comfort. Additionally, the inter-reflections are lower in Baseline 2, due to the smaller aspect ratio.

8.2. Implications

The present work contributes to the ongoing research on passive retrofitting strategies aimed at improving thermal comfort both indoor and outdoor during extreme heat events.

The results of the current study provide valuable insights that can inform future decisions regarding retrofitting planning. Specifically, the results underscore the importance of context-sensitive retrofitting. While some retrofitting strategies may enhance indoor thermal comfort, they could

be detrimental for pedestrian comfort. This implies that facade retrofitting should not be solely evaluated based on their energy performance, but also on the effect they have on the microclimate. Beyond the specific case study, these results suggest that it is of utmost importance that the studies on energy retrofitting, and in general the ones with an energy saving approach, start questioning in their research process the urban consequence that their outcomes have. A more holistic approach is needed.

Furthermore, this work emphasizes the necessity of including urban geometry variables in the evaluation of facade retrofitting strategies. Canyon geometry, such as aspect ratio and sky view factor, plays a crucial role by controlling solar access and influencing wind speed within the canyon. Moreover, at a smaller scale, the geometry of the building itself should be considered in the analysis, as courtyards exhibit different thermal behavior compared to other building configurations.

The findings of the present work raise awareness on the limitation of the current research approach to the cool materials, which tends to generalize their benefits. While these materials may be beneficial in stabilizing the indoor air temperature, their use on vertical surfaces should be carefully evaluated in dense urban areas.

Lastly, this work highlights the necessity for a multi-criteria assessment in the evaluation of retrofitting strategies. It is crucial to integrate geometric factors at both the urban and building scale, along with outdoor and indoor thermal comfort. Such an approach enables interventions to deliver balance benefits across different performance objectives and to inform resilient and context-appropriate design decisions.

8.3. Limitations

This section outlines the main limitations of the present study, which should be taken into account when interpreting the results and considering their applicability to other contexts.

The present research was designed as a controlled-variable experiment. However, despite efforts to minimize the number of variables, many factors still affected the behavior of the simulated scenarios. This prevented a precise quantitative assessment of the relative contribution of each variable to the outcomes. Given the already extensive computational time, conducting a sensitivity analysis of each variable was not doable within a six-month project. Nevertheless, the adopted approach provided clear trends and meaningful insights, which are a strong basis for future research.

The results found for the indoor environment are valid only for a night natural ventilation scenario, with no occupants, internal heat gains, or equipment considered in the model. This choice was made to simplify the model, ensuring more controlled results and reducing variables dependency. However, the findings cannot be extended for other type of ventilated scenarios or to buildings with HVAC systems, which are expected to behave differently. Nonetheless, these simplification allowed to have a clear pattern in the results.

It is important to mention that the outcomes of the present study are strongly dependent on the geometry of the case study. While this represents one of the key conclusions of the study, it also limits the extent to which general remarks on retrofitting strategies can be drawn.

Moreover, the outcomes of the current research can not be taken as comprehensive guidelines for retrofitting strategies, as they are based solely on heatwave conditions and do not consider other scenarios or seasons. The present research aimed to explore the complex trade-offs that arise when retrofitting for energy savings while also accounting for outdoor thermal comfort. However, it does not address the fact that a passive retrofitting strategy must perform effectively throughout the entire year, not only in summer.

8.4. Recommendations

Based on the findings of this study, several recommendations can be made to guide future research and practice.

The present research has examined how different passive retrofitting strategies perform during a heatwave. Future studies should aim to find solutions that have a good thermal performance all over the year - even if it is important to continue studying how buildings respond to heatwaves. This should include the assessment of retrofitting strategies across all seasons. Furthermore, given that the climate is constantly evolving, future climate scenarios must also be considered.

Green facades were not explored in the present work due to computational time constraints. However, assessing the impact of the latent heat flux of a green facade during a heatwave would be an interesting direction for future research. Furthermore, the current study only focused on vertical surfaces of the built environment, while also the horizontal ones, such as roofs and pavements should be evaluated.

A key finding of the current research was the inter-reflection between surfaces that occurred when cool coatings were applied. Further investigation is needed to better understand this phenomenon and to identify strategies to minimize it. For instance, future study could explore directional radiative cooling.

Moreover, the topic of this research is particularly relevant due to the large number of variables involved, spanning diverse fields such as urban morphology, microclimate, facade systems, energy efficiency, thermal comfort. For this reason, it would be interesting to implement a machine learning tool capable of learning from a large dataset of real world cases and draw general guidelines for retrofitting strategies.

Conclusion

This present study contributes in the field of facade engineering and architectural engineering, in particular to that of passive retrofitting strategies research. The main research question:

> *How do different retrofitting strategies influence outdoor and indoor thermal comfort during a heatwave?*

is answered by compiling the key findings of each sub-question.

This research aimed to evaluate how different retrofitting strategies influence both outdoor and indoor thermal comfort. The strategies investigated included cool facades, insulation (external and internal), and their combinations. Based on scenario simulations, it can be concluded that the effectiveness of diverse retrofitting strategies is highly dependent on the geometry and the characteristics of the built environment. Engineers have to assess case specific investigations before retrofitting a building's facade, as the surrounding conditions are different for every case. In this context, if the research on energy efficiency of buildings is extended to human well-being in the built environment, then studies with large samples of buildings lose their validity, as they are not context appropriate.

The first key methodological aspect in bridging indoor and outdoor thermal comfort was the lack of a common metric. Indices used for the indoor environment cannot be applied to outdoor settings, and vice versa, due to the substantially different boundary conditions. A multi-metric approach is therefore required. Based on a comprehensive literature review, SET* was selected for evaluating indoor thermal comfort, while PET was chosen for assessing outdoor thermal comfort. Although these two indices differ in their underlying assumptions, such differences can be reasonably overlooked within the scope of this study.

The parameters influencing indoor and outdoor thermal comfort were divided into facade parameters, environmental parameters, and urban geometry characteristics. To clearly represent the relationship between each parameter, a thermal model was developed. To evaluate and isolate the influence of specific facade and urban geometry parameters on thermal comfort, a matrix of simulation scenarios was defined, with each scenario being tested for both indoor and outdoor.

Cool facades were found to improve indoor thermal comfort, but could be detrimental to outdoor thermal comfort due to the inter-reflection between surfaces, with courtyards being the most affected areas. Insulation showed a negligible effect on outdoor thermal comfort; however, for indoor conditions, internal insulation could lead to overheating of the building. When combined with cool facades, internal insulation exacerbated this overheating issue, whereas combining cool facades with external insulation did not give any significant difference compared to the external insulation case. A wider street canyon resulted in a beneficial effect for indoor thermal comfort, but not for outdoor thermal comfort, where the shaded hours were reduced.

To better understand the implications of these results, future studies could address a wider range of climatic conditions and seasons, explore different strategies and geometry configurations, and evaluate their long-term performance.

The research on retrofitting strategies was being carried in parallel on two binaries: mitigating the urban heat island effect, and improving the energy efficiency of the buildings. The present work contributes to the ongoing research on passive retrofitting strategies by demonstrating, through its methodology and outcomes, the importance of evaluating both indoor and outdoor performance of retrofitting strategies. This integrated approach helps avoid fragmented analysis and partial

evaluation.

The findings of the current work highlight the importance of performing context-appropriate assessments. Energy retrofit studies often analyze large building samples, regardless of their location and surroundings. While this approach could yield more general results, it is debatable whether such results are useful if then they are not applicable to real-world cases. To address this issue, a holistic approach should be incorporated into energy-oriented studies.

Ultimately, this study demonstrates the crucial role of urban geometry in evaluating retrofitting performance. A multi-criteria assessment that integrates outdoor and indoor thermal comfort with both urban and building-scale geometry is essential to ensure interventions are effective and context-sensitive.

Bibliography

[1] UNFCCC. *Seven Ways Cities Can Take Climate Action*. Accessed: 2025-03-17. 2020. URL: https://unfccc.int/news/seven-ways-cities-can-take-climate-action.

[2] Paola Lassandro and Silvia Di Turi. "Multi-criteria and multiscale assessment of building envelope response-ability to rising heat waves". In: *Sustainable Cities and Society* 51 (2019), p. 101755.

[3] Arjan Droste. *Urban Climate*. Lecture notes from the course *CEGM2001 Sustainable Cities*, TU Delft. Accessed during coursework. 2025.

[4] Samah A Abrahem, Susan Abed Hassan, and Wurood Adeeb Khamees. "Impact of Façade Material of Mass Housing on Outdoor Thermal Comfort in Hot-arid Climate". In: *IOP Conference Series: Materials Science and Engineering*. Vol. 881. 1. IOP Publishing. 2020, p. 012006.

[5] Tuukka Petäjä et al. "Chapter 15 - Air quality and the environmental impacts". In: *Air Quality*. Ed. by Ranjeet S. Sokhi. Elsevier, 2025, pp. 439–462. ISBN: 978-0-12-822591-2. DOI: https://doi.org/10.1016/B978-0-12-822591-2.00015-9. URL: https://www.sciencedirect.com/science/article/pii/B9780128225912000159.

[6] Saghar Hashemi. "Assessing Microclimate and Outdoor Thermal Comfort in the Urban Environment: A Case Study of Auckland, New Zealand". PhD thesis. Auckland University of Technology, 2024.

[7] Timothy R Oke. "The energetic basis of the urban heat island". In: *Quarterly journal of the royal meteorological society* 108.455 (1982), pp. 1–24.

[8] Surjamanto Wonorahardjo et al. "Effect of different building façade systems on thermal comfort and urban heat island phenomenon: An experimental analysis". In: *Building and Environment* 217 (2022), p. 109063.

[9] Jihui Yuan, Craig Farnham, and Kazuo Emura. "Effect of different reflection directional characteristics of building facades on outdoor thermal environment and indoor heat loads by CFD analysis". In: *Urban Climate* 38 (2021), p. 100875.

[10] Eduardo L Krüger. "Urban heat island and indoor comfort effects in social housing dwellings". In: *Landscape and Urban Planning* 134 (2015), pp. 147–156.

[11] John Patrick Connors, Christopher S Galletti, and Winston TL Chow. "Landscape configuration and urban heat island effects: assessing the relationship between landscape characteristics and land surface temperature in Phoenix, Arizona". In: *Landscape ecology* 28 (2013), pp. 271–283.

[12] Soha S Tabatabaei and Rima Fayaz. "The effect of facade materials and coatings on urban heat island mitigation and outdoor thermal comfort in hot semi-arid climate". In: *Building and Environment* 243 (2023), p. 110701.

[13] Elmira Jamei et al. "Review on the impact of urban geometry and pedestrian level greening on outdoor thermal comfort". In: *Renewable and Sustainable Energy Reviews* 54 (2016), pp. 1002–1017.

[14] Bouthaina Sayad et al. "Microscale investigation of urban heat island (UHI) in Annaba City: Unveiling factors and mitigation strategies". In: *Sustainability* 16.2 (2024), p. 747.

[15] LCM Itard et al. "Fundamental Aspects of Thermal Comfort". In: (2004).

[16] Xiaoyu Du. "A review of thermal comfort". In: *A+BE | Architecture and the Built Environment* 9.10 (2019), pp. 49–68. DOI: 10.7480/abe.19.10.4103. URL: https://journals.open.tudelft.nl/abe/article/view/4103.

[17] Floriberta Binarti et al. *A review of outdoor thermal comfort indices and neutral ranges for hot-humid regions*. Mar. 2020. DOI: 10.1016/j.uclim.2019.100531.

[18] Noël Djongyang, René Tchinda, and Donatien Njomo. *Thermal comfort: A review paper*. 2010. DOI: 10.1016/j.rser.2010.07.040.

[19] Ata Chokhachian et al. "How material performance of building façade affect urban microclimate". In: *Powerskin 2017*. 2017.

[20] Sijing Liu et al. "Comparative analysis on indoor and outdoor thermal comfort in transitional seasons and summer based on multiple databases: Lessons learnt from the outdoors". In: *Science of the Total Environment* 848 (Nov. 2022). ISSN: 18791026.

[21] Erik Johansson et al. "Instruments and methods in outdoor thermal comfort studies - The need for standardization". In: *Urban Climate* 10 (P2 2014), pp. 346–366. ISSN: 22120955. DOI: 10.1016/j.uclim.2013.12.002.

[22] Agnese Salvati et al. "Impact of reflective materials on urban canyon albedo, outdoor and indoor microclimates". In: *Building and Environment* 207 (2022), p. 108459.

[23] Ken Parsons. *Human thermal environments: the effects of hot, moderate, and cold environments on human health, comfort and performance*. CRC press, 2007.

[24] Andrea Martinez et al. "Fundamentals in façade retrofit practice". In: *Procedia engineering* 118 (2015), pp. 934–941.

[25] Patricia Edith Camporeale and Pilar Mercader-Moyano. "Retrofit strategies to mitigate overheating linking urban climate modeling and urban building simulations with outdoor comfort. An urban sector in Malaga (Spain)". In: *Energy and Buildings* 298 (2023), p. 113531.

[26] Paola Lassandro and Silvia Di Turi. "Façade retrofitting: from energy efficiency to climate change mitigation". In: *Energy Procedia* 140 (2017), pp. 182–193.

[27] Jiayu Li et al. "Study on a full-year improvement of indoor thermal comfort by different vertical greening patterns". In: *Journal of Building Engineering* 35 (2021), p. 101969.

[28] Juan A Acero et al. "Thermal impact of the orientation and height of vertical greenery on pedestrians in a tropical area". In: *Building Simulation*. Vol. 12. Springer. 2019, pp. 973–984.

[29] Lei Zhang et al. "Thermal behavior of a vertical green facade and its impact on the indoor and outdoor thermal environment". In: *Energy and buildings* 204 (2019), p. 109502.

[30] Tiziana Susca, Fabio Zanghirella, and Vincenzo Del Fatto. "Building integrated vegetation effect on micro-climate conditions for urban heat island adaptation. Lesson learned from Turin and Rome case studies". In: *Energy and Buildings* 295 (2023), p. 113233.

[31] SA Palermo and M Turco. "Green Wall systems: where do we stand?" In: *IOP conference series: Earth and environmental science*. Vol. 410. 1. IOP Publishing. 2020, p. 012013.

[32] Alexandra Medl, Rosemarie Stangl, and Florin Florineth. "Vertical greening systems–A review on recent technologies and research advancement". In: *Building and Environment* 125 (2017), pp. 227–239.

[33] Yaolin Lin et al. "A review on the impact of outdoor environment on indoor thermal environment". In: *Buildings* 13.10 (2023), p. 2600.

[34] Hayder Alsaad et al. "The potential of facade greening in mitigating the effects of heatwaves in Central European cities". In: *Building and Environment* 216 (2022), p. 109021.

[35] Xiaoli Hao et al. "Influence of vertical greenery systems and green roofs on the indoor operative temperature of air-conditioned rooms". In: *Journal of building engineering* 31 (2020), p. 101373.

[36] Jiayu Li and Bohong Zheng. "Does vertical greening really play such a big role in an indoor thermal environment?" In: *Forests* 13.2 (2022), p. 358.

[37] Fabiana Convertino et al. "Effect of leaf area index on green facade thermal performance in buildings". In: *Sustainability* 14.5 (2022), p. 2966.

[38] Ratih Widiastuti, Juliana Zaini, and Wahyu Caesarendra. "Field measurement on the model of green facade systems and its effect to building indoor thermal comfort". In: *Measurement* 166 (2020), p. 108212.

[39] Dongjin Cui et al. “Effects of different vertical façade greenery systems on pedestrian thermal comfort in deep street canyons”. In: *Urban Forestry & Urban Greening* 72 (2022), p. 127582.

[40] Carmen María Calama-González et al. “Optimal retrofit solutions considering thermal comfort and intervention costs for the Mediterranean social housing stock”. In: *Energy and Buildings* 259 (2022), p. 111915.

[41] Francesca Stazi et al. “Retrofitting using a dynamic envelope to ensure thermal comfort, energy savings and low environmental impact in Mediterranean climates”. In: *Energy and Buildings* 54 (2012), pp. 350–362.

[42] Zhaosong Fang et al. “The effect of building envelope insulation on cooling energy consumption in summer”. In: *Energy and Buildings* 77 (2014), pp. 197–205.

[43] Lucienne G Basaly et al. “Effects of retrofit strategies on thermal comfort and energy performance in social housing for current and future weather scenarios”. In: *Buildings* 15.1 (2024), p. 80.

[44] Elisabeth Kossecka and Jan Kosny. “Influence of insulation configuration on heating and cooling loads in a continuously used building”. In: *Energy and buildings* 34.4 (2002), pp. 321–331.

[45] Hylke E. Beck et al. “Present and future köppen-geiger climate classification maps at 1-km resolution”. In: *Scientific Data* 5 (2018). ISSN: 20524463. DOI: 10.1038/sdata.2018.214.

[46] Mohamed H. Elnabawi and Neveen Hamza. “Review on Gaps and Challenges in Prediction Outdoor Thermal Comfort Indices: Leveraging Industry 4.0 and ‘Knowledge Translation’”. In: *Buildings* 14 (4 Apr. 2024). ISSN: 20755309. DOI: 10.3390/buildings14040879.

[47] Tsuyoshi Honjo. “Thermal comfort in outdoor environment”. In: *Global environmental research* 13.2009 (2009), pp. 43–47.

[48] Dayi Lai et al. *A comprehensive review of thermal comfort studies in urban open spaces*. Nov. 2020. DOI: 10.1016/j.scitotenv.2020.140092.

[49] Manuel Carlos Gameiro da Silva. “Spreadsheets for the calculation of thermal comfort indices”. In: *Scribd* (2013).

[50] Fergus Nicol, Michael Humphreys, and Susan Roaf. *Adaptive thermal comfort: principles and practice*. Routledge, 2012.

[51] Richard De Dear and Gail Schiller Brager. “Developing an adaptive model of thermal comfort and preference”. In: (1998).

[52] Wenjie Ji et al. “Interpretation of standard effective temperature (SET) and explorations on its modification and development”. In: *Building and Environment* 210 (2022), p. 108714.

[53] Noah Sandoval et al. “Cooling–not weatherization–ensures access to livable indoor conditions for residential buildings in Los Angeles”. In: (2024).

[54] Janelle Pickup, Richard de Dear, et al. “An outdoor thermal comfort index (OUT_SET*)-part I-the model and its assumptions”. In: *Biometeorology and urban climatology at the turn of the millenium. Selected papers from the Conference ICB-ICUC*. Vol. 99. 2000, pp. 279–283.

[55] Oded Potchter et al. *Outdoor human thermal perception in various climates: A comprehensive review of approaches, methods and quantification*. Aug. 2018.

[56] Wenqiang Jing et al. “Evaluating thermal comfort indices for outdoor spaces on a university campus”. In: *Scientific Reports* 14.1 (2024), p. 21253.

[57] Peter Höppe. “The physiological equivalent temperature–a universal index for the biometeorological assessment of the thermal environment”. In: *International journal of Biometeorology* 43 (1999), pp. 71–75.

[58] Taiyang Huang et al. “Assessment of human thermal comfort during short-term exposure in hot and humid urban outdoor areas”. In: (2022).

[59] Edouard Walther and Quentin Goestchel. “The PET comfort index: Questioning the model”. In: *Building and Environment* 137 (2018), pp. 1–10.

[60] U.S. Department of Energy. *EnergyPlus*. https://energyplus.net. Accessed: 2025-07-04. 2025.

[61] Yung-Chang Chen et al. "Concepts and new implements for modified physiologically equivalent temperature". In: *Atmosphere* 11.7 (2020), p. 694.

[62] Peter Bröde et al. "Deriving the operational procedure for the Universal Thermal Climate Index (UTCI)". In: *International journal of biometeorology* 56.3 (2012), pp. 481–494.

[63] Dusan Fiala et al. "UTCI-Fiala multi-node model of human heat transfer and temperature regulation". In: *International journal of biometeorology* 56.3 (2012), pp. 429–441.

[64] George Havenith et al. "The UTCI-clothing model". In: *International journal of biometeorology* 56.3 (2012), pp. 461–470.

[65] Yung-Chang Chen Andreas Matzarakis. "Modification of physiologically equivalent temperature". In: *Journal of Heat Island Institute International* 9-2 (2014).

[66] Charles H Simpson. "Comment on Havenga et al.(2022): Standard heat stress indices may not be appropriate for assessing marathons". In: *South African Journal of Science* 120.1/2 (2024).

[67] YH Yau and BT Chew. "A review on predicted mean vote and adaptive thermal comfort models". In: *Building Services Engineering Research and Technology* 35.1 (2014), pp. 23–35.

[68] A Cengel Yunus et al. "Heat transfer: a practical approach". In: *MacGraw Hill, New York* 210 (2003).

[69] Yunus A Cengel and Afshin Jahanshahi Ghajar. *(TEE-815): Heat and Mass Transfer: Fundamentals and Applications (Chap No. 15, 16 & 17 Includes)*. McGraw-Hill Education, 2020.

[70] Araz Azarnejad and Ardeshir Mahdavi. "Implications of façades' visual reflectance for buildings' thermal performance". In: *Journal of Building Physics* 42.2 (2018), pp. 125–141.

[71] Chao Hong et al. *Cool facades to mitigate urban heat island effects*. 2022.

[72] Rossano Albatici et al. "Assessment of the thermal emissivity value of building materials using an infrared thermovision technique emissometer". In: *Energy and buildings* 66 (2013), pp. 33–40.

[73] Christoph Reinhart. *4.401/4.464 Environmental Technologies in Buildings - Lecture 12: Thermal Mass and Heat Flow*. Accessed: 27-Feb-2025. 2018. URL: https://ocw.mit.edu/courses/4-401-environmental-technologies-in-buildings-fall-2018/c03cdb9ea591216d81a3f2febd616a3c_MIT4_401F18_lec12.pdf.

[74] H Lin, Y Xiao, and F Musso. "Shading effect and heat reflection performance of green facade in hot humid climate area: measurements of a residential project in Guangzhou, China". In: *IOP Conference Series: Earth and Environmental Science*. Vol. 146. 1. IOP Publishing. 2018, p. 012006.

[75] B Bechtel et al. *Generating WUDAPT Level 0 data–Current status of production and evaluation. Urban Clim. 27, 24–45*. 2019.

[76] Matthias Demuzere et al. "Combining expert and crowd-sourced training data to map urban form and functions for the continental US". In: *Scientific data* 7.1 (2020), p. 264.

[77] Noushig Kaloustian and Benjamin Bechtel. "Local climatic zoning and urban heat island in Beirut". In: *Procedia Engineering* 169 (2016), pp. 216–223.

[78] Cyril Goutte and Eric Gaussier. "A probabilistic interpretation of precision, recall and F-score, with implication for evaluation". In: *European conference on information retrieval*. Springer. 2005, pp. 345–359.

[79] Vincenzo Corrado, Ilaria Ballarini, and Stefano Paolo Corgnati. *Building Typology Brochure – Italy / Fascicolo sulla Tipologia Edilizia Italiana*. Luglio 2014. Politecnico di Torino – Dipartimento Energia, Gruppo di Ricerca TEBE, 2014. ISBN: 978-88-8202-065-1.

[80] Comune di Milano. *Geoportale del Comune di Milano – Censimento Urbanistico Storico*. Accessed: 2025-05-06. 2025. URL: https://geoportale.comune.milano.it/portal/apps/webappviewer/index.html?id=933b770d3eb54af98cb9c6305251028f.

[81] Gianfranco Pertot, Roberta Ramella, et al. *Milano 1946. Alle origini della ricostruzione. La città bombardata, il Censimento urbanistico, gli studi per il nuovo piano, le questioni di tutela.* Silvana editoriale, 2016.

[82] Copernicus Climate Change Service. *Extreme heat - European State of the Climate 2022*. https://climate.copernicus.eu/esotc/2022/extreme-heat. Accessed: 2025-03-29. 2023.

[83] ARPA Lombardia. *Meteorological and Climate Data Request Form*. https://www.arpalombardia.it/temi-ambientali/meteo-e-clima/form-richiesta-dati/. Accessed: 2025-04-03. 2025.

[84] Copernicus Atmosphere Monitoring Service. *CAMS Atmospheric Data Portal*. https://atmosphere.copernicus.eu/data. Accessed: 2025-04-17. 2025.

[85] *ENVI-met*. https://envi-met.com. Accessed: 2025-03-14.

[86] Anna Laura Pisello. "State of the art on the development of cool coatings for buildings and cities". In: *Solar Energy* 144 (2017), pp. 660–680.

[87] EVS Kiran Kumar Donthu et al. "Development of a simplified cool coating thermal model for predicting street canyon air temperature". In: *Building and Environment* 251 (2024), p. 111207.

[88] Ángel Luis León-Rodríguez et al. "Design and performance of test cells as an energy evaluation model of facades in a mediterranean building area". In: *Energies* 10.11 (2017), p. 1816.

[89] Nuno M Mateus, Armando Pinto, and Guilherme Carrilho Da Graça. "Validation of EnergyPlus thermal simulation of a double skin naturally and mechanically ventilated test cell". In: *Energy and Buildings* 75 (2014), pp. 511–522.

[90] Mohammad Taleghani et al. "Urban cooling: Which façade orientation has the most impact on a microclimate?" In: *Sustainable Cities and Society* 64 (2021), p. 102547.

[91] Ronnen Levinson. "Using solar availability factors to adjust cool-wall energy savings for shading and reflection by neighboring buildings". In: *Solar Energy* 180 (2019), pp. 717–734.

[92] Silvana Flores Larsen, Celina Filippín, and Graciela Lesino. "Thermal behavior of building walls in summer: Comparison of available analytical methods and experimental results for a case study". In: *Building Simulation*. Vol. 2. 1. Springer. 2009, pp. 3–18.

[93] Maxime Chaumont et al. "Influence of the thermal insulation position in standard and cool roofs on their contribution to urban heating during heatwaves". In: *Energy and Buildings* 324 (2024), p. 114907.

[94] Haotian Wu. *LCZ Factsheet: Milan, Italy*. Software Version 1.1.2, Retrieved from https://lcz-generator.rub.de. 2021.

A

Additional figures

Figure A.1: LCZ map 1

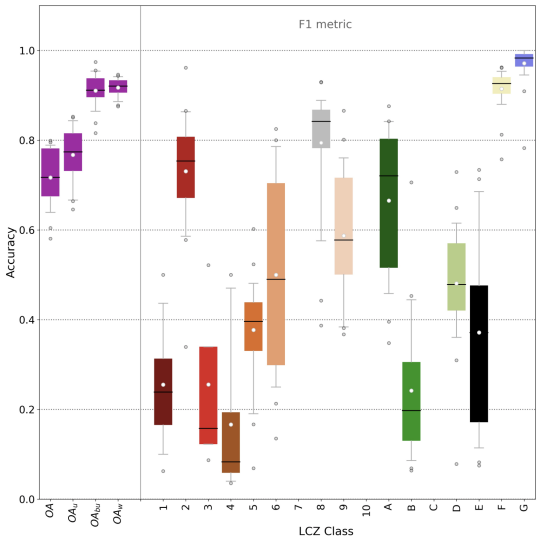

Figure A.2: F1 metric map 1

Figure A.3: LCZ map 2

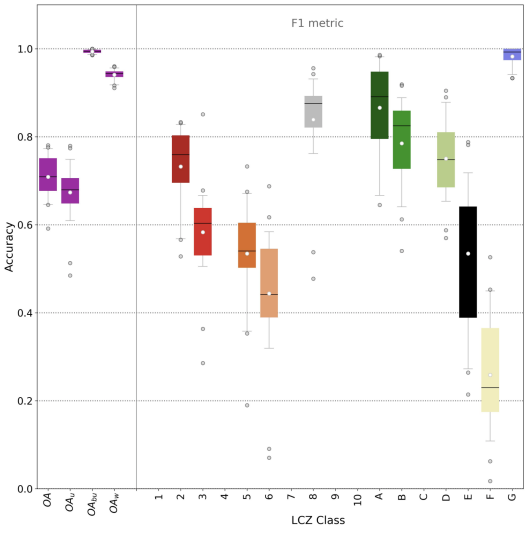

Figure A.4: F1 metric map 2

Figure A.5: LCZ map 3

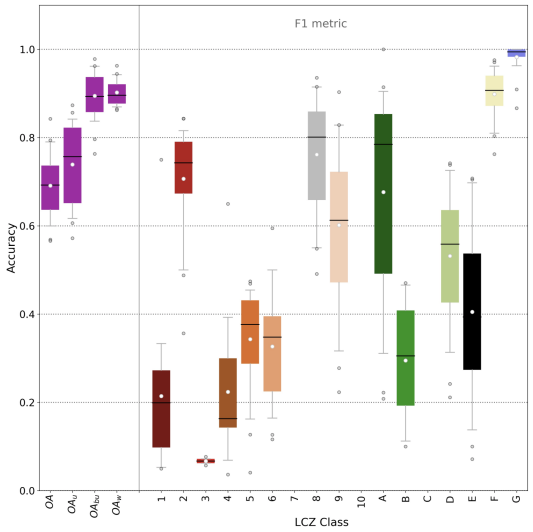

Figure A.6: F1 metric map 3

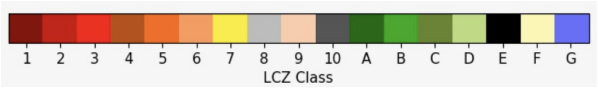

Figure A.7: LCZ classification per color according to the Factsheet of [94]

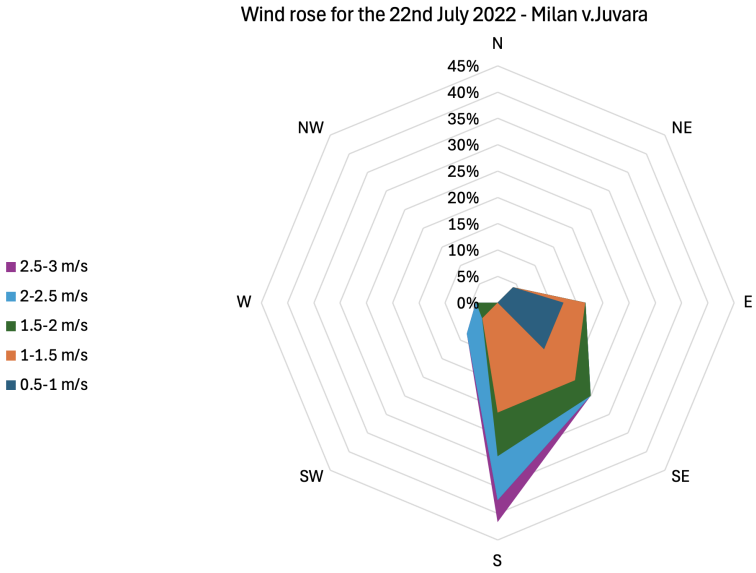

Figure A.8: Windrose for the 22nd of July 2022

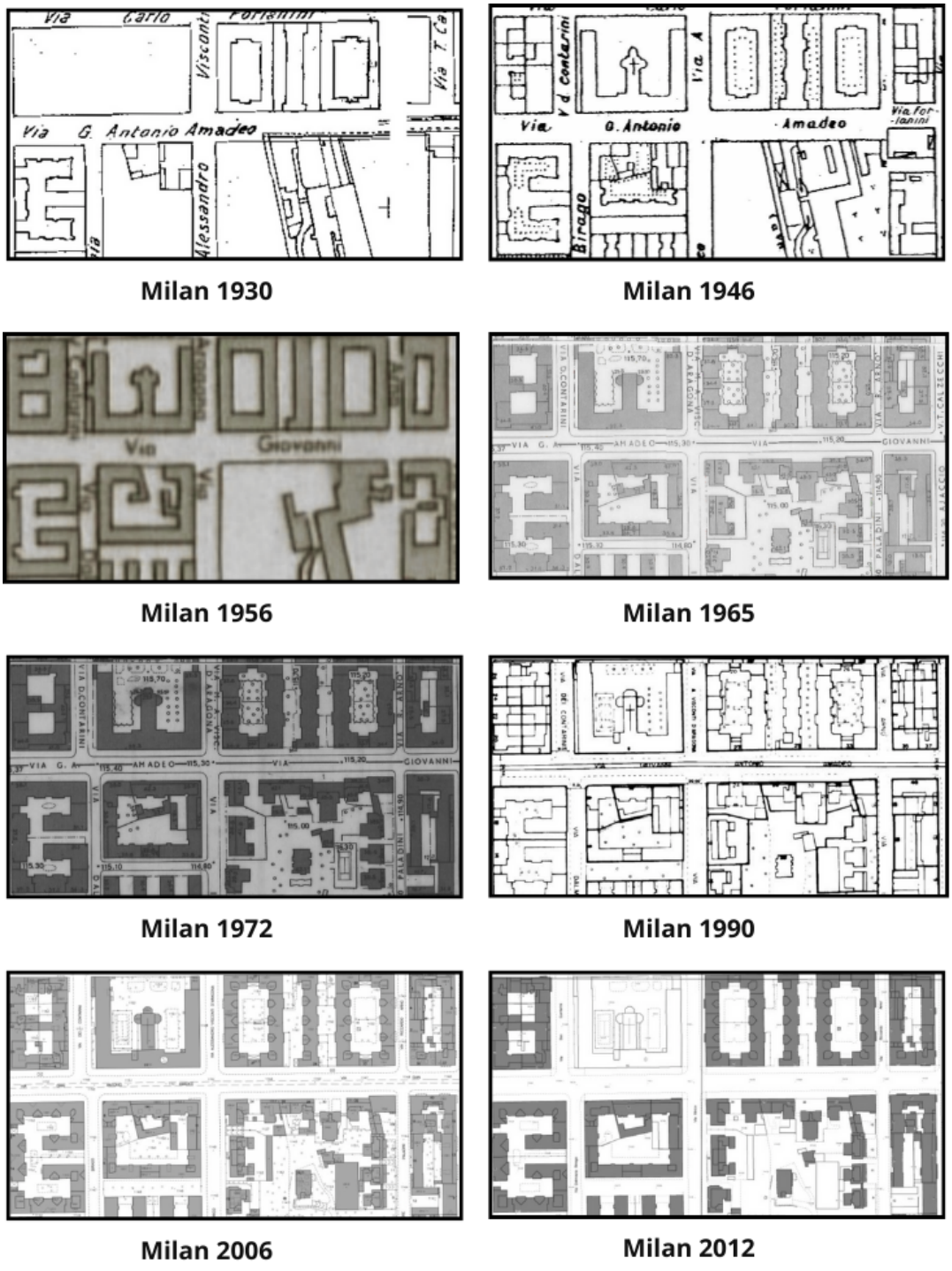

Figure A.9: Historical maps from Comune di Milano Geoportale[80]

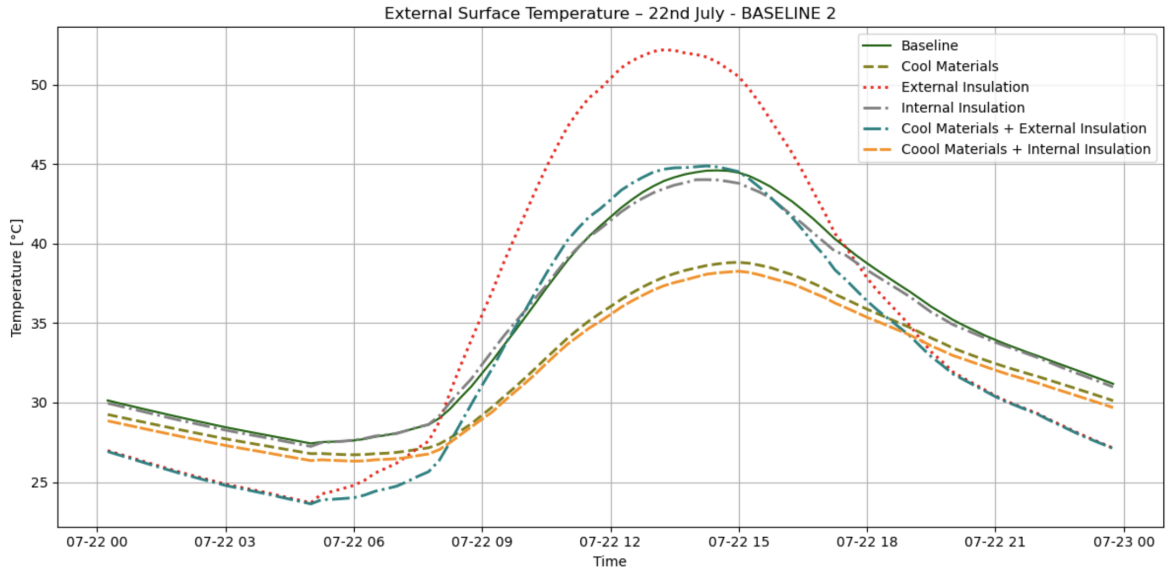

Figure A.10: External Surface Temperature - BASELINE 2

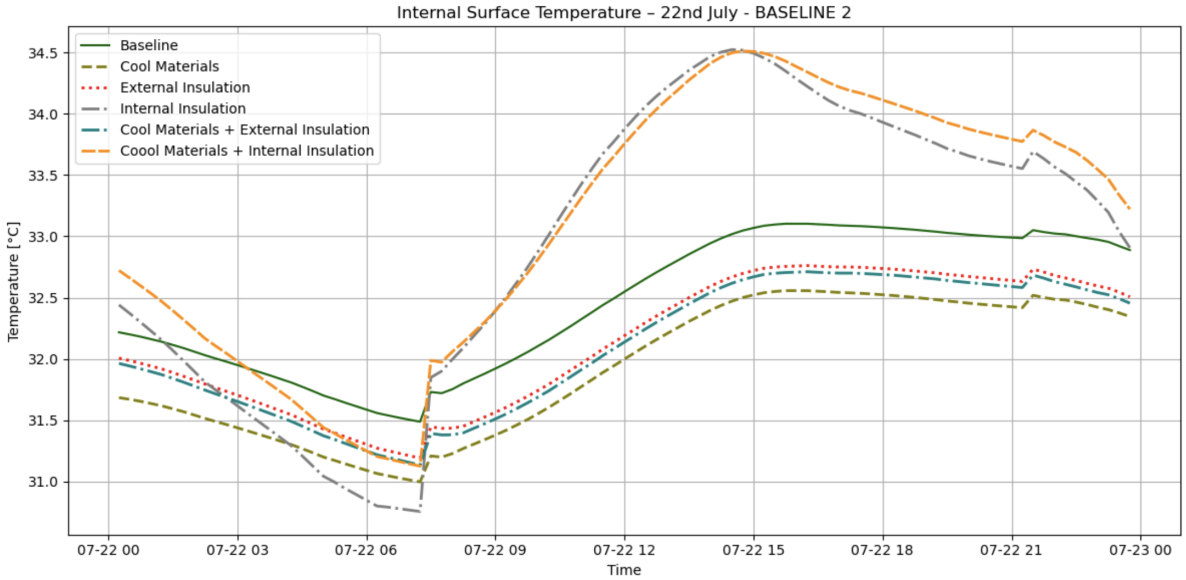

Figure A.11: Internal Surface Temperature - BASELINE 2

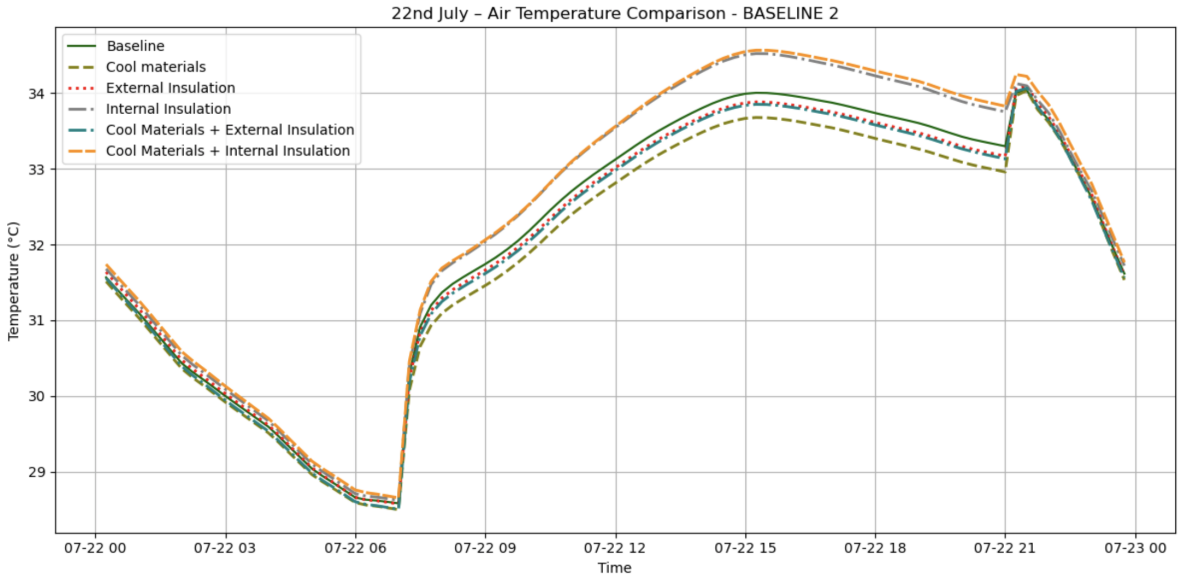

Figure A.12: Air Temperature - BASELINE 2

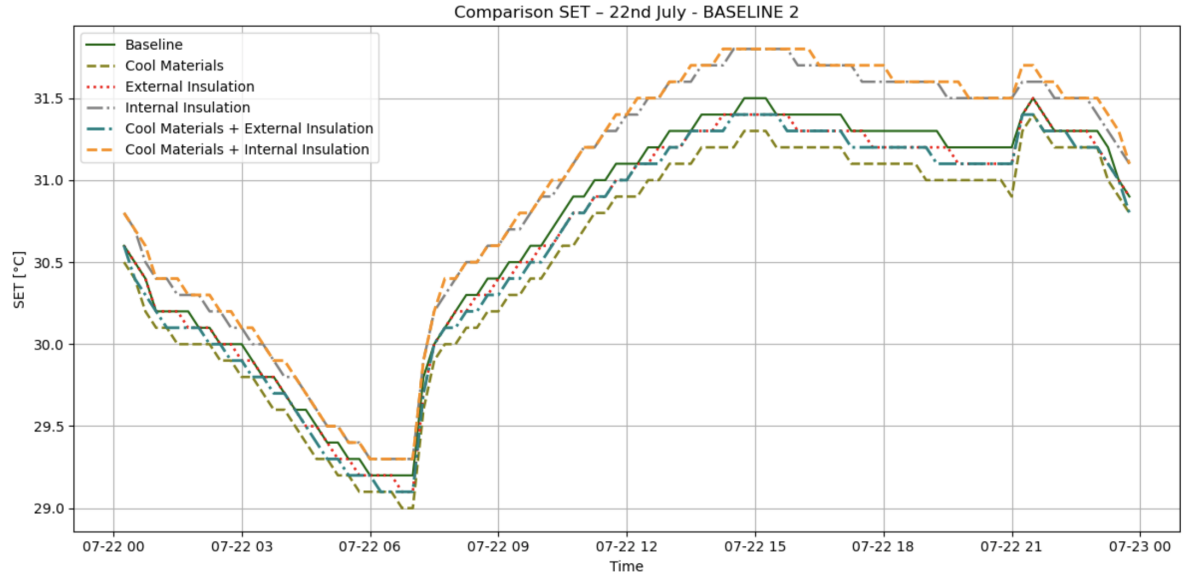

Figure A.13: SET - BASELINE 2

B

Calculations

B.1. Python Code

Simulation day selection

```
#!/usr/bin/env python
# coding: utf-8

# # EPW file creation

# In[112]:


import pandas as pd
import numpy as np
import matplotlib.pyplot as plt
from io import StringIO


# ### Importing a TMY file for Milan Linate

# In[113]:


# All the EPW file is read as text lines
with open("ITA_LM_Milano-Linate.AP.160800_TMYx.2007-2021/ITA_LM_Milano-
    Linate.AP.160800_TMYx.2007-2021.epw", "r") as f:
     lines = f.readlines()

# The first eitht lines are headers
epw_header = lines[:8]

# The ones after are hourly data
epw_data_lines = lines[8:]


# In[114]:


# The lines of the hourly data are imported in a DataFrame
epw_df = pd.read_csv(StringIO("".join(epw_data_lines)), header=None)
```

```

# In[115]:


# The lines of July are isolated
luglio_df = epw_df[epw_df[1] == 7]


# ### Incorporating CAMS dataset into the EPW file

# In[116]:


# All CAMS data are imported (skipping the headers)
cams_df = pd.read_csv("d63a36b1e9f17fd9970708619f29422e.csv", skiprows
    =42, sep=";")
cams_df.columns = [
    "time",       # column 0
    "col_2",      # column 1
    "col_3",      # column 2
    "col_4",      # column 3
    "col_5",      # column 4
    "col_6",      # column 5
    "GHI",        # column 6      EPW col 14
    "col_8",      # column 7
    "DHI",        # column 8      EPW col 16
    "DNI",        # column 9      EPW col 15
    "col_11"      # column 10
]


# In[117]:


# Find the indices of July's lines
luglio_idx = epw_df[epw_df[1] == 7].index

# Converting columns 14, 15, 16 in float64
epw_df[13] = epw_df[13].astype(float)
epw_df[14] = epw_df[14].astype(float)
epw_df[15] = epw_df[15].astype(float)

# Substituting CAMS' data in the right columns of the EPW file
epw_df.loc[luglio_idx, 13] = cams_df["GHI"].values      # column 14 EPW
epw_df.loc[luglio_idx, 14] = cams_df["DNI"].values      # column 15 EPW
epw_df.loc[luglio_idx, 15] = cams_df["DHI"].values      # column 16 EPW


# ### Including ARPA dataset into the EPW fie

# In[118]:


# Importing ARPA data
path = "RW_20250521110343_694146/"
```

```
91
92 arpa_temp = pd.read_csv(path + "RW_20250521110343_694146_5909_1.csv",
       names=["sensore", "timestamp", "valore"])
93 arpa_rh   = pd.read_csv(path + "RW_20250521110344_694146_6179_1.csv",
       names=["sensore", "timestamp", "valore"])
94 arpa_dir  = pd.read_csv(path + "RW_20250521110344_694146_6044_1.csv",
       names=["sensore", "timestamp", "valore"])
95 arpa_wind = pd.read_csv(path + "RW_20250521110344_694146_19242_1.csv",
       names=["sensore", "timestamp", "valore"])
96
97 # Parsing timestamp
98 for df in [arpa_temp, arpa_rh, arpa_dir, arpa_wind]:
99     df["timestamp"] = pd.to_datetime(df["timestamp"])  # lascia  l ora
           com'
100    df.set_index("timestamp", inplace=True)
101
102 # Isolating July 2022
103 start = "2022-07-01␣00:00"
104 end = "2022-08-01␣00:00"
105 arpa_temp_july = arpa_temp.loc[start:end]
106 arpa_rh_july   = arpa_rh.loc[start:end]
107 arpa_dir_july  = arpa_dir.loc[start:end]
108 arpa_wind_july = arpa_wind.loc[start:end]
109
110 # Making the columns foat
111 epw_df[6] = epw_df[6].astype(float)   # Dry bulb temperature
112 epw_df[8] = epw_df[8].astype(float)   # Relative Humidity
113 epw_df[20] = epw_df[20].astype(float) # Wind direction
114 epw_df[21] = epw_df[21].astype(float) # Wind speed
115
116 # Substituting ARPA's data in the right columns of the EPW file
117 epw_df.loc[luglio_idx, 6]  = arpa_temp_july["valore"].astype(float).
       values    # Dry bulb temperature
118 epw_df.loc[luglio_idx, 8]  = arpa_rh_july["valore"].astype(float).
       values      # Relative Humidity
119 epw_df.loc[luglio_idx, 20] = arpa_dir_july["valore"].astype(float).
       values     # Wind direction
120 epw_df.loc[luglio_idx, 21] = arpa_wind_july["valore"].astype(float).
       values    # Wind speed
121
122 #print("Lunghezza EPW luglio:", len(luglio_idx))
123 #print("Lunghezza dati ARPA temperatura luglio:", len(arpa_wind_july["
       valore"]))
124
125
126 # ### Dew Point Temperature Calculation
127 #
128 # The **dew point temperature** $T_{\text{dew}}$ is calculated from the
       air temperature $T$ (in  C ) and relative humidity $RH$ (in %)
       using the Magnus formula.
129 #
130 # 1. Compute the intermediate variable ($\gamma$):
131 #
132 # $$
133 # \gamma = \frac{a \cdot T}{b + T} + \ln\left(\frac{RH}{100}\right)
134 # $$
```

```
#
# 2. Compute the dew point temperature:
#
# $$
# T_{\text{dew}} = \frac{b \cdot \gamma}{a - \gamma}
# $$
#
# Constants used:
#
# - \( a = 17.625 \)
# - \( b = 243.04 \)
#
#
#
# (Source: Lawrence, M. G. (2005). The relationship between relative
    humidity and the dewpoint temperature in moist air: A simple
    conversion and applications. Bulletin of the American
    Meteorological Society, 86(2), 225-234.)

# In[119]:


# Magnus' constants
a = 17.625
b = 243.04

# Temperature and relative humdity from ARPA's data
T = arpa_temp_july["valore"].astype(float).values  # in  C
RH = arpa_rh_july["valore"].astype(float).values   # in %

# Calculating gamma
gamma = (a * T) / (b + T) + np.log(RH / 100.0)

# Calculating dew point temperature
T_dew = (b * gamma) / (a - gamma)

# Substituting the column in the EPW file
epw_df.loc[luglio_idx, 7] = T_dew


# ### Checks

# In[120]:


# Visualizing the first 5 lines of the month of July in the EPW file
#pd.set_option("display.max_columns", None)  # Mostra tutte le colonne
#epw_df.loc[luglio_idx].head()


# In[121]:


# Extract July data using the existing boolean mask
july_data = epw_df.loc[luglio_idx]
time_july = range(len(july_data))
```

```
188
189 # COLUMN MAPPING (zero-based index in EPW):
190 # 6  = Dew Point Temperature
191 # 8  = Relative Humidity
192 # 20 = Wind Direction
193 # 21 = Wind Speed
194
195 variables = {
196     'Dry Bulb Temperature ( C )': 6,
197     'Dew Point Temperature ( C )': 7,
198     'Relative Humidity (%)': 8,
199     'Global Horizontal Radiation (Wh/m  )': 13,
200     'Direct Normal Radiation (Wh/m  )': 14,
201     'Diffuse Horizontal Radiation (Wh/m  )': 15,
202     #'Wind Direction (  )': 20,
203     'Wind Speed (m/s)': 21
204 }
205
206 # Plot for July (x-axis = hours)
207 for label, col in variables.items():
208     plt.figure(figsize=(15, 4))
209     plt.plot(time_july, july_data.iloc[:, col], label=label, color='
        teal')
210     plt.title(f'{label} - July')
211     plt.xlabel('Hour')
212     plt.ylabel(label)
213     plt.grid(True)
214     plt.legend()
215     plt.tight_layout()
216     plt.show()
217
218
219 # In[122]:
220
221
222 # Plot for Full Year
223 for label, col in variables.items():
224     plt.figure(figsize=(15, 4))
225     plt.plot(time_full, epw_df.iloc[:, col], label=label, color='
        darkorange')
226     plt.title(f'{label} - Full Year')
227     plt.xlabel('Hour of the Year')
228     plt.ylabel(label)
229     plt.grid(True)
230     plt.legend()
231     plt.tight_layout()
232     plt.show()
233
234
235 # In[124]:
236
237
238 # Saving modified EPW file
239 output_path = "epw_luglio_modificato.epw"
240 epw_df.to_csv(output_path, index=False, header=False)
241 print(f"EPW file saved in: {output_path}")
```

```

# In[125]:


# Add the original header of the TMY file
with open("ITA_LM_Milano-Linate.AP.160800_TMYx.2007-2021/ITA_LM_Milano-Linate.AP.160800_TMYx.2007-2021.epw", "r") as f:
    epw_lines = f.readlines()

epw_header = epw_lines[:8]

# Convert in EPW format
data_lines = epw_df.apply(lambda row: ",".join(row.astype(str)), axis=1).tolist()

# Save
with open("epw_luglio_modificato.epw", "w") as f:
    f.writelines(epw_header)
    for line in data_lines:
        f.write(line + "\n")

print("EPW file saved as: epw_luglio_modificato.epw")
```

Listing B.1: Simulation day selection

EPW file creation

```
#!/usr/bin/env python
# coding: utf-8

# In[25]:


import pandas as pd
import matplotlib.pyplot as plt
import seaborn as sns
import numpy as np


# In[26]:


file_path = "/Users/margherita/Desktop/dati_arpa_3.xls"

# Read the Excel file
df = pd.read_excel(file_path, engine="xlrd", header=None)  # Use "openpyxl" if it's an .xlsx file, "xlrd" if it is a .xls file

# Rename the columns
df.columns = ["Day", "Mean_daily_Temperature", "Mex_mean_hourly_Temperature"]

# Display the first few rows
#print(df.head())
```

```
26
27
28 # In[27]:
29
30
31 # Convert "Day" column to datetime format
32 df["Day"] = pd.to_datetime(df["Day"])
33
34 # Add a Month column
35 df["Month"] = df["Day"].dt.month_name()
36
37 # Find the maximum temperature for each month
38 monthly_max = df.groupby("Month")["Mex_mean_hourly_Temperature"].max().
       sort_values(ascending=False)
39
40 print("Maximum␣temperature␣per␣month:")
41 print(monthly_max)
42
43 # Get the month with the highest value
44 worst_month = monthly_max.idxmax()
45 max_temp = monthly_max.max()
46
47 print(f"\nThe␣hottest␣month␣was␣{worst_month},␣with␣a␣maximum␣daily␣
       temperature␣of␣{max_temp:.1f} C .")
48
49
50 # In[28]:
51
52
53 file_path = "/Users/margherita/Desktop/dati_arpa_2.xls"
54
55 # Read the Excel file
56 df = pd.read_excel(file_path, engine="xlrd", header=None)  # Use "
       openpyxl" if it's an .xlsx file, "xlrd" if it is a .xls file
57
58 # Rename the columns
59 df.columns = ["Day", "Time", "Mean_Temperature"]
60
61 # Display the first few rows
62 #print(df.head())
63
64
65 # In[32]:
66
67
68 # Find the daily maximum temperature
69 daily_max_temps = df.groupby("Day")["Mean_Temperature"].max().
       reset_index()
70
71 # Plot the data
72 #plt.figure(figsize=(12, 6))
73 #plt.bar(daily_max_temps["Day"], daily_max_temps["Mean_Temperature"],
       color="#800020", alpha=0.7)
74
75 # Formatting the plot
76 #plt.xlabel("Date")
```

```
#plt.ylabel("Maximum Temperature ( C )")
#plt.title("Daily Maximum Temperatures for July 2022")
#plt.xticks(daily_max_temps["Day"], rotation=90)
#plt.show()


# In[33]:


daily_max_temps["Day"] = pd.to_datetime(daily_max_temps["Day"]).dt.date
print(f"The␣hottest␣day␣was␣{daily_max_temps.loc[daily_max_temps['
    Mean_Temperature'].idxmax(),␣'Day']}␣with␣a␣maximum␣temperature␣of␣
    {daily_max_temps['Mean_Temperature'].max()} C .")
```

Listing B.2: EPW file creation

EPW file for Baseline 1

```
#!/usr/bin/env python
# coding: utf-8

# # EPW file for Baseline Simulation 1

# In[21]:


import pandas as pd
import matplotlib.pyplot as plt


# #### Importing the EPW file created before

# In[22]:


epw_path = "epw_luglio_modificato.epw"

# Load the EPW data (skip the first 8 header lines)
epw_df = pd.read_csv(epw_path, skiprows=8, header=None)

# Display the first few rows
#epw_df.head()


# #### Importing the .xls file for Baseline Simulation 1 (i=125, j=66,
    k=8)

# In[23]:


envi_path = "excel_files/baseline125D_AT__125_66_8.xls"
envi_df = pd.read_excel(envi_path)

# Combine 'date' and 'time' columns into a single datetime column
envi_df['datetime'] = pd.to_datetime(envi_df['Date'].astype(str) + '␣'
    + envi_df['Time'].astype(str), dayfirst=True, format='%d.%m.%Y␣%H.%
```

```
    M.%S')

# Check
#envi_df[['Date', 'Time', 'datetime']].head()


# #### Filtering ENVI-met data and keeping only the 22nd of July

# In[24]:


# Filter rows for 22 July only
envi_22july = envi_df[envi_df['datetime'].dt.month == 7]
envi_22july = envi_22july[envi_22july['datetime'].dt.day == 22].
    reset_index(drop=True)

# Check
#envi_22july.head()


# #### Isolating the lines of the 22nd of July on the EPW file

# In[25]:


# Creating a Datetime index from the EPW
epw_df.index = pd.to_datetime({
    'year':  epw_df.iloc[:, 0],
    'month': epw_df.iloc[:, 1],
    'day':   epw_df.iloc[:, 2],
    'hour':  epw_df.iloc[:, 3] - 1  # da 1  24   a 0  23
})

# Corregge l'offset semantico di mezzanotte (24:00)     00:00 del
    giorno successivo
midnight_rows = epw_df.iloc[:, 3] == 24
epw_df.index = epw_df.index.where(~midnight_rows, epw_df.index + pd.
    Timedelta(days=1))


# Isolate rows corresponding to July 22nd
july_22_mask = (epw_df.index.month == 7) & (epw_df.index.day == 22)
epw_july22 = epw_df.loc[july_22_mask]

# Check the number of rows (should be 24)
print("Number␣of␣records␣for␣July␣22:", len(epw_july22))
#epw_july22.head()


# #### Replacing the EPW values for the 22nd of July with the values
    from ENVI-met

# In[26]:


print(envi_df.columns)
```

```
88
89
90  # In[27]:
91
92
93  # Ensure the ENVI-met data is filtered to July 22 only
94  envi_july22 = envi_df[envi_df['datetime'].dt.day == 22]
95
96  # Double check lengths match
97  assert len(envi_july22) == len(epw_df.loc[july_22_mask]), "Row␣count␣
        mismatch!"
98
99  # Replace the values in epw_df
100 epw_df.loc[july_22_mask, 21] = envi_july22["Wind␣Speed␣␣(m/s)"].values
101 epw_df.loc[july_22_mask, 20] = envi_july22["Wind␣Direction␣␣(deg)"].
        values
102 epw_df.loc[july_22_mask, 6]  = envi_july22["Potential␣Air␣Temperature␣␣
        ( C )"].values
103 epw_df.loc[july_22_mask, 8]  = envi_july22["Relative␣Humidity␣␣(%)"].
        astype(float).values
104
105
106 # #### Visual checks
107
108 # In[28]:
109
110
111 # Print the modified rows for July 22
112 epw_df.loc[july_22_mask, [6, 8, 20, 21]].head(20)
113
114
115 # #### Comparative plots
116
117 # In[29]:
118
119
120 epw_original = pd.read_csv("epw_luglio_modificato.epw", skiprows=8,
        header=None)
121 epw_original.columns = epw_df.columns
122 epw_original.index = epw_df.index
123
124
125 # In[30]:
126
127
128 # Subset July 22 data
129 original_july22 = epw_original.loc[july_22_mask]
130 modified_july22 = epw_df.loc[july_22_mask]
131
132 # Ordina solo il dataframe modificato per plotting
133 modified_july22_sorted = modified_july22.sort_index()
134
135 # L'asse X dei grafici rimane quello dell'originale
136 time_july22 = modified_july22_sorted.index
137
138 # Mapping: {Label: EPW column number}
```

```
variables = {
    'Dry Bulb Temperature ( C )': 6,
    'Relative Humidity (%)': 8,
    'Wind Direction (  )': 20,
    'Wind Speed (m/s)': 21
}

# Plot comparisons
for label, col in variables.items():
    plt.figure(figsize=(15, 4))
    plt.plot(time_july22, original_july22[col], label='Original EPW',
        linestyle='--', color='gray')
    plt.plot(time_july22, modified_july22_sorted[col], label='Modified
        (ENVI-met)', color='teal')
    plt.title(f'{label} - July 22')
    plt.xlabel('Hour')
    plt.ylabel(label)
    plt.grid(True)
    plt.legend()
    plt.tight_layout()
    plt.show()


# In[31]:


print(modified_july22.shape)
print(modified_july22.index)


# In[32]:


envi_july22[["Wind Speed   (m/s)", "Wind Direction   (deg)"]].describe()


# The values from the ENVI-met results for the wind speed and wind
    direction appeares as straight lines. This is because the data have
     a really low standard deviation. This can be explained because in
    the ENVI-met simulations, the values for wind direction and wind
    speed were not fully forced, but a mean was applied for the wind
    speed (v=1.6m/s) and a wind rose was done to establish the average
    wind direction (160 C ). This choice was made due to the numerical
    instability of ENVI-met under changing wind data. In order to keep
    consistency between the outdoor and the indoor simulations, the
    wind data from ENVI-met will be used, even if they are highly
    simplifying the real wind pattern.

# #### Concistency check

# Checking that for all the rows the Dew Point Temperature is lower
    than the Dry Bulb Temperature.

# In[33]:


```

```
july_22_data = epw_df.loc[july_22_mask]

invalid_dewpoint = july_22_data[july_22_data[7] > july_22_data[6]]
print(f"{len(invalid_dewpoint)} rows where Dew Point > Dry Bulb")


# Relative humidity must be between 0% and 100% for all the rows.

# In[34]:


invalid_rh = july_22_data[(july_22_data[8] < 0) | (july_22_data[8] >
    100)]
print(f"{len(invalid_rh)} rows where Relative Humidity is outside [0%,
    100%]")


# Wind speed must be positive for all the rows.

# In[35]:


invalid_wind_speed = july_22_data[july_22_data[21] < 0]
print(f"{len(invalid_wind_speed)} rows where Wind Speed < 0")


# Wind direction must be between 0 C  and 360 C  for all the rows

# In[36]:


invalid_wind_direction = july_22_data[(july_22_data[20] < 0) | (
    july_22_data[20] > 360)]
print(f"{len(invalid_wind_direction)} rows where Wind Direction is
    outside 0   360   range")


# #### No NaNs

# In[37]:


july_22_data = epw_df.loc[july_22_mask]

cols_to_check = [6, 7, 8, 20, 21]

nan_check = july_22_data[cols_to_check].isna().sum()
#print("NaN values per column:\n", nan_check)

if nan_check.sum() == 0:
    print("No NaN values found in modified columns.")
else:
    print("There are NaN values in the modified columns.")


# #### Saving
```

```
234
235 # In[38]:
236
237
238 output_epw_path = "epw_baseline1.epw"
239
240 # Save header
241 with open("epw_luglio_modificato.epw", 'r') as f:
242     epw_header = [next(f) for _ in range(8)]
243
244 # Convert to EPW format
245 data_lines = epw_df.apply(lambda row: ",".join(row.astype(str)), axis
    =1).tolist()
246
247 # Save
248 with open(output_epw_path, "w") as f:
249     f.writelines(epw_header)
250     for line in data_lines:
251         f.write(line + "\n")
252
253 print(f"␣EPW␣file␣saved␣as:␣{output_epw_path}")
254
255
256 # In[ ]:
```

Listing B.3: EPW file for Baseline 1